

Eesti Maaülikooli doktoritööd

**Doctoral Thesis of the
Estonian University of Life Sciences**



**ON USING MATHCAD SOFTWARE FOR
MODELLING, VISUALIZATION AND
SIMULATION IN MECHANICS**

MATHCADI TARKVARAPÕHINE MODELLEERIMINE,
VISUALISEERIMINE JA SIMULEERIMINE MEHAANIKAS

AARE AAN

A Thesis
for applying for the degree of Doctor of Philosophy
in Production Engineering

Väitekiri
filosoofiadoktori kraadi taotlemiseks tootmistehnika erialal

Tartu 2015

Institute of Technology,
Eesti Maaülikool, Estonian University of Life Sciences

According to verdict No 1-4/30 of September 25, 2015, the Doctoral Committee of the Engineering Sciences of the Estonian University of Life Sciences has accepted the thesis for the defence of the degree of Doctor of Philosophy in Production Engineering.

Opponent: **Professor Valery Ochkov**, DSc (Eng)
Department of Power Plants,
National Research University Moscow Power
Engineering Institute

Opponent: **Leading Research Scientist Jüri Majak**, DSc
(Math)
Department of Machinery,
Faculty of Mechanical Engineering,
Tallinn University of Technology

Supervisor: **Professor Mati Heinloo**, DSc (Math)
Institute of Technology
Estonian University of Life Sciences

Defence of the thesis:
Estonian University of Life Sciences, room B136, Kreutzwaldi 56,
Tartu on November 06, 2015, at 9:15.

Publication of this thesis is supported by the
Estonian University of Life Sciences.



© Aare Aan, 2015
ISSN 2382-7076
ISBN 978-9949-569-02-1 (trükis)
ISBN 978-9949-569-03-8 (pdf)

CONTENTS

LIST OF ORIGINAL PUBLICATIONS	8
INTELLECTUAL PROPERTY	10
ABBREVIATIONS AND SYMBOLS	11
INTRODUCTION.....	14
1. Literature overview	15
1.1 Visualization.....	15
1.2 On using simulations in teaching.....	16
1.3 Overview of the virtual models and their motion simulations in the program Mathcad.....	18
1.4 The purpose and tasks of the doctoral thesis	23
2. Materials and Methods.....	26
2.1 Foreword.....	26
2.2 Overview of some mass point equations in kinematics and dynamics.....	26
2.2.1 On the mass point motion of Curved planar trajectories	26
2.2.2 Mass point motion on a rotating disc	27
2.2.3 Mass point motion on a moving inclined plane	28
2.3 Overview of the Lagrange and Hamilton's equations	29
2.4 Overview of the equations in the Mechanics of machinery	29
2.5 IV order Runge-Kutta algorithm for differential equations' numerical solutions.....	33
3. Using the program Mathcad.....	34
3.1 Mathcad worksheet.....	34
3.2 Implementation of the Runge-Kutta method using a Mathcad worksheet	35
3.3 Motion simulation on a Mathcad worksheet	38

3.4	On the visualization of geometric vectors on a Mathcad worksheet	40
4.	Overview of the research papers written by the author of the thesis	42
4.1	On the creative teaching of engineering mechanics	42
4.2	On research regarding linkages	43
4.2.1	Study of the V-engine	43
4.2.2	Study of the double connecting-rod linkage.....	45
4.2.3	Study of the Theo Jansen walking mechanism	48
4.3	On research on mass point motion	50
4.3.1	Mass point motion on curved trajectories	50
4.3.2	Study of a granule's motion on a fertilizer spreading disc.....	51
4.3.3	A sea buckthorn berry's motion on a conveyor belt ..	52
4.4	Synthesis of a cam-follower mechanism.....	53
4.5	Study on the chaotic motion of a double pendulum	57
4.6	Small oscillations of coupled pendulums	57
	SUMMARY AND CONCLUSIONS.....	59
	REFERENCES.....	63
	KOKKUVÕTE.....	70
	ACKNOWLEDGEMENTS	73
	PUBLICATIONS	74
	CURRICULUM VITAE	174
	ELULOOKIRJELDUS.....	176
	ETTEKANDED	178

LIST OF ORIGINAL PUBLICATIONS

- I. **Aan, A.**, Aarend, E., Heinloo, M. 2011. On chaotic motion of a double pendulum. *Agronomy Research*, Volume 9, 5–12.
- II. **Aan, A.**, Heinloo, M., Aarend, E. 2011. Interactive Computer Aided Learning and Teaching of Analytical Mechanics. *Int. J. Engn. Pedagogy (iJEP)*, Volume 1(3), pp. 4–8.
- III. **Aan, A.**, Heinloo, M. 2011. On creative teaching of engineering mechanics. *Proc. 22nd International DAAAM World Symposium*, pp. 1081–1082.
- IV. **Aan, A.**, Heinloo, M., Aarend, E., Mikita, V. 2012. Analysis of four-stroke cycle internal combustion V-engine in Mathcad environment. *Proceedings of 8th International Conference of DAAAM Baltic Industrial Engineering*, Tallinn, pp 389–394.
- V. **Aan, A.**, Heinloo, M. 2012. Computer based comparison analysis of single and double-connecting-rod slider-crank linkages. *Agronomy Research*, Volume 10, pp. 3–10.
- VI. **Aan, A.**, Heinloo, M. 2012. Visualization of the kinematics of a material point. *Engineering for Rural Development: Proceedings 11th International Scientific Conference - Engineering for Rural Development*, Jelgava, pp. 204–209.
- VII. **Aan, A.**, Heinloo, M. 2013. Composing and solving differential equations for small oscillations of mathematical spring-coupled pendulum. *Agronomy Research*, Volume 11(1). Pp. 223–230.
- VIII. **Aan, A.**, Heinloo, M. 2014. Motion of a granule on fertilizer spreading disc. *Proc. 42nd Int. symp. “Actual Tasks on Agricultural Engineering”*, Opatia, pp. 101 - 111.
- IX. **Aan, A.**, Heinloo, M., Allas, J. 2014. Design of a radial cam for the cam-follower mechanism. *Proceedings of 9th International DAAAM Baltic Conference in Estonia: INDUSTRIAL ENGINEERING*, Tallinn, pp. 11 – 16.
- X. **Aan, A.**, Heinloo, M. 2014. Analysis and synthesis of the walking linkage of Theo Jansen with a flywheel. *Agronomy Research*, Volume 12(2), pp. 657–662.
- XI. **Aan, A.**, Heinloo, M. 2015. Dynamics of a frozen sea buck-thorn berry in a separator. *Procedia Engineering*, Volume 100, pp. 689–698.

The author's contribution to the paper:

Paper	Study design	Data collection	Data processing	Manuscript preparation
I	MH, AA, EA	MH, AA	AA, MH	AA, MH
II	AA, MH, EA	AA	AA	AA, MH
III	MH, AA	AA, MH	AA, MH	AA
IV	MH, AA	AA, MH	AA, MH, EA	AA, MH, VM
V	MH, AA	AA, MH	AA, MH	AA, MH
VI	MH, AA	MH, AA	AA, MH	AA, MH
VII	MH, AA	AA, MH	AA, MH	AA, MH
VIII	MH, AA	MH, AA	AA, MH	AA, MH
IX	AA, MH, JA	AA, MH	AA, MH	AA, MH, JA
X	MH, AA	MH, AA	AA, MH	AA, MH
XI	MH, AA	MH, AA	AA, MH	AA, MH

AA - Aare Aan, MH - Mati Heinloo, EA - Eino Aarend, VM - Villu Mikita, JA - Jaanus Allas

INTELLECTUAL PROPERTY

I. Title: Device for the separation of deep-frozen sea-buckthorn berries from twigs

Patent number: EE 05717 B1
Filing date of the application: 19.07.2012
Priority date: 19.07.2012
Publication date: 15.04.2014
Inventors' names: Nõmm, P., **Aan, A.**

The author's contribution to the paper:

Document	Study design	Preparation and elaboration activities	Study of prior art	Manuscript preparation
I	PN, AA	AA	AA	AA, PN

AA - Aare Aan, PN - Peeter Nõmm

ABBREVIATIONS AND SYMBOLS

$rkfixed(a, t_0, t_N, N, D)$ —function in the program Mathcad, which uses the algorithm of the Runge-Kutta fourth order method

FRAME—animation parameter used to define the variable for the generation of simulations on a Mathcad worksheet

Symbols

A	fertilizer granule's current position; berry surface's frontal area
A_0	fertilizer granule's initial position
$a; a_x, a_y$	acceleration; projections of the acceleration
$b(t)$	vector module in vector function $F(t, \gamma, b, n)$
b	notation of $b(t)$ of the vector \vec{b} in vector function $F(t, \gamma, b, n)$
c_d	air resistance constant
D	notation of the vector $D(t, y)$
D	piston diameter
F_1	friction force projection on axis ξ between the spreading disc and the vane
F_2	inertial force projection on axis ξ
F_3	friction force projection on axis ξ
F_4	projection of the Coriolis inertial force
F_k	magnitude of the resisting force
f	friction coefficient
H	Hamiltonian; follower stroke
I	moment of inertia; matrix of the shape of a vector in the vector function $F(t, \gamma, b, n)$
I_r	reduced moment of inertia
I_{r0}	value of the reduced moment of inertia at the beginning of a cycle
L	Lagrangian
l	width of the conveyor belt; length
M_r	magnitude of the resisting torque on link one
M_u	pivot's resisting torque
M_m	constant driving torque of the link
m	mass
N	number of intervals between t_0 and t_N

n	coefficient of dimensions in vector function $F(t, \gamma, b, n)$
p	gas pressure in the engine cylinder
p_k	generalized momentum
$p_{\theta_1}, p_{\theta_2}$	generalized momentum of the double pendulum
Q_k	generalized force
q_k	generalized coordinates
R	spreading disc radius
$R(t)$	radius of the curvature
R_0	cam base circle radius
r	distance between the centre of the disc and a fertilizer granule in the current position
r_0	distance between the centre of the disc and a fertilizer granule in the initial position
Z	used to define function $rkfixed(a, t_0, t_N, N, D$
s	axis along the conveyor belt
s''	berry's acceleration
T	kinetic energy; denotes the transposed matrix in a vector function $F(t, \gamma, b, n)$
t_0	first time value
t_N	last value, where N marks last value
V_0	matrix of origin in vector function $F(t, \gamma, b, n)$
v	velocity
v_x, v_y	projections of the velocity
v_k	velocity of the conveyor belt; magnitude of the velocity
Greek	
α	pressure angle
α_k	angle between force and velocity
$\alpha(t)$	centre of the curvature x coordinate
$\beta(t)$	centre of the curvature y coordinate
β	inclination angle of the conveyor belt
ΔT	change in linkage kinetic energy
δ	coefficient of speed fluctuation
ε	eccentricity of the follower
θ_1, θ_2	inclination angles of the double pendulum
ξ	axis between initial A_0 and current positions A of a fertilizer granule
Π	potential energy
ρ	air density
ϕ_r	follower rise angle

ϕ_h	follower high dwell angle
ϕ_f	follower fall angle
ϕ_l	follower low dwell angle
ψ_0	adjusting angle of the vane
ψ	angle between the polar radii of a fertilizer granule and the direction of the vane
Ω	matrix of transformation of the rotation in the vector function $F(t, \gamma, b, n)$
ω, ω_1	angular velocity
ω_u	pivot's angular velocity
ω_0	value of ω at the beginning of a cycle

INTRODUCTION

Learning and research are becoming increasingly more computer-based, which is supported by both the development of computing technology and better results in studying, teaching and research into engineering problems. According to Chonacky, 2006, computer modelling and simulation are some of the best methodologies that have been applied in science and engineering.

This doctoral thesis develops computer-based learning and research methods in engineering mechanics, analytical mechanics and machinery mechanics. The results can be used in both teaching and practical engineering. In the current doctoral thesis, the objects that are automatically generated on the computer screen using a mathematical model are called virtual models for short. The process of creating images that correspond to calculation results (graphs, virtual models, simulations, etc.) is called visualization. The simulation of the movement of virtual models gives an idea of the movement of the object of study and the veracity of the solution calculated on the basis of the mathematical model. The use of computer-based visualization in teaching is very important. The analysis Höffler & Leutner, 2007 showed that the learning outcome improved by 37% on average when a simulation (animation) was used instead of a static picture. The simulations in the current thesis correspond to Recchi, et al., 2006 definition: an effective computer simulation is built on a mathematical model, which describes the process that is being studied. Visualization is interdisciplinary by nature, drawing on simulations, the psychology of perception, graphic art, computer graphics, picture editing, data management, etc. (Haber, 1990).

The mechanical problems explored in the current thesis have been solved with a computer on a PTC Mathcad worksheet. Unlike other mathematics programs, in which the formulas have to be programmed as well, the engineering calculations software Mathcad allows writing formulas the way we are used to seeing them in books and writing them ourselves. The formulas and variables on a Mathcad worksheet can be changed on the computer screen and the changes in results can be directly observed in drawings, virtual models and motion simulations for the virtual models.

1. Literature overview

1.1 Visualization

The visualization of the study object's mathematical model helps a greater number of scientists, engineers and students to understand the work processes of physical systems, while taking into account the special types of people with increased neural activity.

Russian psychologist I. Pavlov divided people into three categories according to their neural activity: artistic, thinking and middle types (Leppik, 2001; Leppik, 2008). The memory of the artistic type is closely connected to senses, especially sight. In order to understand problems - this bears great significance in the learning process - it is important for the artistic type to see a diagram, picture, model, graph, film, etc. The studies have shown that these people value imagery over concreteness. Additionally, it has been found that they respond to stimuli more directly, they have a closer connection to real experiences and react to reality more unwillingly than thinkers (Leppik, 2008). Thinkers are characterised by abstract thinking, logical analysis and good memory. They are good at math. Most thinkers are introverts: quiet, withdrawn and attentive. Teachers like this type of students. They are satisfied when the study material is verbal and abstract, relying on logic and analysis when absorbing information. They remember new material mostly semantically (conceptually). Generally, they do not need visual explanation and enjoy abstract analysis and discussion instead (Leppik, 2008). The people who fall in the middle category extract information from the outside world using the strategies of both the previously described types. It has been found that the middle type is successful in both scientific and creative fields (Leppik, 2008). It is important for the teacher, lecturer or trainer to be aware of the different learning types. Consequently, they should use teaching methods that are suitable for the discussed types (Leppik, 2001).

Studies in cognitive psychology have proven that imagery is more important in teaching than the concrete presentation of information. The importance of imagery is regarded as twofold:

1. it helps some of the students to understand new material. The material that has been understood is stored in long-term memory;
2. it helps to create associative connections, which means that information is stored more efficiently and it can later be easily retrieved from long-term memory.

Primary schools and kindergartens traditionally engage all senses, but the teaching in higher grades and institutions of higher education is often verbal, which means that the teacher actually works with only some of the students. As a result, the teacher thinks that the students are not learning and this leads to teacher-student conflicts. Engaging all senses becomes especially important when presenting new material in class. Verbal and abstract methods can later be used when revising, practising and storing information, especially among older students (Leppik, 2001).

There are plenty of ways to engage different senses that are suitable for different subjects and ages, for instance:

1. demonstrations, experiments and models;
2. observation of the objects of study;
3. pictures, tables, diagrams;
4. slideshows;
5. video clips and films;
6. computer research;
7. field trips (Leppik, 2001).

Above all, visualization helps the artistic type to understand the presented material. Mathcad's interactive worksheets along with motion simulation offer better visualization compared to printed text.

1.2 On using simulations in teaching

Two groups were compared, one of which received traditional guidance in a classroom, whereas the other used additional computer simulations. The students' understanding of kinematics was studied, whereas the topic was motion in the Earth's gravitational field. The students who used computer simulations showed significantly better results in solving the task given to them. It was concluded that computer simulations are useful tools for understanding velocity and acceleration (Jimoyiannis & Komis, 2001; Rutten, et al., 2012). In

another study, two groups of students had to study particle kinetics. One group only studied in the classroom, whereas the other studied both in class and using computer simulations. The test results of the group who used computer simulations were better (Cohen's $d=0.81$), even though the overall results of the test were low (Rutten, et al., 2012; Stern, et al., 2008). A comparative study of a traditional class and simulation-supported class was conducted in the field of genetics. The students were assessed in two ways, firstly, using statements (true/false) and secondly multiple choice questions. The study revealed that the class that used simulations achieved better results. When answering the question of whether the statement was true/false $d=0.87$ and $d=0.80$ when multiple choice questions were used (Rutten, et al., 2012; Gelbart, et al., 2009). In the field of forestry, students used computer simulation to practise managing a forest plot. The study assessed the simulation's influence on solving the task and explaining the solution. The study found that in order to receive better results, it is useful to combine lessons with creating the opportunity for the students to figure things out themselves and to use computer simulations for practice (Riess & Mischo, 2010; Rutten, et al., 2012). Students' interest in the studied material when using computer simulations has also been explored. For this, two simulations were created for the cell's respiratory chain. The first simulation included tasks that needed to be solved and the second had examples which were designed to explain a specific part. The simulations with fully developed examples had a positive effect on the students' interest. However, the students did not show heightened interest in the simulations that used tasks. The students who had little interest in the subject beforehand expanded their factual knowledge despite the simulation type. The general understanding of the subject was created via simulations, which visualized the material (Melek, et al., 2008). A study conducted at a high school physics course involved a group of students learning physics using special simulation software. The control group was taught in the traditional way without using this kind of software. The number of students in both groups was 15 and their age was in the range of 17 to 19. A test at the end of the course showed that the group of students who used simulation software scored 3.07 points more out of the maximum of 20 points on average than the control group (El Hassan, et al., 2014).

The aforementioned studies clearly show that the use of simulations improves students' learning performance. The materials prepared in

relation to the current doctoral thesis have not been used in comparative groups and are based on other studies on the positive influence of simulations on learning and understanding.

The computer simulations presented in this doctoral thesis correspond to the solution of a specific task. For instance, the website Mekanizmalar offers numerous computer simulations (flash animations) for the field of mechanics and technology, which visualize the work of mechanisms, but these are not based on solutions to specific tasks (Mekanizmalar). The learning process shows that the students understand the methodology of creating computer simulations on a Mathcad worksheet. It is important that each student can create these in order to visualize and check the solution to a specific task. The advantages of Mathcad in teaching mechanics have been highlighted by Novohatska, et al., 2014; Broman & Östholm, 1997; Soutas-Little, et al., 2008; Bertjaev, 2005 and Soutas-Little, et al., 2008.

1.3 Overview of the virtual models and their motion simulations in the program Mathcad

In their studies Heinloo & Olt, 2004a; 2004b and 2004c used the scheme in Figure 1.1a to create a virtual model of the disk-ridging tool on a Mathcad worksheet (Figure 1.1b) for studying the work process and simulations. The work process simulation of the virtual model is presented in the video clip Heinloo, 2015.

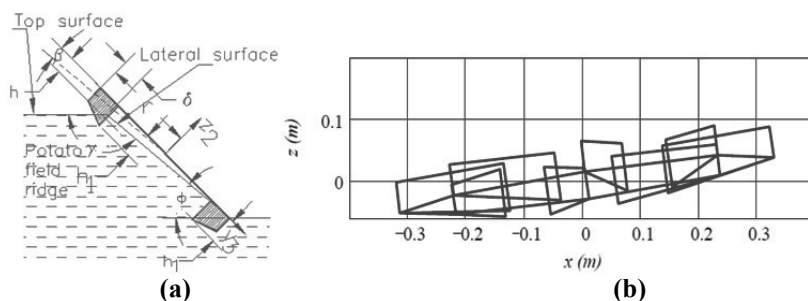


Figure 1.1. Scheme (a) and virtual model (b) of a disk-ridging tool (Heinloo & Olt, 2006).

In their studies Heinloo, et al., 2005; Heinloo & Leola, 2006a; 2006b and 2007 used the scheme in Figure 1.2a to generate a virtual model of a scraper performing press manure removal (Figure 1.2b). They used this virtual model to investigate the work process of the scrap-

er. This virtual model is displayed in action in the video clip Heinloo, 2011a.

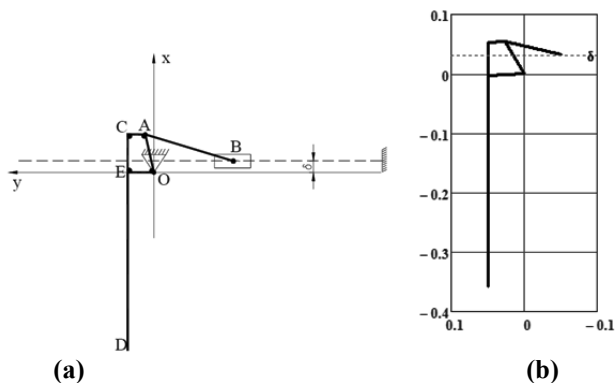


Figure 1.2. Scheme (a) and virtual model (b) of a device for press manure removal (Heinloo, et al., 2005).

In the study Heinloo, 2007a composed a program on a Mathcad worksheet for the automatic generation of a four-bar linkage virtual model (Figure 1.3), which is often used in machine design linkage structures. If the user of this program defines the lengths of the links and the four-bar is kinematically possible, the virtual model is displayed and the motion simulation can be executed. The four-bar virtual model's motion simulation is displayed in the video clip Heinloo, 2011c.

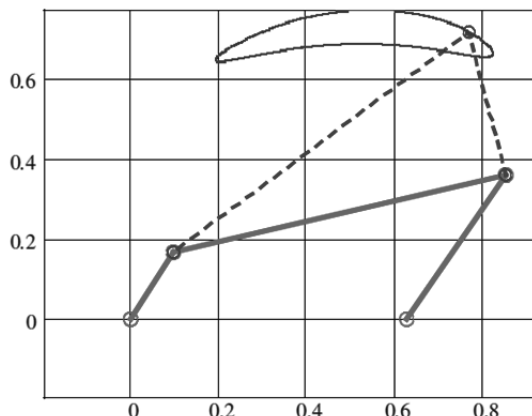


Figure 1.3. Virtual model of the four-bar with the trajectory of a point of the connecting-rod (Heinloo, 2007a).

In the study Heinloo, 2007b a virtual model of a blueberry harvester picking reel was prepared on a Mathcad worksheet (Figure 1.4) owing to derived equations. A video clip of the motion simulation of the picking reel's virtual model upon simulating the harvesting process was prepared (Heinloo, 2014). In the video clip, the four-rake picking reel's straight movement along the virtual field and the reel's rotating movement with the rakes can be observed.

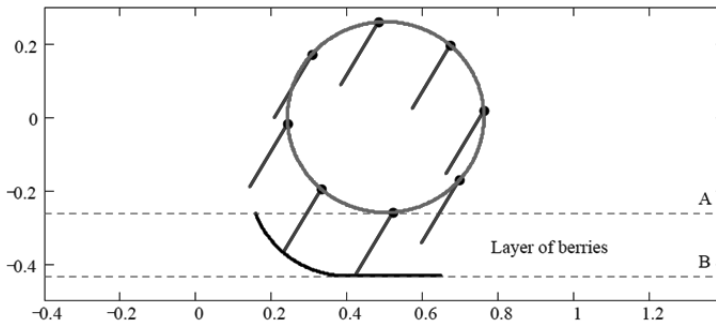


Figure 1.4. Virtual model of a blueberry harvester's picking reel (Heinloo, 2007b).

In the study Olt & Heinloo, 2011a, the authors composed a virtual model of a plough stone protector according to derived equations on a Mathcad worksheet to study the device's motion over stones. In this work, the stone protector linkage's movement over stones was simulated and the linkage pivots' velocities are displayed with vectors (Figure 1.5). In the video clip Heinloo, 2009, a stone protector's virtual model's simulated movement over "stone" is presented.

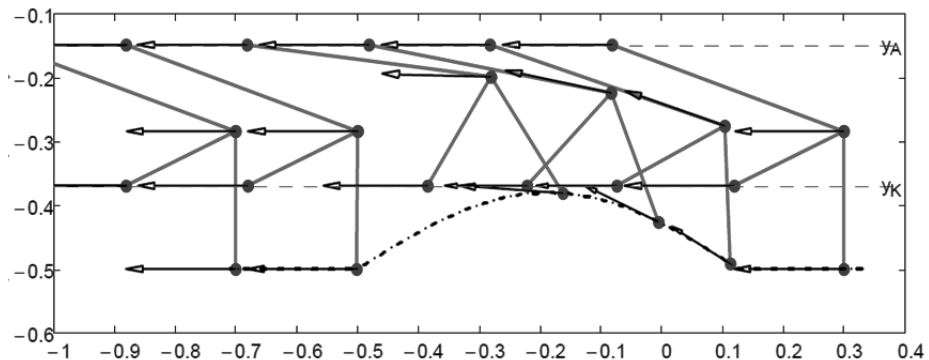


Figure 1.5. Positions of the virtual model of a stone protector in passing a „stone“ (Olt & Heinloo, 2011a).

In the study Heinloo, 2010a, the author researched the motion of virtual fertilizer granules in a virtual fertilizer's spreading disc. The fertilizer granules are in complex motion: they rotate with the spreading disc and move along the disc's vane. In the video clip Heinloo, 2010c, the virtual fertilizer granules' motion in the four-vane virtual spreading disc is presented. Later on, this work was developed further with research on the effect of different vane angles (Olt & Heinloo, 2011a and 2011b).

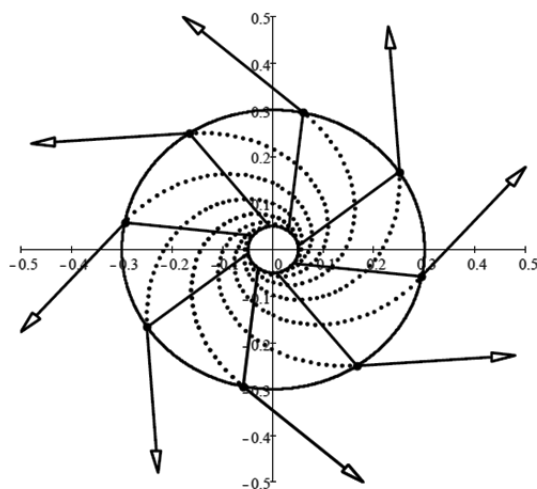


Figure 1.6. Virtual model of the spreading disc together with the trajectories of fertilizer granules and the vectors of their velocities at the contour of the disc (Heinloo, 2010a).

Zhang, et al., 2010 studied linkage that can be used in a feeding mechanism in the Mathcad environment. They composed a mathematical model for the mechanism and a respective mathematical model they used to simulate the movement of the linkage.

Hess, et al., 2014 simulated the movement of a synchronous motor on a Mathcad worksheet. The simulation depends on different input values, which are adjustable: measurements, quantity of the magnetic poles and slots per pole, power and torque, simulation duration and step, etc. Accordingly, input values of the virtual model of the synchronous motor's cross-section are displayed. On the cross-section, a stator corresponding to input measurements, slots, a rotor, arrows to visualize magnetic field, etc. (Figure 1.7) can be observed.

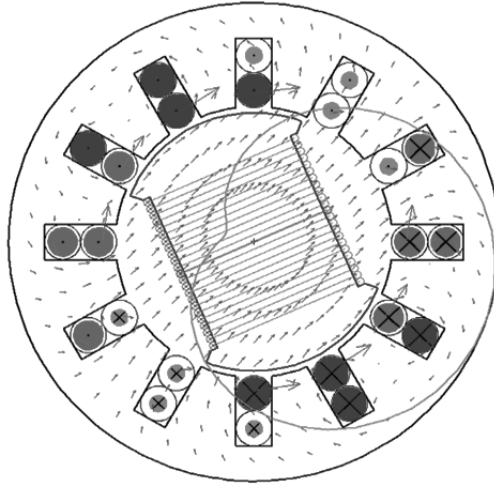


Figure 1.7. Virtual model of the cross-section of a synchronous motor (Hess, et al., 2014).

Different mechanisms have been simulated on a Mathcad worksheet by the author V. Ochkov. He has studied steam engines (Ochkov, 2011a), car windshield wipers (Ochkov, 2011b), the Chebyshev mechanism (Ochkov, 2011c), the Theo Jansen walking mechanism (Ochkov, 2011d), (Ochkov, 2013), etc.

1.4 The purpose and tasks of the doctoral thesis

Purpose

Developing computer-based learning and research methods in mechanics.

In order to fulfil the purpose, tasks were set for each of the three categories of mechanics: analytical mechanics, engineering mechanics and machinery mechanics.

Tasks for developing learning methods:

1. Devising an interactive learning method in analytical mechanics. Demonstrate the compilation and use of interactive study notes for analytical mechanics. Create a system of Hamilton's differential equations, well-known in analytical mechanics, for a physical double pendulum as a more specific example, along with the virtual model of the double pendulum and its motion simulation.
2. In the field of machinery mechanics, the task is to demonstrate how to make computer-based calculations for the kinematics and dynamics of the V-engine, along with creating a virtual model and its motion simulation.
Demonstrate a method for finding an optimal profile for a radial cam in a cam-follower mechanism. Create a simulation of the movement of the optimal cam and its follower.
3. In the field of engineering mechanics, the task is to simulate the change in a mass point's velocity and acceleration vectors, the centre of curvature, circle of trajectory curvature and evolute of the trajectory upon its movement on given trajectories.
4. Demonstrate the use of Mathcad's symbolic calculation function and the Laplace transform for composing and solving motion equations for coupled pendulums along with the motion simulation of a virtual model.

Tasks for developing research methods:

1. Create mathematical and virtual models for single and double connecting-rod slider-crank mechanisms. Simulate their motion and perform a comparative analysis of the forces acting on it during motion. Present the results.

2. Create mathematical and virtual models for Jansen walking mechanism. Simulate the motion of the virtual model. Study the resisting environment's influence on the fluctuation of the step and the possibilities of minimising it using a flywheel. Present the results.
3. Simulate the motion of fertilizer granules on a rotating spreading disc. Study the dependency of the motion on the adjusting angle of the vane, initial position of fertilizer granules and friction coefficient between a fertilizer granule and the spreading disc. Present the results.
4. Simulate the motion of a frozen berry (mass point) on a moving conveyor belt and in free fall after leaving the belt. Study the dependency of the berry's motion on the inclination angle of the belt, velocity of the belt and friction coefficient between the berry and belt. Present the results.

The presented results and methods can be used in designing the aforementioned or other similar mechanisms.

The relevance of the doctoral thesis:

1. Using the possibilities of information technology to expand the teaching methods for mechanics increases the efficiency of teaching and learning and makes the learning process more mobile and interesting for the students.
2. Increasing the number of computer-based research methods for problems related to mechanics provides the engineers and scientists with better tools for research and development.
3. The visualization of the objects of study using virtual models and motion simulation is an easy way to check the accuracy of the solutions and a better way to understand the object than the alternative of conducting research and teaching only with the help of equations and their solutions.

Novelty:

The features of the computer program Mathcad are used in this thesis for solution of the problems in analytical mechanics, engineering mechanics, mechanics of machinery and in agricultural machinery.

Solved new Mathcad based problems in this thesis:

1. Numerical analysis of chaotic motion for double pendulum.
2. E-teaching and e-training methods for analytical mechanics.
3. Visualization of kinematics of a material point.
4. Comparative analysis of motions the new double-connecting-rod and a single-rod linkages.
5. Optimization method of the profile a cam in a cam-follower mechanism.
6. Virtual model for the v-engine, simulation and analysis the motion of this model.
7. Virtual model for the Theo Jansen walking mechanism, simulation its motion and optimization the trajectory of a leg endpoint.
8. Composition and solving the differential equations for spring-coupled pendulum by using symbolic calculus.
9. Simulation the motion of a granule on the rotating spreading disc and the analysis the dependency of this motion from various parameters.
10. Analysis the motion of a berry in the separator of sea-buckthorn berries.

2. Materials and Methods

2.1 Foreword

This chapter explores the mathematical and mechanical equations and principles used in published papers. Some elementary principles like Newton laws, kinetic energy formula, etc. have been left out.

2.2 Overview of some mass point equations in kinematics and dynamics

In studies on material bodies, it is common to leave out minor and arbitrary influencers and to focus only on properties that are relevant. This way, material bodies can be treated as abstractions - the material body is represented by a model. For example, when the dimensions of the body make no difference in view of the motion of the body or the difference is small, dimensions are not important then a body can be described as a mass point. In the mechanical sense, a mass point is one of the most common material body models. A mass point can be used for different applications: planets, berries, bombshells, cars, etc. (Butenin, et al., 1983; Kenk & Kirs, 2013; Lepik & Roots, 1971; Ruina & Pratap, 2014).

2.2.1 On the mass point motion of curved planar trajectories

If the curve is represented with the parametric equations $x = x(t)$, $y = y(t)$ that also refer to the law of motion of a material point, then according to Piskunov, 1981, the radius of curvature $R(t)$, and the x – and y – coordinates $\alpha(t)$ and $\beta(t)$ of the centre of curvature (centre of the circle of a curvature) at the point $(x(t), y(t))$ are

$$R(t) = \frac{v(t)^3}{|a_y(t)v_x(t) - a_x(t)v_y(t)|}, \quad (2.1)$$

$$\alpha(t) = x(t) - \frac{v(t)^2 v_y(t)}{a_y(t)v_x(t) - v_y(t)a_x(t)}, \quad (2.2)$$

$$\beta(t) = y(t) + \frac{v(t)^2 v_x(t)}{a_y(t)v_x(t) - v_y(t)a_x(t)},$$

accordingly, where

$$v_x(t) = \frac{dx(t)}{dt}, v_y(t) = \frac{dy(t)}{dt}, a_x(t) = \frac{d^2x(t)}{dt^2}, a_y(t) = \frac{d^2y(t)}{dt^2}$$

$$v(t) = \sqrt{v_x(t)^2 + v_y(t)^2}, a(t) = \sqrt{a_x(t)^2 + a_y(t)^2}.$$

Paper VI is based on those equations.

2.2.2 Mass point motion on a rotating disc

On Figure 2.1, the scheme of a disc spreading fertilizer has been depicted.

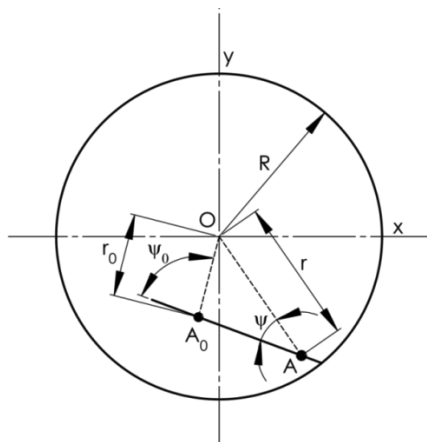


Figure 2.1. The scheme of a spreading disk: R - spreading disc radius, ψ_0 - adjusting angle of the vane, ψ - angle between the polar radii of a fertilizer granule and the direction of the vane, r - distance between the centre of the disc and fertilizer granule in the current position A , r_0 - distance between the centre of the disc and fertilizer granule in the initial position A_0 (Paper VIII).

Differential equation of the compound motion of a mass point (fertilizer granule) on the spreading disk

$$m \frac{d^2}{dt^2} \xi = F_1 + F_2 + F_3 + F_4 \quad (2.3)$$

was composed in the study Reintam, 1995 The formulas for the determination of these forces have been provided below

$$F_1 = -fmg, F_2 = m\omega^2 r \cos \psi, F_3 = -fm\omega^2 r \sin \psi, \quad (2.4)$$

$$F_4 = -2fm\omega \frac{d}{dt} \xi(t).$$

Placing forces from equations (2.4) in the equation (2.3) and dividing them by m results in an ordinary differential equation with the constant coefficients

$$\frac{d^2}{dt^2} \xi(t) + 2f\omega \frac{d}{dt} \xi(t) - \omega^2(r\cos\psi - fr\sin\psi) + fg = 0. \quad (2.5)$$

Paper VIII is based on the solution of the differential equation (2.5).

2.2.3 Mass point motion on a moving inclined plane

The moving inclined plane in Paper XI is a belt conveyor belt's surface, whereupon a sea buckthorn berry is moving owing to gravity, and it is modelled as a mass point (Figure 2.2).

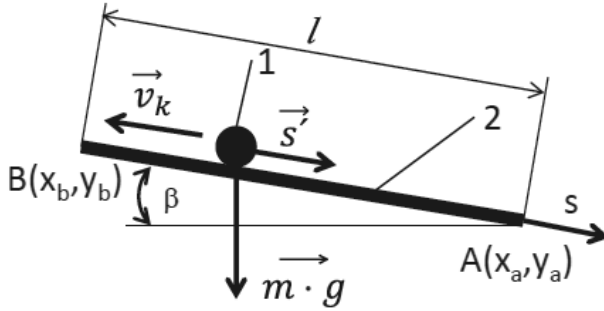


Figure 2.2. Computational scheme of a conveyor belt and berry: 1 - berry, 2 - conveyor belt between points AB , l - width of the belt (distance between points AB), v_k - velocity of the conveyor belt, s - axis starting at point B along the conveyor belt, s' - berry's velocity, β - inclination angle of the conveyor belt, m - berry particle mass, g - acceleration of gravity (Paper XI).

In a resisting environment, a mass point's motion can be described with a nonlinear differential equation

$$m\dot{s} = mg \sin \beta - fmg \cos \beta - \frac{1}{2}\rho \cdot (\dot{s} - v_k)^2 c_d A. \quad (2.6)$$

The motion of a free falling mass point can be described with a nonlinear differential equation

$$m\ddot{y} = -mg + \frac{1}{2}\rho\dot{y}^2 c_d A, \quad (2.7)$$

$$m\ddot{x} = -\frac{1}{2}\rho \dot{x}^2 c_d A, \quad (2.8)$$

where \ddot{x} , \dot{y} , \dot{x} and \dot{y} are mass point (berry) accelerations and velocities during the free fall respectively.

Paper XI is based on the solutions of the differential equations (2.5), (2.7) and (2.8).

2.3 Overview of the Lagrange and Hamilton's equations

Hamilton's canonical equations are (Lepik & Roots, 1971; Goldstein, et al., 2000; Thornton & Marion, 2007):

$$\begin{aligned} \dot{q}_k &= \frac{\partial H}{\partial p_k}, \\ \dot{p}_k &= -\frac{\partial H}{\partial q_k}, \end{aligned} \quad (2.9)$$

where $k = 1; 2; \dots ; s$.

Hamiltonian is defined as follows in equation (2.9):

$$H = \sum_{j=1}^k p_j \cdot \dot{q}_j - L, \quad (2.10)$$

where L is Lagrangian, which is equal to the subtraction ($L = T - \Pi$) of a mechanical system's kinetic and potential energy.

Hamilton's equations (2.9) were used in Paper I.

Second type Lagrange equations are (Lepik & Roots, 1971; Goldstein, et al., 2000; Thornton & Marion, 2007; Butenin, et al., 1986; Targ, 1968):

$$\frac{d}{dt} \left(\frac{\partial T}{\partial \dot{q}_k} \right) - \frac{\partial T}{\partial q_k} = Q_k \quad (2.11)$$

Second type Lagrange equations (2.11) were used in Paper VII.

2.4 Overview of the equations in the mechanics of machinery

All limiting conditions that restrict the motion of the mass point system are called restrictions in mechanics. Mathematically, restrictions

are expressed with the equations of restrictions, where the point coordinates that form a system must be satisfied (Lepik & Roots, 1971).

For example, the equations of restrictions (also circle equations) (Molian, 1982)

$$\begin{aligned} (x_B - x_A(\varphi))^2 + (y_B - y_A(\varphi))^2 &= AB^2, \\ (x_B - OC)^2 + (y_B - y_C)^2 &= BC^2, \end{aligned} \quad (2.12)$$

prescribe that a four-bar's (Figure 2.3) links AB and BC have constant lengths during the entire movement.

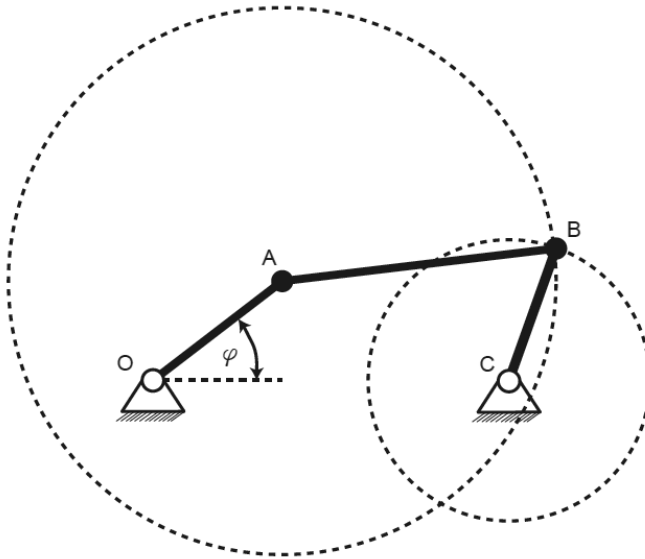


Figure 2.3. Determination of a four-bar's equations of restrictions for point B .

The variable pressure angle is important for machinery. If we look at the linkages, the pressure angle is the angle between the linkage point's velocity and applied force vector (Figure 2.4). The lower the pressure angle, the more work the force is doing and the lower are the reaction forces and friction losses (Kleis, 1988).

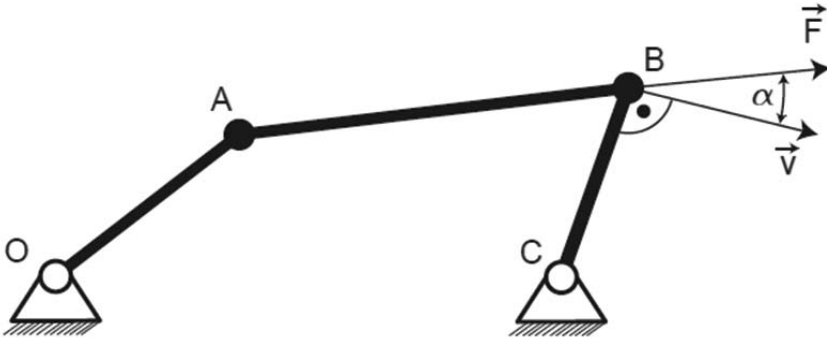


Figure 2.4. Fourbar: F - force, v - velocity, α - pressure angle.

The pressure angle must be taken into account in the synthesis of the cam mechanisms. On the cam mechanism, the pressure angle is the angle between the cam follower's common normal and the follower (Figure 2.5). It must be in the range $-30^\circ \leq \alpha \leq 30^\circ$ (Norton, 2009).

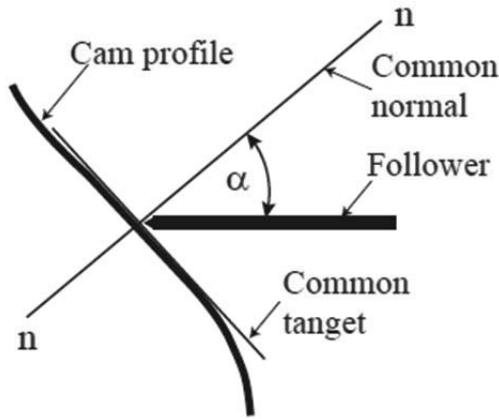


Figure 2.5. The pressure angle α between the cam and follower (Paper IX).

In radial cam mechanisms, it is possible to calculate the pressure angle with the following equation (Norton, 2009; Kleis, 1988):

$$\alpha(R_0, \varepsilon) = \arctan\left(\frac{v - \varepsilon}{s + \sqrt{R_0^2 - \varepsilon^2}}\right). \quad (2.13)$$

It can be derived from the equations (2.13) that the value of the pressure angle depends on two variables R_0 and ε , but their values are unknown. To find the pressure angle, Norton, 2009 suggests considering eccentricity $\varepsilon = 0$ and calculating the desired pressure angle

according to the base circle radius, then optimizing the pressure angle value with the value of eccentricity.

The following equation is used in the mechanics of machinery to reduce the forces acting on the link (Artobolevski, 1961):

$$M_r \omega_1 = \sum_k (F_k v_k \cos \alpha_k) + \sum_u (M_u \omega_u). \quad (2.14)$$

The kinematic chain's reduced moment of inertia on the linkage input link can be determined with the following equation (Artobolevski, 1961):

$$I_r = m_1 \left(\frac{v_1}{\omega_1} \right)^2 + I_1 \left(\frac{\omega_1}{\omega_1} \right)^2 + m_2 \left(\frac{v_2}{\omega_1} \right)^2 + I_2 \left(\frac{\omega_2}{\omega_1} \right)^2 + \dots + m_k \left(\frac{v_k}{\omega_1} \right)^2 + I_k \left(\frac{\omega_k}{\omega_1} \right)^2. \quad (2.15)$$

A linkage input link's angular velocity can be determined with the following equations (Artobolevski, 1961):

$$\omega_1 = \sqrt{\frac{I_{r0} \omega_0^2}{I_r} + \frac{2}{I_r} \Delta T}. \quad (2.16)$$

The precise calculation of angular velocity ω_0 is impossible, therefore, it is recommended to use an approximate formula (Lepikson, 1998)

$$\omega_0 = \frac{n \omega_1}{\sum_{i=0}^n \sqrt{\frac{I_r(0)}{I_{r_i}} + \frac{4 \Delta T_i}{I_{r_i} \omega_1^2}}}. \quad (2.17)$$

In equation (2.16), the change in the linkage's kinetic energy is determined with the following equation

$$\Delta T(\varphi) = M_m \varphi + \int_0^\varphi M_r(\varphi) d\varphi. \quad (2.18)$$

The coefficient of speed fluctuation is important for machines and mechanisms, and it can be determined with the following equation (Shigley, et al., 2004):

$$\delta = \frac{\max(\omega) - \min(\omega)}{0.5(\max(\omega) + \min(\omega))}. \quad (2.19)$$

Equations of the mechanics of machinery were used in Papers IV, V, IX and X.

2.5 IV order Runge-Kutta algorithm for differential equations' numerical solutions.

Mathematical models of mechanical problems must be solved with numerical algorithms in case we are dealing with nonlinear differential equations (Tamme, 1973).

Runge-Kutta algorithms are some of the most common numerical algorithms for solving nonlinear differential equations. Carl Runge came up with the idea for these algorithms and it was improved by Wilhelm Kutta (Tamme, 1973).

The IV order Runge-Kutta algorithm is used the most because it is sufficiently precise (Tamme, 1973; Levin & Ulm, 1966). When people talk about the Runge-Kutta algorithm, they mostly mean the fourth order method without mentioning the number (Tamme, 1973).

When we use Runge-Kutta algorithms to solve differential equations, the values of function $y = f(x)$ will be calculated from the argument sequence $x_0 < x_1 < x_2 \dots y_i = f(x_i)$ and $x_1 - x_0 = h$. When it is known in case of the algorithm how to find a starting point (x_0, y_0) and the next point (x_1, y_1) on the line, we can find y_i with all the values of i by repeating the algorithm.

IV order Runge-Kutta algorithm is defined with the next equations:

$$\begin{aligned}k_1 &= hf(x_0, y_0), \\k_2 &= hf\left(x_0 + \frac{h}{2}, y_0 + \frac{k_1}{2}\right), \\k_3 &= hf\left(x_0 + \frac{h}{2}, y_0 + \frac{k_2}{2}\right), \\k_4 &= hf(x_0 + h, y_0 + k_3), \\k &= \frac{1}{6}(k_1 + 2k_2 + 2k_3 + k_4), \\y_1 &= y_0 + k.\end{aligned}\tag{2.20}$$

The Runge-Kutta algorithm was used in Papers I and XI.

3. Using the program Mathcad

3.1 Mathcad worksheet

The computer program Mathcad enables to write equations in the form we are accustomed to reading from books and writing on paper, differently from other mathematical programs (Matlab, Maple, Mathematica), where equations must be programmed. Additionally, there are built-in algorithms in Mathcad, for example, the IV order Runge-Kutta algorithm (2.20). Communication with built-in algorithms is achieved with special functions. These functions' variables are easily changed and the changed parameters can be immediately observed from the results and virtual models.

A typical Mathcad worksheet is shown in Figure 3.1. In the top part of Figure 3.1, we can see the heading, then the angle φ 's range of change, sine and cosine functions are defined, and, finally, there is a graph of the functions. Changing the angle φ or functions $f_1(\varphi)$ and $f_2(\varphi)$ will automatically change the graphs on the worksheet.

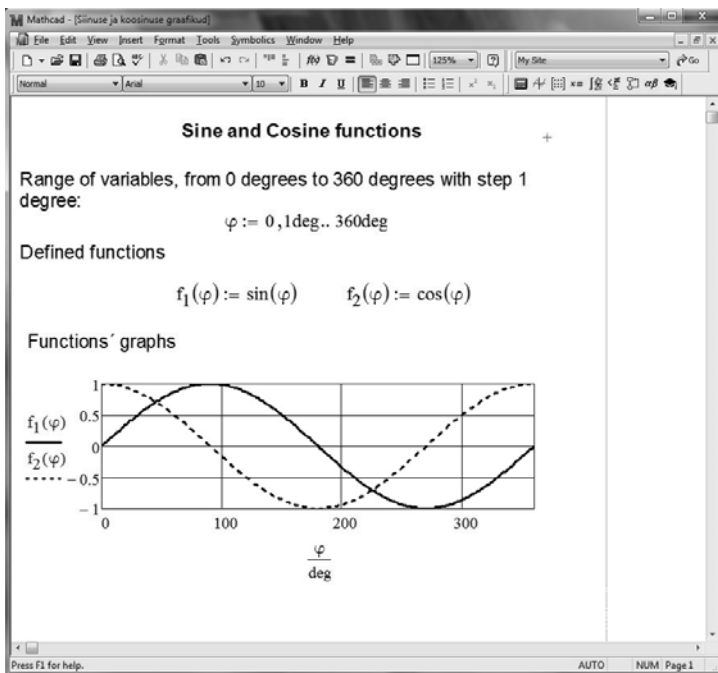


Figure 3.1. Example of a Mathcad worksheet.

It can be observed from Figure 3.1 that the style of writing equations on a Mathcad worksheet is the same as in mathematic books. While using this worksheet for extra learning material, it is possible to show, or the students can try how the equations “work”, which is difficult with static books. Based on (Leppik, 2001; Leppik, 2008), these kinds of interactive worksheets will help artist-type students (ca 40% humans) understand mathematics, mechanics, physics and other sciences in a better manner.

All the problems featured in this thesis were solved using Mathcad worksheets.

3.2 Implementation of the Runge-Kutta method using a Mathcad worksheet

IV order Runge-Kutta algorithm (2.20) is a built-in function in Mathcad and it can be used with the function

$$rkfixed(a, t_0, t_N, N, D). \quad (3.1)$$

Differential equation system

$$y'(t) = D(t, y), \quad (3.2)$$

where y is a one column matrix (vector) that is composed of the required functions

$$y = \begin{pmatrix} y_1(t) \\ y_2(t) \\ \dots \\ y_n(t) \end{pmatrix}. \quad (3.3)$$

In the function (3.1), $D(t, y)$ is a vector that is composed of the right-side equations in a differential equation system (3.2)

$$D(t, y) = \begin{pmatrix} f_1(t, y) \\ f_2(t, y) \\ \dots \\ f_n(t, y) \end{pmatrix} \quad (3.4)$$

and

$$y'(t) = \begin{pmatrix} y'_1(t) \\ y'_2(t) \\ \dots \\ y'_n(t) \end{pmatrix} \quad (3.5)$$

is a vector derived from the desired values.

In the function (3.1), a is a vector which is composed of the right sides of a given differential equation system's initial conditions $y'_1(t_0) = y_{10}, y'_2(t_0) = y_{20}, \dots, y'_n(t_0) = y_{n0}$

$$a = \begin{pmatrix} y_{10} \\ y_{20} \\ \dots \\ y_{n0} \end{pmatrix}. \quad (3.6)$$

The next members in the function (3.1) are t_0 and t_N , which are argument t 's first and last values respectively. The member N is a number of integration interval, between the values t_0 and t_N . D is a notation of vector $D(t, y)$

For example, in the case of a double pendulum (Figure 3.2), the first two elements in the vector a of a Hamilton's equations' (2.9) initial conditions (3.7) are the pendulums' angles $(\theta_{10}, \theta_{20})$ at the beginning of the oscillation, and two next elements are the pendulums' initial impulses $(p_{\theta_{10}}, p_{\theta_{20}})$ (Paper I):

$$a = \begin{pmatrix} \theta_{10} \\ \theta_{20} \\ p_{\theta_{10}} \\ p_{\theta_{20}} \end{pmatrix}. \quad (3.7)$$

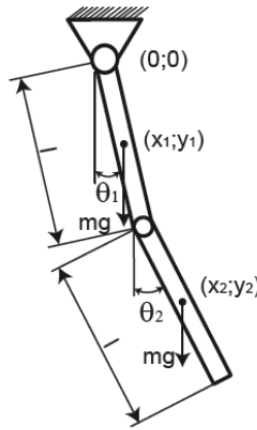


Figure 3.2. A physical double pendulum: m - mass of the pendulum, l - length of the pendulum, θ_1, θ_2 - inclination angles of the pendulum (Paper I).

In the case of a double pendulum in the function (3.1), the value t_0 is the first time value and t_N is the last time value. The greater the value of the integration interval N , the smaller the $\frac{t_N - t_0}{N}$ calculation

step. In the case of a double pendulum's Hamilton's equation, vector D is

$$D(t, y) = \begin{pmatrix} f_1(m, l, y) \\ f_2(m, l, y) \\ f_3(m, l, g, y) \\ f_4(m, l, g, y) \end{pmatrix} \quad (3.8)$$

where

$$f_1(m, l, y) = \frac{6}{ml^2} \frac{2y_2 - 3y_3 \cos(y_0 - y_1)}{16 - 9 \cos^2(y_0 - y_1)},$$

$$f_2(m, l, y) = \frac{6}{ml^2} \frac{8y_3 - 3y_2 \cos(y_0 - y_1)}{16 - 9 \cos^2(y_0 - y_1)},$$

$$f_3(m, l, g, y) = -\frac{ml^2}{2} \left(A(y) + \frac{3g}{l} \sin(y_0) \right),$$

$$f_4(m, l, g, y) = \frac{ml^2}{2} \left(A(y) - \frac{g}{l} \sin(y_1) \right),$$

where

$$A(y) = \frac{36}{m^2 l^4} \frac{[2y_2 - 3y_3 \cos(y_0 - y_1)][8y_3 - 3y_2 \cos(y_0 - y_1)]}{16 - 9 \cos^2(y_0 - y_1)^4} \sin(y_0 - y_1).$$

In case of a Hamilton's equation, the results of the function (3.1) are in a matrix, which can have the notation Z . In this case, a result can be calculated like it is shown in Figure 3.3.

	0	1.571	0	0	0
	0.1	1.567	$1.015 \cdot 10^{-5}$	$-1.103 \cdot 10^3$	$-4.123 \cdot 10^{-3}$
	0.2	1.556	$1.624 \cdot 10^{-4}$	$-2.206 \cdot 10^3$	-0.131
	0.3	1.538	$8.221 \cdot 10^{-4}$	$-3.309 \cdot 10^3$	-0.998
	0.4	1.512	$2.599 \cdot 10^{-3}$	$-4.408 \cdot 10^3$	-4.204
	0.5	1.479	$6.351 \cdot 10^{-3}$	$-5.501 \cdot 10^3$	-12.833
	0.6	1.438	0.013	$-6.582 \cdot 10^3$	-31.935
	0.7	1.39	0.024	$-7.641 \cdot 10^3$...

Figure 3.3. Result matrix: first column - time, second to fourth columns - desired variables.

There are time t values with the step $\frac{t_N - t_0}{N}$ in the first column of the matrix Z . The first pendulum's inclination angle values are in the second column and the second pendulum's inclination angle values are in the third column. The first pendulum's impulse values are in the fourth column and the second pendulum's impulse values are in the fifth column.

Function (3.1) was used in Papers I and XI.

3.3 Motion simulation on a Mathcad worksheet

To simulate the motion of the virtual models with the computer program Mathcad 15's worksheet, the dialogue window "Record Animation" (Figure 3.4) must be used. The dialogue window can be opened from the drop-down menu "Tools" by selecting "Animation" and "Record". The animation variable FRAME initial value "From" and final value "To" must be defined in the "Record Animation" window. The value Frames/Sec will define the speed with which the video frames will change. Holding down the left button of the mouse and moving the mouse arrow over the worksheet, a frame which can be used to select objects for simulation will appear. After selecting the object and clicking on the button "Animate", the variable FRAME will start to display values. When the starting value is "From=0", value steps will be 0, 1, 2, 3, etc. until the value of "To" is reached. When the FRAME value reaches the "To" value, the simulation ends and a new dialogue window pops up, where we can see the simulation's video clip and also save it by clicking on the button "Save as" and selecting "video file". To create simulations on a Mathcad worksheet, one must be find the parameter, the values of which define the simulated object's positions, and express this parameter with the variable FRAME (Heinloo, 2010b).

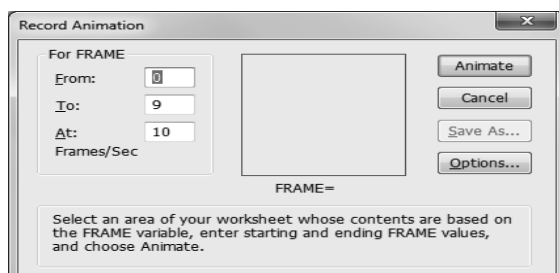


Figure 3.4. Dialogue window to start animation on a Mathcad worksheet.

Examine the mechanism (Figure 3.5) of motion simulation.

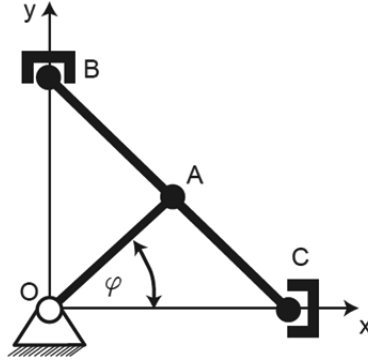


Figure 3.5. Kinematic scheme of an ellipse mechanism.

Let us agree that the length of the link OA is $l = 0.3 \text{ m}$. It is rotating around the joint O counter-clockwise and it is connected from the centre of the link BC to joint A . The length of link BC is $d = 2l$. Joints B and C (sliders) can move vertically on the y -axis and horizontally on the x -axis (Heinloo, 2010b).

Joint A coordinates are

$$x_A(\varphi) = l\cos(\varphi), y_A(\varphi) = l\sin(\varphi), \quad (3.9)$$

slider B coordinates are

$$x_B = 0, y_B(\varphi) = 2y_A(\varphi), \quad (3.10)$$

slider C coordinates are

$$x_C(\varphi) = 2x_A(\varphi), y_C = 0. \quad (3.11)$$

To visualize this mechanism on a Mathcad worksheet figure, let us define the vectors

$$OA_x(\varphi) = \begin{pmatrix} 0 \\ x_A(\varphi) \end{pmatrix}, \quad OA_y(\varphi) = \begin{pmatrix} 0 \\ y_A(\varphi) \end{pmatrix}, \quad (3.12)$$

$$BC_x(\varphi) = \begin{pmatrix} x_B \\ x_C(\varphi) \end{pmatrix}, \quad BC_y(\varphi) = \begin{pmatrix} y_B(\varphi) \\ y_C \end{pmatrix}.$$

The vectors in the Figure 3.6 are a visualized virtual model of the mechanism, when the angle $\varphi = 1 \text{ rad}$.

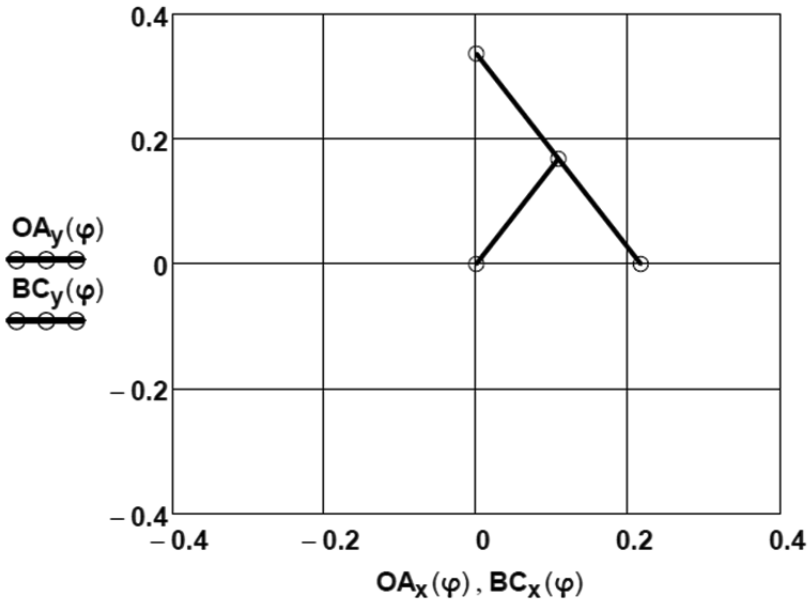


Figure 3.6. Virtual model of an ellipse mechanism.

To simulate the motion of the virtual model (Figure 3.6), the value of angle φ must be defined with the variable FRAME. In this case: $\varphi = 0.02\pi \text{FRAME}$. When the variable FRAME has automatic values $0, 1, 2, 3, \dots, 100$, the values of angle φ are $0, 0.02\pi, 0.04\pi, \dots, 2\pi$ and the motion of the virtual model will be simulated. This virtual model simulation can be seen in the video clip Aan, 2014a.

3.4 On the visualization of geometric vectors on a Mathcad worksheet

In dealing with mechanical problems, it is often necessary to use vectors to show velocity applied to a point, acceleration or a force's direction and value. Vectors in motion can be visualized on a Mathcad worksheet through a special program, which defines functions (3.13) (Bertjaev, 2005). The arguments of this function are time t , γ for the notation of the direction angle function $\gamma(t)$, b for the notation of the vector module function $b(t)$ and n - the coefficient of dimensions, which enables to make the vectors' measures suitable for the figures. Before using the function (3.13) the laws governing the vector's initial point's change and the vector's module must be defined: $x = x(t)$, $y = y(t)$.

$$\begin{aligned}
F(t, \gamma, b, n) = & \\
& \left. \begin{aligned}
& x \leftarrow x(t) \\
& y \leftarrow y(t) \\
& V_o \leftarrow \begin{pmatrix} x & x & x & x & x & x \\ y & y & y & y & y & y \end{pmatrix}^T \\
& I \leftarrow \begin{pmatrix} 0.00 & 0.85 & 0.85 & 1.00 & 0.85 & 0.85 \\ 0.00 & 0.00 & 0.03 & 0.00 & -0.03 & 0.00 \end{pmatrix}^T, \\
& \Omega \leftarrow \begin{pmatrix} \cos(\gamma(t)) & \sin(\gamma(t)) \\ -\sin(\gamma(t)) & \cos(\gamma(t)) \end{pmatrix} \\
& V_o + nb(t)I\Omega
\end{aligned} \right\} \quad (3.13)
\end{aligned}$$

where $x = x(t)$ and $y = y(t)$ are the co-ordinates of origin, $\gamma = \gamma(t)$ is the direction angle.

The function for the visualization of the vectors was used in Papers I, V, VI, VIII, X. Vectors which are visualized with the function $F(t, \gamma, b, n)$ can be seen in Figure 4.5, Figure 4.7 and Figure 4.9.

4. Overview of the research papers written by the author of the thesis

4.1 On the creative teaching of engineering mechanics

This subject is featured in the author's published Papers II and III.

In Paper III the idea of how to teach engineering and machine mechanics interactively is explored. It is presented in video clips of the motion simulations of a four-bar, material point and double pendulum, which can be used to visualize the teaching process.

Paper II discusses the interactive teaching of analytical mechanics, which the current doctoral thesis defines as a teaching method, which allows both the teacher and student to be actively involved in calculations made in the course of the subject that is being taught and to observe the influence of the changes on the computer screen. The paper provides an overview of the compiled collection of interactive revision notes on analytical mechanics, the different parts of which are connected to links that allow quick movement between different parts of the revision notes. The examples include links to Mathcad worksheets, which can be used interactively for visualizing and revising the theoretical part of the study notes. Even though the article concentrates on analytical mechanics, the discussed methodology can be also used for teaching other subjects.

An interactive learning and teaching method is an active alternative for lecture-type learning, in which the students absorb information passively via one-way communication with a teacher or from a book (Manapa, et al., 2012; Preszler, et al., 2007).

In an interactive environment, the students are not simply trying to remember information, but their relationship with the materials is more cognitive. The more interesting the material, the more the student learns. Interactive materials allow the student to use them at home in order to study in their own way and choose their own pace. This saves teachers' time, as school and university teachers are often overburdened and cannot offer individual guidance (Smith).

Interactive learning can be divided into three styles which are based on the way of engaging the student in the learning process. The first style is based on learner-content interaction, in which the student works with the material individually. The second style involves learner-instruction interaction, in which case the student learns with the help of an instructor. The third style is based on learner-learner interaction, in which case the course content is studied with a fellow student. The interactive revision notes discussed in Paper II are designed for the learner-instructor learning style, the theoretical part of the notes is to be introduced by the teacher and the student will then acquire extra knowledge by solving interactive examples on a Mathcad worksheet.

Papers II and III can be used to plan teaching.

4.2 On research regarding linkages

4.2.1 Study of the V-engine

Paper IV is an interactive V-engine (Figure 4.1) research guide on a Mathcad worksheet for the students of the Tallinn University of Technology (Lepikson, 1998).

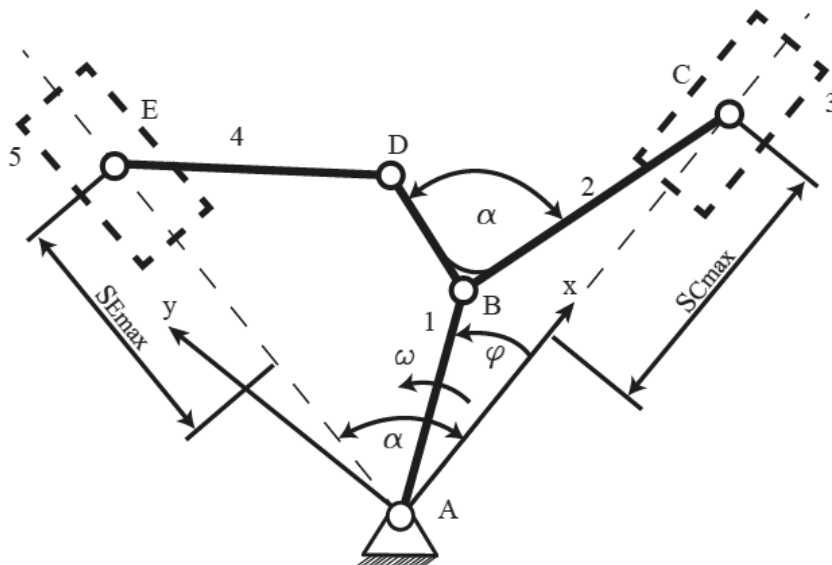


Figure 4.1. Kinematic scheme of a V-engine (Paper IV).

To study kinematics, the following form of the equations of restrictions was used:

$$\begin{aligned}
 (x_D - x_B)(x_C - x_B) - (y_D - x_B)y_B &= l_{BC}l_{BD} \cos \alpha, \\
 (x_D - x_B)^2 + (y_D - x_B)^2 &= l_{BD}^2, \\
 y_E &= x_E \tan \alpha, \\
 (x_E - x_D)^2 + (y_E - y_D)^2 &= l_{DE}^2
 \end{aligned}
 \tag{4.1}$$

and employed to find the displacements of the pistons 3 and 5 (Figure 4.1). To find the velocities and accelerations of the pistons, equations (4.1) were differentiated in view of time. In the equation system (4.1), the first equation angle α between links BC and BD must have a constant value during the entire movement of the V-engine. In the third equation, the pivot E must move along the line AE . In the second and fourth equations, the lengths of the links BD and DE must have constant values during the entire movement of the V-engine.

In Paper IV, a different method compared to Lepikson, 1998 was used to find from $p - V$ indicator diagram the burning gas pressure exerted on the pistons. The $a - p - V$ indicator diagram was converted to a $p - S$ indicator diagram (Figure 4.2). The $p - S$ indicator diagram shows pressure inside the engine cylinder according to the displacement of the piston in Cartesian coordinates.

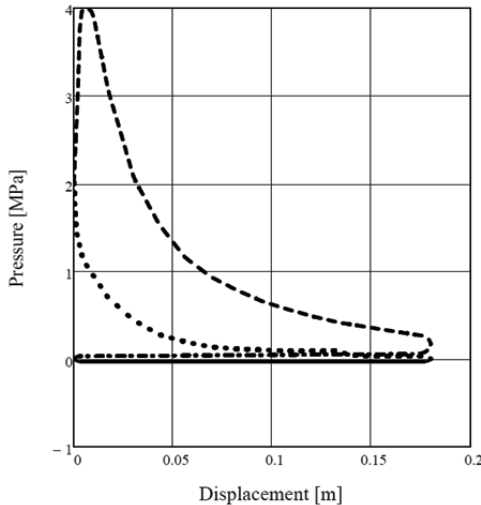


Figure 4.2. P-S indicator diagram: p - pressure, S - piston displacement (Paper IV).

In Figure 4.2, the continuous line indicates gas pressure change in the cylinder during intake stroke and while the piston is moving from the top dead centre to the bottom dead centre. The dotted line indicates gas pressure changes during compression stroke. The dash line indicates gas pressure changes during power stroke and the dash dot line during exhaust stroke.

Accordingly, the $p - S$ indicator diagram's (Figure 4.2) pressure values of the forces on the pistons were determined

$$F = p \frac{\pi \cdot d^2}{4}. \quad (4.2)$$

All the reaction forces were found in consideration of the calculated accelerations, links' mass and forces exerted on the pistons.

In the video clip Heinloo, 2012a, the motion simulation of the V-engine is displayed. The method demonstrated in Paper IV can be used in the teaching process and for engineering research.

4.2.2 Study of the double connecting-rod linkage

In Paper V, a double connecting-rod linkage (Evert) and the single connecting-rod linkage (Figure 4.3) very common in internal combustion engines were compared.

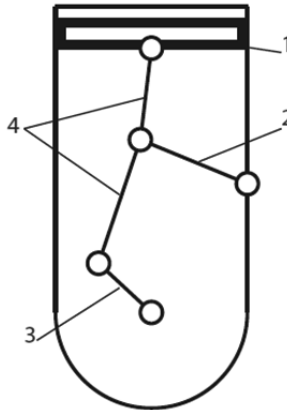


Figure 4.3. The scheme of a double-connecting-rod linkage: 1 - piston, 2 - swivel arm, 3 - crankshaft, 4 - two-part connecting rod.

Equations of restrictions were prepared and used to study the linkages' positions, displacements, velocities and accelerations. The calculated values were compared in figures. Pressure angle and reaction

forces between pistons and cylinder walls were compared separately. It was found that double connecting-rod linkage pressure angles and reaction forces are lower on average.

The comparison of the linkages' displacement was visualised in a video clip Aan & Heinloo, 2012a. In the video clip, one can observe the comparison of the displacement according to the crank rotation angle φ' and its current value (dots) when the rotation angle is φ (upper part on the Figure 4.4). The lower part of the figure features the simulation of the linkages' movement.

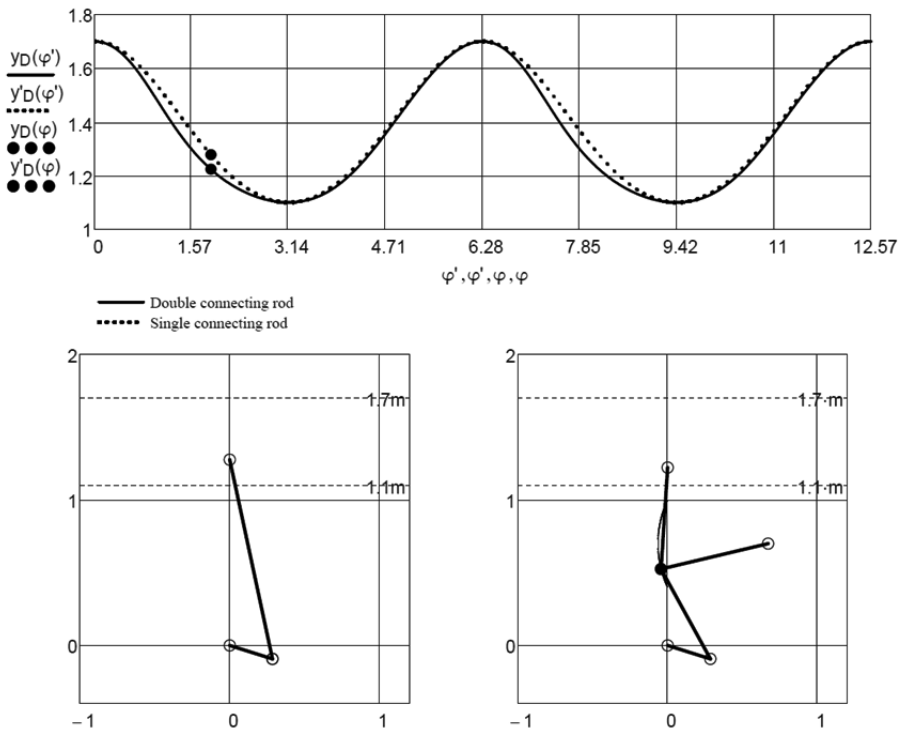


Figure 4.4. Frame from video clip (Aan & Heinloo, 2012a).

A video clip Aan & Heinloo, 2012b, where forces applied to the pistons according to the rotation angle φ and their current value (dots) when the rotation angle is φ' (Figure 4.5) are displayed in the upper part of the figure. In the lower part of the figure, a simulation of the linkages' movement with velocities and accelerations vectors can be observed.

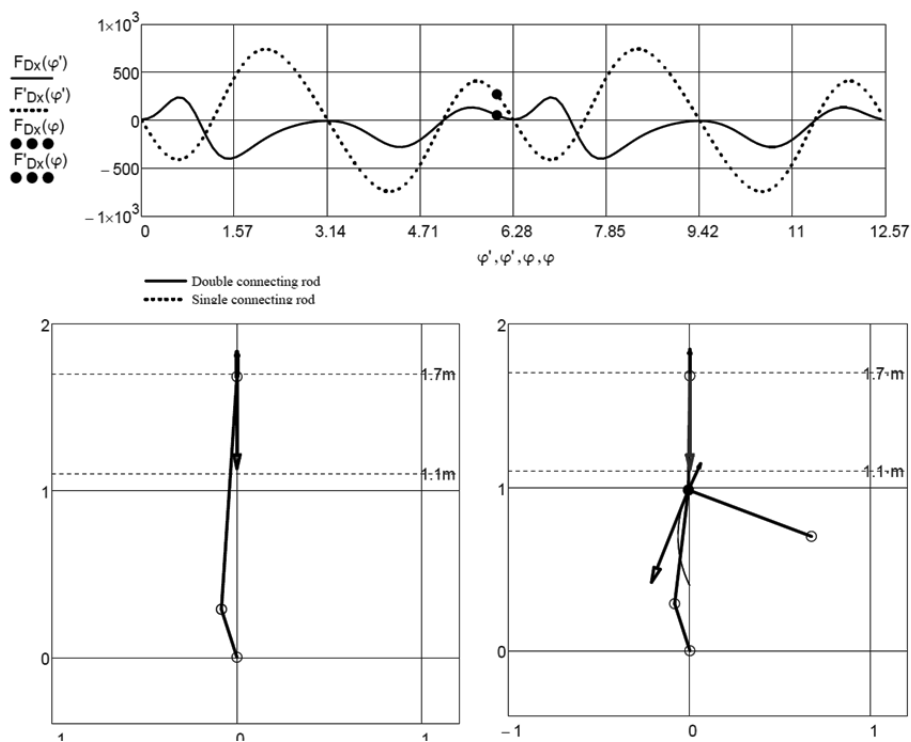


Figure 4.5. Frame from the video clip (Aan & Heinloo, 2012b).

The method presented in paper V can be used in the teaching process and for engineering.

4.2.3 Study of the Theo Jansen walking mechanism

In Paper X, a 12-bar walking mechanism (Figure 4.6) that Theo Jansen used to create wind-powered walking machines was studied (Jansen, 2007).

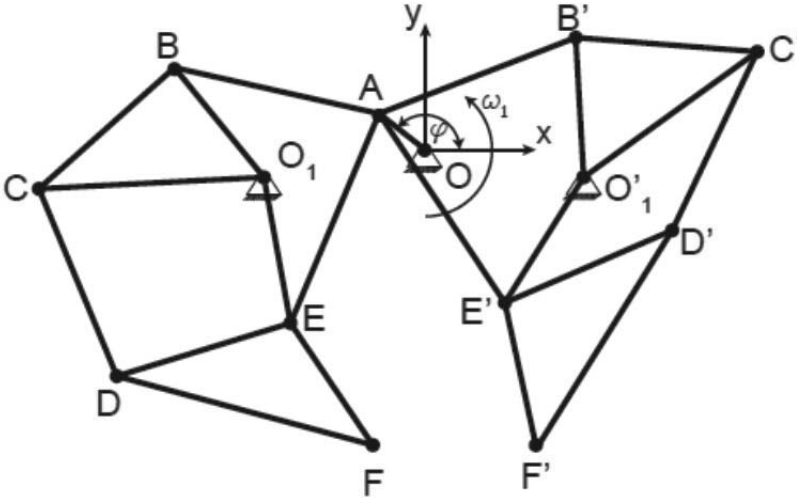


Figure 4.6. A kinematic scheme of the walking linkage (Paper X).

All the pivot coordinates were determined and pivot F and F' trajectories calculated with the equations of restrictions according to the input link (link OA) rotation angle φ . After the differentiation of the equations of restrictions, the velocities and accelerations were determined. After analysing the pivot F and F' 's trajectories, the input link angle range was determined for when the pivot F and F' are connected to the ground and when are they moving. Resisting forces were applied on the pivot F and F' to simulate their movement in a resisting environment. To reduce the input link's fluctuation coefficient, a flywheel was synthesised on the input link OA (equations (2.14)–(2.19)). A motion simulation of the Jansen mechanism's virtual model with velocities and accelerations vectors is presented in the video clip Aan, 2014b. A frame of the video clip is shown in Figure 4.7.

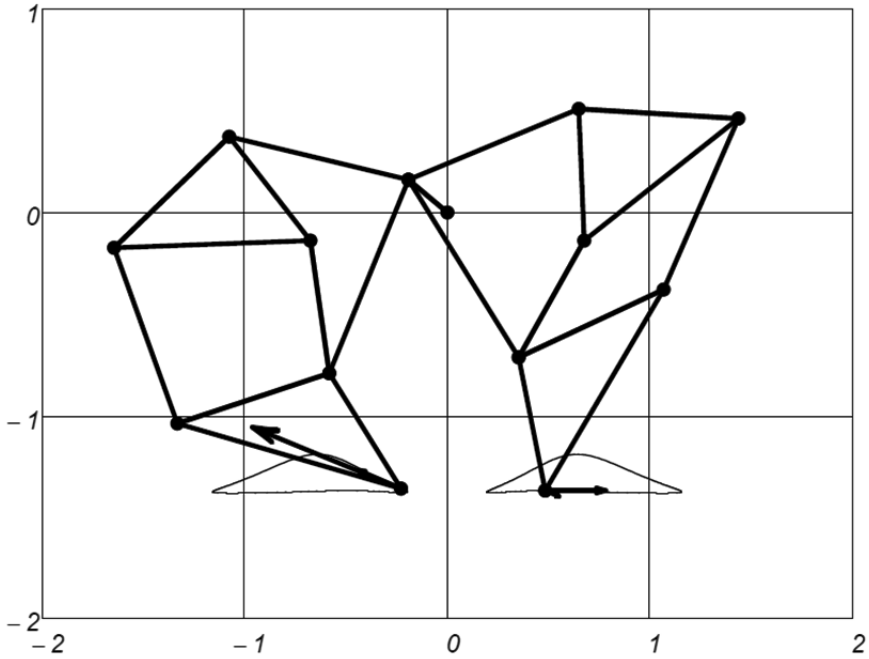


Figure 4.7. A frame from the video clip (Aan, 2014b).

The method presented in paper X can be used in the teaching process and for designing walking machines.

4.3 On research on mass point motion

4.3.1 Mass point motion on curved trajectories

In Paper VI the authors studied mass point motion on curved trajectories, which are mathematically based on equations (2.1) and (2.2). In the video clips Heinloo, 2011b and Heinloo, 2012b, simulations of the mass point on elliptical and sinusoidal trajectories with the circle of trajectory curvature, formation of the evolute of the trajectory, velocity and accelerations vectors are displayed. All the mentioned trajectories and vectors shown in Figure 4.8 apply in case of a sinusoid mass point trajectory.

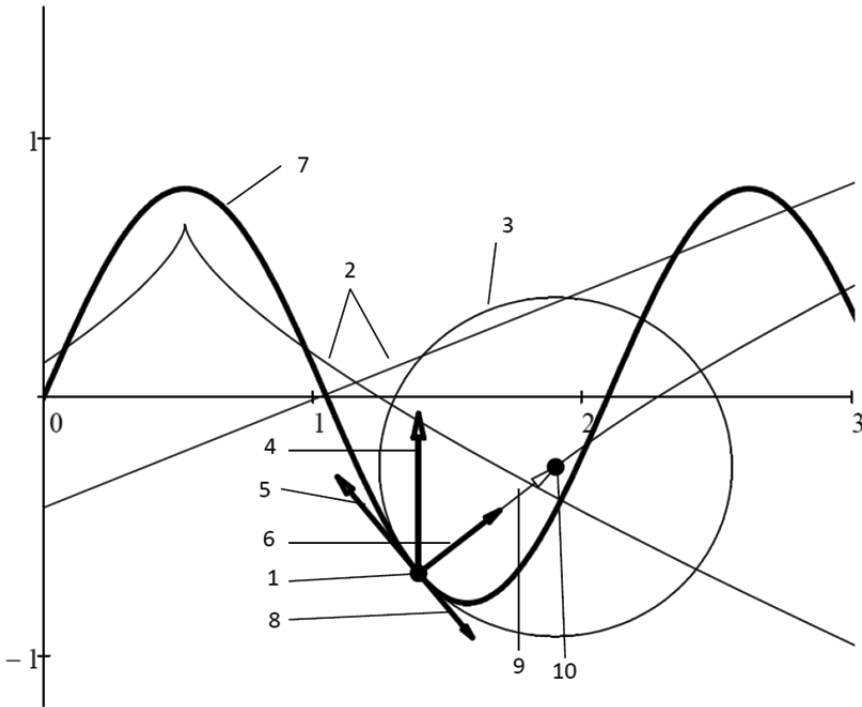


Figure 4.8. Point motion on sinusoidal trajectory: 1 - point M , 2 - evolute of the trajectory of the point M , 3 - circle of trajectory curvature at point M , 4 - full acceleration at point M , 5 - tangential acceleration of point M , 6 - normal acceleration at point M , 7 - trajectory of the point, 8 - velocity of point M , 9 - vector connecting point M and the centre of curvature, 10 - centre of trajectory curvature at point M .

A frame from the video clip Heinloo, 2011b is displayed in Figure 4.9.

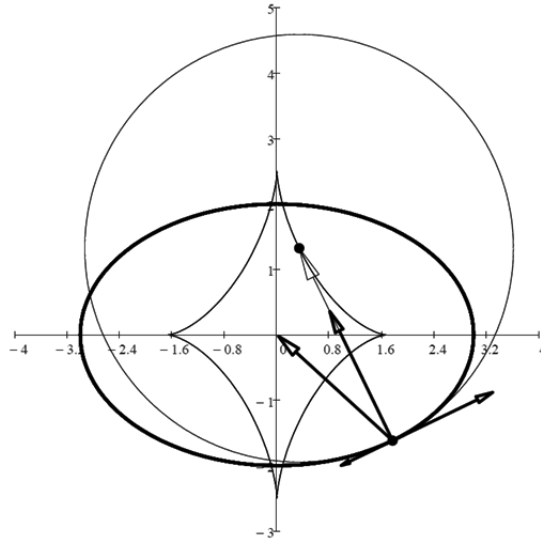


Figure 4.9. Frame from the video clip (Heinloo, 2011b).

Methods, results and video clips presented in Paper VI can be used to teach kinematics. Additionally, users who learn this method can create mass point motion simulations with different trajectories on a Mathcad worksheet.

4.3.2 Study of a granule's motion on a fertilizer spreading disc

In Paper VIII the mass point was modelled as a fertilizer granule on a spreading disc (Figure 2.1). The differential equation (2.5) was solved for fertilizer motion modelling.

In Paper VIII, fertilizer granule outlet time and velocity equations were calculated. The granule trajectories were compared with different spreading disc vane angles. Additionally, it was studied how outlet time and velocity are influenced by the coefficient of friction, vane angle and the initial position of the granule. Fertilizer granule motion simulations on a disc with four vanes are displayed in the video clips Heinloo, 2013a and Heinloo, 2013b. A frame from the video clip showing the moment in time before the granule leaves the rotating spreading disc can be observed in Figure 4.10. Fertilizer granules (dots), granules' trajectories and their velocities' vectors are shown in Figure 4.10.

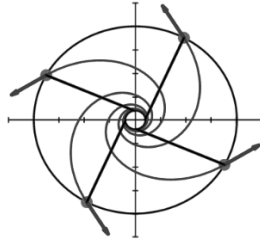


Figure 4.10. A frame from the video clip (Heinloo, 2013a).

The results and methods of Paper VIII can be used in teaching the processes involved in the work and design of a spreading disc.

4.3.3 A sea buckthorn berry's motion on a conveyor belt

In Paper XI, a sea buckthorn berry serves as a mass point, the movement of which is studied on a berry separator conveyor belt (Figure 4.11a) and during free fall after leaving the belt.

Paper XI is based on Patent I that describes the mechanical separation of frozen sea buckthorn berries from branches, leaves and other twigs. The separation is performed in two stages, firstly with a sieve and secondly with a conveyor belt. The separator belt has an inclination angle to assure that the berries will roll and be guided into a gathering box. The twigs that the sieve does not separate and that cannot roll (branches, leaves) will be transported away by the belt (Figure 4.11b).

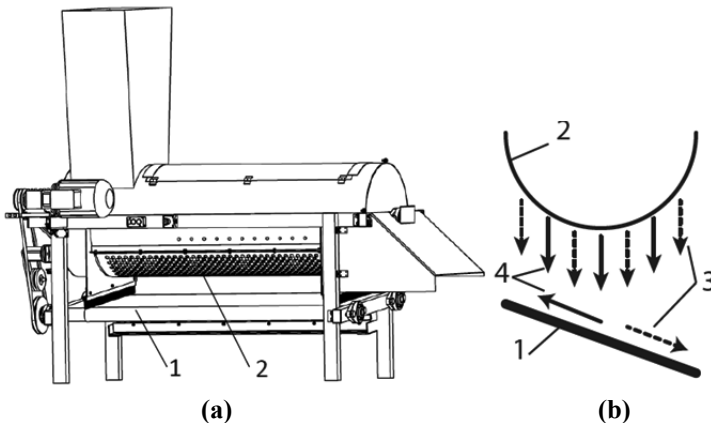
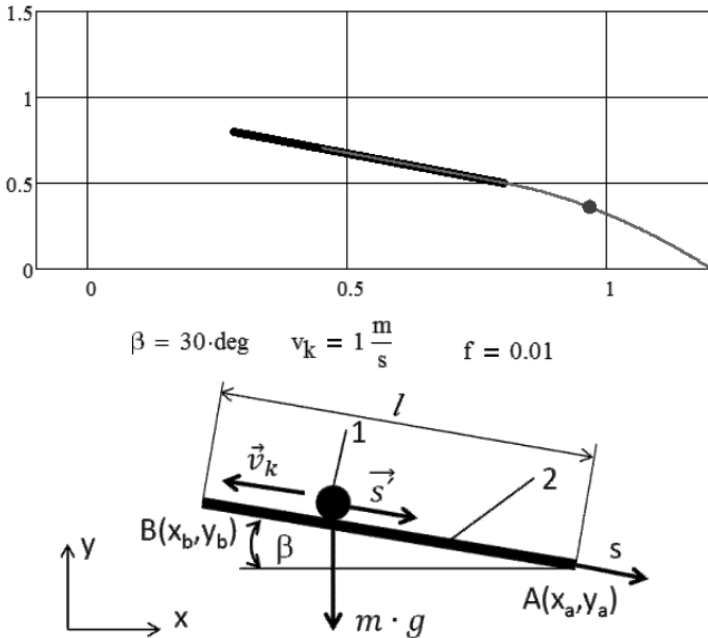


Figure 4.11. A device for the separation of deep-frozen sea buckthorn berries from twigs (a) and (b) a principal scheme of the sea buckthorn berries' separator sieve and conveyor belt, where: 1 - inclined conveyor belt, 2 - sieve, 3 - sea buckthorn berries, 4 - leaves and small branches (Paper XI).

Non-linear differential equations (2.6), (2.7) and (2.8) were solved on a Mathcad worksheet with the IV order Runge-Kutta algorithm (sections 2.5 and 3.2). It was studied berry displacement, velocity and total motion time in view of different belt inclination angles, velocities and coefficients of friction. The motion of the berry on the conveyor belt and in the air after leaving the belt was simulated in a video clip Aan, 2014c. A frame of the video clip is shown in Figure 4.12.



The scheme of the belt conveyor: 1 – berry particle, 2 – conveyor’s belt between points AB, l – width of the belt (distance between points AB), v_k – velocity of the conveyor’s belt, s – axis along the conveyor’s belt, s' – berry’s particle velocity, β – inclination angle of the conveyor’s belt, m – berry’s particle mass, g – gravitational acceleration

Figure 4.12. A frame from the video clip (Aan, 2014c).

The results presented in Paper XI can be used for teaching and in designing conveyors.

4.4 Synthesis of a cam-follower mechanism

The optimal profile synthesis of a cam-follower mechanism (Figure 4.13) in a radial cam was studied in Paper IX. Restrictions are ap-

plied on the follower's maximum displacement and pressure angles in view of the synthesis.

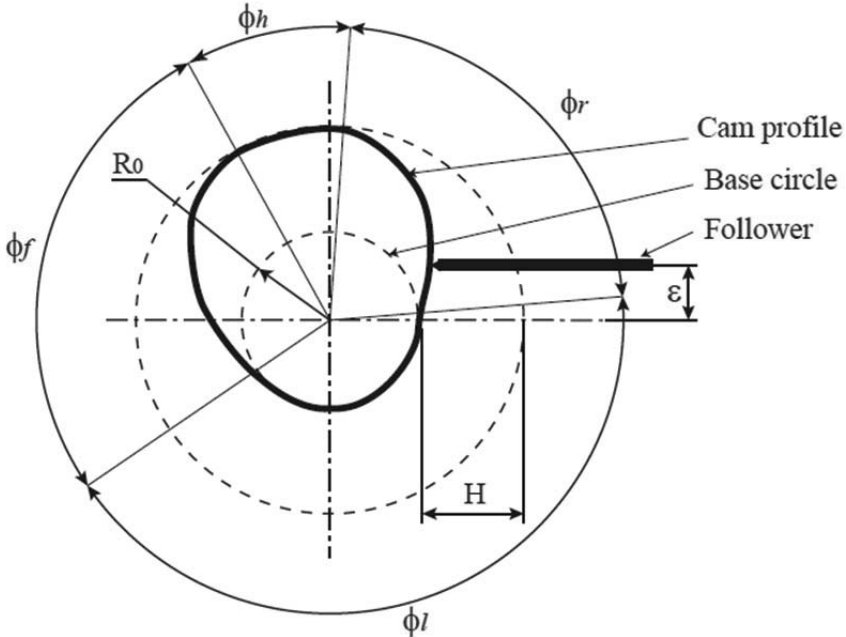


Figure 4.13. The scheme of a cam mechanism, where ϕ_r - rise angle, ϕ_h - high dwell angle, ϕ_f - fall angle, ϕ_l - low dwell angle, ε - eccentricity, H - follower stroke (Paper IX).

It is useful to use a Mathcad worksheet program (4.3) to find displacement, velocity and acceleration values, because the cam profile is described by a piecewise function. The program (4.3) connects the cam rotation angle to different follower phases: rise, high dwell, low dwell and fall, which are determined with the cam curve. Different cam curves can be found from handbooks (Norton, 2009; Kleis, 1988; Norton, 1992). The following program and cam curve was used for calculating displacement in Paper IX

$$s(\varphi) = \begin{cases} s_1(\varphi) & \text{if } 0 \leq \varphi \leq \phi_r \\ s_1(\phi_r) & \text{if } \phi_r < \varphi \leq \phi_r + \phi_h \\ s_2(\varphi) & \text{if } \phi_r + \phi_h < \varphi \leq \phi_r + \phi_h + \phi_f \\ 0 & \text{otherwise} \end{cases} \quad (4.3)$$

where the displacement cam curve function for rise and fall is

$$s_1(\varphi) = H \left[35 \left(\frac{\varphi}{\phi_r} \right)^4 - 84 \left(\frac{\varphi}{\phi_r} \right)^5 + 70 \left(\frac{\varphi}{\phi_r} \right)^6 - 20 \left(\frac{\varphi}{\phi_r} \right)^7 \right],$$

$$s_2(\varphi) = H - H \left[35 \left(\frac{\varphi - \phi_r - \phi_h}{\phi_f} \right)^4 - 84 \left(\frac{\varphi - \phi_r - \phi_h}{\phi_f} \right)^5 + 70 \left(\frac{\varphi - \phi_r - \phi_h}{\phi_f} \right)^6 - 20 \left(\frac{\varphi - \phi_r - \phi_h}{\phi_f} \right)^7 \right].$$

A similar program was used to find follower velocity and acceleration (Paper IX).

According to Norton, 2009, the cam-follower mechanism's pressure angle α must be between $-30^\circ \leq \alpha \leq 30^\circ$. The impact of the pressure angle value on the cam profile is determined with the function (2.13). In Paper IX, the following cam profile optimal pressure angle synthesis task was solved:

Find such values for R_0 and ε that guarantee the satisfaction of the restriction

$$\alpha(\varphi, R_0, \varepsilon) = \alpha_e \quad (4.4)$$

in the rise, and restriction

$$\alpha(\varphi, R_0, \varepsilon) = \alpha_n \quad (4.5)$$

in the fall, when $\alpha_e = 20^\circ$, $\alpha_n = -24^\circ$ (Paper IX).

Figure 4.14 shows pressure angle dependence on cam rotation angle before optimization and Figure 4.15 after optimization.

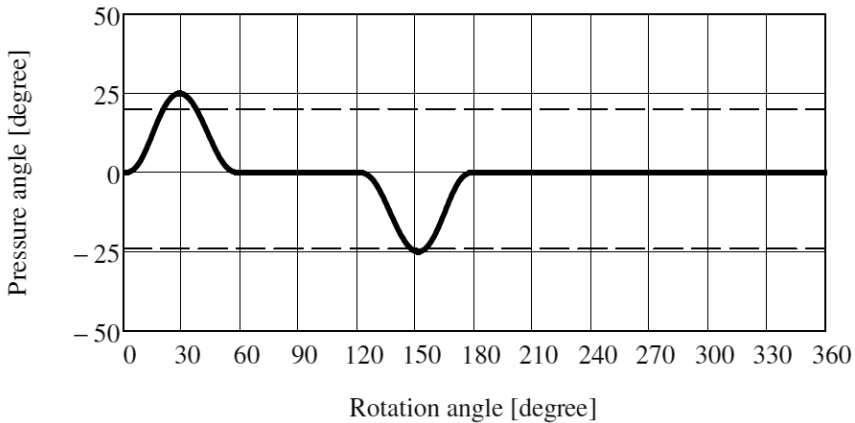


Figure 4.14. Cam mechanism's pressure angle before optimization.

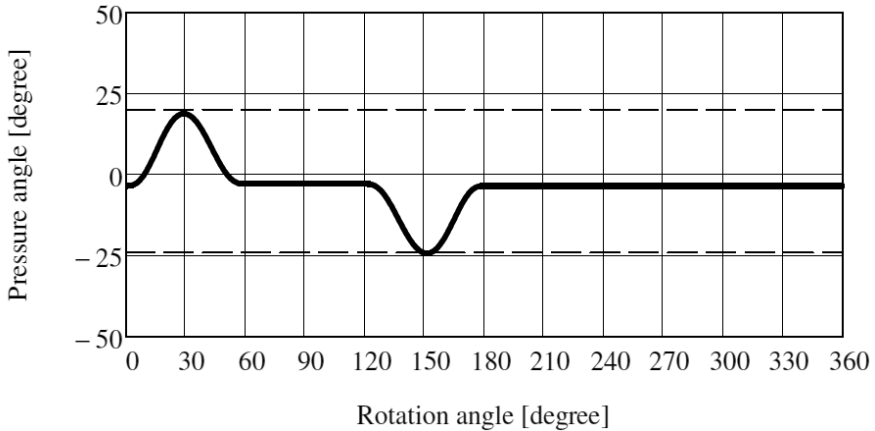


Figure 4.15. Cam mechanism's pressure angle after optimization.

In the video clip Aan, 2013, the motion simulation of the optimal cam profile and follower is displayed. A frame of the video clip, where follower displacement, velocity and acceleration values can be also observed is shown in Figure 4.16.

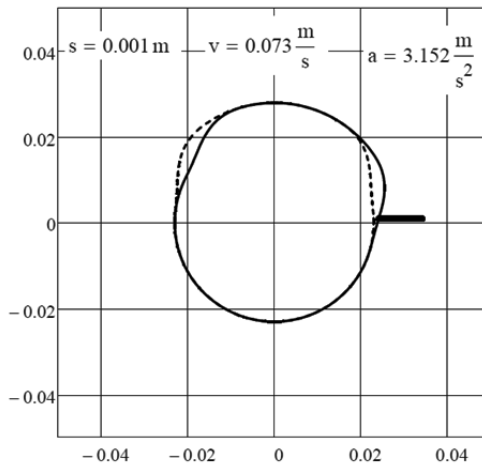


Figure 4.16. A frame from the video clip (Aan, 2013).

The Cartesian coordinates of the cam profile were also given, and these can be used to manufacture the cam with a CNC mill (Paper IX).

The methods presented in Paper IX can be used for teaching and designing radial cams.

4.5 Study on the chaotic motion of a double pendulum

In Paper I, the author studied the physical double pendulum (Figure 3.2), which is composed of two links connected with pivots. It was assumed that the links are similar and that the only acting force is gravitation. The centre of masses (x_1, y_1) and (x_2, y_2) applied gravitation force mg , where m is mass and g gravitational acceleration are shown in Figure 3.2. The lengths of the links is l and the inclination angles are θ_1 and θ_2 . The double pendulum is discussed in many mechanics books (Kenk & Kirs, 2013; Lepik & Roots, 1971; Butenin, et al., 1986).

Nonlinear differential equations in Hamilton form (2.9) and (2.10) were composed for the double pendulum. The double pendulum nonlinear differential equations were solved numerically with the IV order Runge-Kutta algorithm on a Mathcad worksheet (sections 2.5 and 3.2). A video clip Heinloo, 2010d was made, which shows that large oscillations of the double pendulum are chaotic. A frame from the video clip Heinloo, 2010d is shown in Figure 4.17.

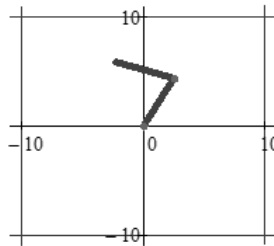


Figure 4.17. A frame from the video clip (Heinloo, 2010d).

The methods presented in Paper I can be used for teaching and studying similar mechanisms with chaotic motion.

4.6 Small oscillations of coupled pendulums

In Paper VII, it was demonstrated on a Mathcad worksheet how to compile equations on the motion of coupled pendulums (Figure 4.18) with the help of Lagrange's equation of the second type (2.11). Additionally, pendulum motion equations were solved with symbolic calculations and the Laplace transform in case of small oscillations.

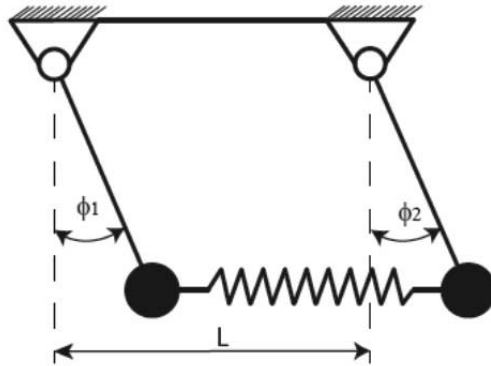


Figure 4.18. Mathematical spring-coupled pendulums: L - length between pendulums' pivots, ϕ_1, ϕ_2 - inclination angles of the pendulums (Paper VII).

The coupled pendulum has three types of oscillations: in phase, opposite phase and beating phase (Picciarelli & Stella, 2010). With the obtained results, it is possible to show all three types of oscillations on a Mathcad worksheet, when the correct initial positions are determined for the pendulums. A video clip was made on the motion simulation of coupled pendulums Aan & Heinloo, 2011 to visualise the results. A frame from the video clip is shown on Figure 4.19.

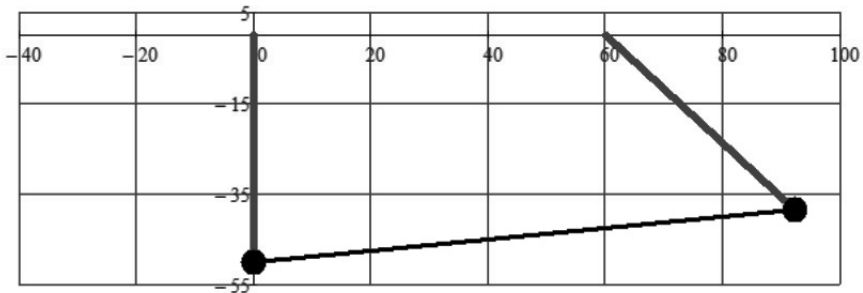


Figure 4.19. A frame from the video clip (Aan & Heinloo, 2011).

The method presented in Paper VII can be used for teaching and studying other oscillating mechanisms where symbolic calculations and the Laplace transform are used.

SUMMARY AND CONCLUSIONS

This doctoral thesis presents 11 publications and one patent, which are used to demonstrate how virtual models and their motion simulations can be created for the fields of engineering, analytical and machinery mechanics, and used in teaching or studying problems. Creating a virtual model of the object of study using a mathematical model and simulating its motion allows gaining better understanding of the problem at hand. This is especially important for people of the artistic type high neural activity, who need visualizing images of different objects in order to understand problems (Leppik, 2001; Leppik, 2008). The problem solutions found in the course of the work have been visualized as virtual models and motion simulations of the objects of study.

The following topics were discussed with regard to the development of learning methods:

1. On the creative teaching of engineering mechanics

The doctoral thesis presents two articles on this topic. Article III explains how engineering and machinery mechanics could be taught creatively. The article gives examples of the solutions to problems in mechanics, which have been solved on a Mathcad worksheet and which were then used to produce video clips simulating the objects' motion. Article II demonstrates how to use interactive examples when composing interactive revision notes for the subject Analytical Mechanics. The method can also be used for composing interactive revision notes for engineering mechanics and machinery mechanics.

Paper I explored the large oscillations of a double pendulum on a Mathcad worksheet as a more specific example of the interactive revision notes for analytical mechanics. The dependencies of the values of the angles determining the positions of the double pendulums on time were calculated by solving the Hamilton differential equations' system using the IV order Runge-Kutta method. A video clip was made of the motion simulation of the double pendulum's virtual model, which demonstrates the pendulum's chaotic movement in detail.

2. Computer-based study of the V-engine and cam mechanism

Article IV demonstrated how to make computer-based calculations of the kinematics and dynamics of a V-engine and to create a virtual model and its motion simulation. The kinematics and dynamics of the model were discussed, whereas the determination of the force acting on pistons was based on the indicator diagram of the four-stroke engine. The motion simulation of the engine's virtual model was shown in a video clip.

Paper IX demonstrated the computer-based synthesis of an optimal radial cam. A program was devised on a Mathcad worksheet, which combines the equations for the follower's rise and fall. Drawings were made to show the dependence of displacement, velocity, acceleration and pressure angle on the cam's rotation angle. Optimal values for the base circle radius and the follower's eccentricity were calculated in order to find the optimal profile for the cam. The paper provided Cartesian coordinates for an optimal cam, which can be used for cutting the cam. The cam's rotation and the motion of the follower's virtual model were simulated in a respective video clip.

3. Tasks related to mass point motion

This topic is discussed in three articles in the current doctoral thesis. Article VI discussed mass point motion on a curved planar trajectory. The video clip simulated mass point motion on some curved trajectories, on which the normal acceleration, tangential acceleration, full acceleration and velocity were marked with geometric vectors. The video clip shows the mass point's given trajectory, vector directed from the location of the mass point at the centre of curvature, the circle of trajectory's curvature at the point corresponding to the location of the mass point and evolute, which is formed by the centre of the circle of trajectory curvature.

4. Study of coupled pendulums using symbolic calculation and the Laplace transform

Paper VII demonstrated how to derive differential equations for coupled pendulums in case of small oscillations and solve these using both the symbolic calculation function in Mathcad as well as the Laplace transform. The motion simulation of the coupled pendulum's virtual model was shown in a video clip.

The following topics were discussed in relation to the development of research methods:

1. Study and visualization of the virtual models of some linkage mechanisms

Article V compared the single connecting-rod slide-crank mechanism common in internal combustion engines and the double connecting-rod slide-crank mechanism, which has not been put to wider use. The piston displacements, velocities and accelerations were found for both mechanisms. The calculated values were compared in the same drawings. The sliders' pressure angle and reaction forces a piston would apply on the cylinder wall were compared separately. Two comparative motion simulations were created for the mechanisms. The first simulation compared slider displacements and the other velocities, accelerations and pressure angles. The study revealed that both the values of the pressure angle and the reaction force for double connecting-rod slider-crank mechanism are smaller on average than those of a single connection-rod linkage mechanism. Article X discusses a mechanism consisting of 12 links, which moves similarly to a walking leg. It is presupposed that the motion of the observed mechanism takes place in a restricting environment. Changing drag force and inertia cause fluctuations in the speed of the input link. In order to decrease the fluctuation of this speed, the article shows how to find a flywheel for this kind of mechanism. A motion simulation was created for the mechanism.

2. Study of problems related to mass point motion and motion simulation

In article VIII, a fertilizer granule was modelled as a mass point. The study explored the trajectories of a fertilizer granule on a spreading disc, time spent on the disc and the velocity of leaving the spreader with different values for the angles of the spreading disk's vane, friction coefficient and the initial position of the fertilizer granule. The motion simulation of the fertilizer granule was shown in a video clip. Paper XI studied the motion of a sea buckthorn berry, modelled as a mass point, during the separation of berries from twigs on a conveyor belt and after it has left the belt. A mathematical model was created, which describes the mo-

tion of the berry on a conveyor belt and in the air after it has left the belt. The values for the berry's displacement, velocity and general time in motion were calculated depending on the velocity of the conveyor belt, inclination angle and the friction coefficient between the berry and belt. A virtual model of the conveyor belt was created, which also depicted the berry. The motion of the berry on the conveyor belt at different inclination angles and after it has left the conveyor belt was illustrated in a video clip.

Conclusions

The methods and results presented in this thesis can be implemented in the teaching process of engineering subjects to visualize the solutions of mechanical problems and simulate the motion of composed virtual models on the screen of a computer.

The computer program Mathcad can be used as convenient tool for the composition of interactive lecture materials. It gives the possibility of experimenting with lecture materials. Composing simulations by students makes studying engineering subjects interesting and attractive for them.

The computer program Mathcad can be used as a convenient tool for engineers for the calculation and simulation of the motion of studied objects to verify and visualize the obtained solutions.

REFERENCES

- Aan, A. 2013. Cam-follower mechanism. Available at: <http://youtu.be/c43JIq7-rvc> (11.11.2014).
- Aan, A. 2014a. Elliptical mechanism. Available at: <http://youtu.be/1YnapCGOvQ4> (31.10.2014).
- Aan, A. 2014b. Jansen linkage. Available at: https://www.youtube.com/watch?v=B_dR2_O3ujc (4 11 2014).
- Aan, A. 2014c. Particle of the berry on inclined moving conveyor belt. Available at: <http://youtu.be/g0Axx5gmwIk> (10.11.2014).
- Aan, A. & Heinloo, M. 2011. Oscillations of pendulums, coupled by a spring. Available at: http://youtu.be/Or9kAUY_gT8 (12.11.2014).
- Aan, A. & Heinloo, M. 2012a. Comparison of piston displacements. Available at: <http://youtu.be/LG2h8oiyjIU> (4.11.2014).
- Aan, A. & Heinloo, M. 2012b. Comparison of piston velocities accelerations and reactions. Available at: <http://youtu.be/QvyZAo-Q3Rk> (4 11 2014).
- Artobolevski, I. 1961. Mehhanismide ja masinate teooria (in Estonian). Tallinn: Eesti Riiklik Kirjastus.
- Bertjaev, B. D. 2005. Mathcad-based Training in Theoretical Mechanics (in russian). Sankt-Peterburg.
- Broman, G. & Östholm, S. 1997. Mathcad in Teaching Rotor and. International journal of engineering education Structural Dynamics, 13(6), pp. 426-432.
- Butenin, N., Lunts, J. & Merkin, D. 1983. Teoreetiline mehaanika: Staatika ja Kinemaatika. Tallinn: Valgus.
- Butenin, N., Lunts, J. & Merkin, D. 1986. Teoreetiline mehaanika. Dünaamika. (in Estonian). Tallinn: Valgus.
- Chonacky, N. 2006. Special thanks to CiSE's peer reviewers. Computing in Science and Engineering, Volume 8(1), p. 14.
- El Hassan, E. H., Fatiha, K., Abdelrhani, E. & Anouar, A. 2014. Teaching / Learning mechanics in high school with the help of Dynamic software. Procedia - Social and Behavioral Sciences, Volume 116, pp. 4617-4621.

- Evert, A. Buckle- and Double-Connecting-Rod. Available at: <http://www.evert.de/ef774e.htm> (3.11.2014).
- Gelbart, H., Brill, G. & Yarden, A. 2009. The impact of a web-based research simulation in bioinformatics on students' understanding of genetics. *Research in Science*, Volume 39(5), pp. 725-751.
- Goldstein, H., Poole, C. & Safko, J. 2000. *Classical mechanics*, third edition. Addison Wesley.
- Haber, R. B. 1990. Visualization techniques for engineering mechanics. *Computing Systems in Engineering*, Volume 1(1), pp. 37-50.
- Heinloo, M. 2007a. Automatic generation virtual models of fourbars for visualized e-courses of interactive engineering mechanics. *Balkan Agricultural Engineering Review*, Volume 10, p. 6.
- Heinloo, M. 2007b. A Virtual Reality Technology-Based Method for the Study of the Working Process of a Blueberry Harvester's Picking Reel. *Agricultural Engineering International: the CIGR Ejournal*, Volume 9.
- Heinloo, M. 2009. Manipulaator 2. Available at: <http://youtu.be/MNTztcBsBoA> (5.1.2015).
- Heinloo, M. 2010a. Ketaslaoturi laotusketta virtuaalse tööprotsessi visualiseerimine (in Estonian). *Agraarteadus*, Volume 21(1), pp. 3-7.
- Heinloo, M. 2010b. Mathcad algajaile. Available at: http://www.e-ope.ee/_download/euni_repository/file/623/MC%20Osa%202.xmcd?download=true (20.10.2014).
- Heinloo, M. 2010c. Villet 4 vanes. Available at: <http://youtu.be/bTxqdhjBOCU> (5.1.2015).
- Heinloo, M. 2010d. Physical double pendulum. Available at: <http://youtu.be/BFIJTAzYdvo> (11.11.2014).
- Heinloo, M. 2011a. Manure skraperi manipulaator 1. Available at: <https://www.youtube.com/watch?v=9TpXx2Xx3Rw> (5.1.2015).
- Heinloo, M. 2011b. Cinematics of a Point. Available at: <http://youtu.be/zFbVcd4GOJw> (31.10.2014).
- Heinloo, M. 2011c. Four bar linkage. Available at: <http://youtu.be/GgEra0JPoDU> (5.1.2015).

- Heinloo, M. 2012a. V-engine. Available at: <https://www.youtube.com/watch?v=OyAiXVzfQkI> (3.11.2015).
- Heinloo, M., 2012b. Cinematics of a point 1. Available at: <https://www.youtube.com/watch?v=2gPSalH9lxU&feature=youtu.be> (7.11.2014).
- Heinloo, M., 2013a. Motion the granules on fertilizer spreading disc 1. Available at: http://youtu.be/ZEh0Zv_gixQ (7.11.2014).
- Heinloo, M., 2013b. Motion the granules on fertilizer spreading disc 2. Available at: <http://youtu.be/8d9EYzzxw1s> (7.11.2014).
- Heinloo, M. 2014. Blueberry harvester picking reel. Available at: <http://youtu.be/aRR80hbAIU0> (5.1.2015).
- Heinloo, M. 2015. Disk ridging tool. Available at: <http://youtu.be/bJqVqO0Ijzk> (6.3.2015).
- Heinloo, M. & Leola, T. 2006a. Virtual reality method supported synthesis of a plane manipulator. Proceedings 5th Int. DAAAM Conf. "Industrial Engineering – Adding Innovation Capacity of Labour Force and Entrepreneurs", Tallinn.
- Heinloo, M. & Leola, T. 2006b. Multiparametric Synthesis the Manipulator of the Scraper of the Press Manure Removal. Journal of Agricultural Science, Volume 17(2), pp. 88-95.
- Heinloo, M. & Leola, T. 2007. Development of Virtual Reality Methods Based Analysis and Synthesis of Mechanisms. Proceedings 12-th World Congress in Mechanism and Machine Science, Besancon.
- Heinloo, M., Leola, T. & Veinla, V. 2005. Synthesis of the Manipulator for the Scraper of a Press Manure Removal. Agricultural Engineering International: the CIGR Ejournal, Volume 7.
- Heinloo, M. & Olt, J. 2004a. The Imagination of the Forced Driven Disk-ridging Tool and it's Working Process in the Mathcad Environment. Proceedings 4th Int. DAAAM Conf. "Industrial Engineering – Innovation as Competitive Edge For SME", Tallinn.
- Heinloo, M. & Olt, J. 2004b. Animation of Motion of the Disk-ridging Tool. Proceedings Int. Conf. "Energy Efficiency and Agricultural Engineering". Rouse, pp. 137 – 135.

- Heinloo, M. & Olt, J. 2004c. Animation of the Working Process of the Disk-ridging Tool. CD Papers Int. Conf. AgEng2004, Leuven.
- Heinloo, M. & Olt, J. 2006. The Method of Virtual Reality for Creation a Disk-Ridging Tool. Agricultural Engineering International: the CIGR Ejournal, Volume 8.
- Hess, H., Johnson, B. & Chapman, C. 2014. Synchronous machine winding layout & flux animation tool. Indianapolis.
- Höffler, T. N. & Leutner, D. 2007. Instructional animation versus static pictures: A meta-analysis. Learning and Instruction, Volume 17, pp. 722-738.
- Jansen, T. 2007. Theo Jansen: The Great Pretender. Rotterdam: 010 Publisher.
- Jimoyiannis, A. & Komis, V. 2001. Computer simulations in physics teaching and learning: a case study on students' understanding of trajectory motion. Computers & Education, Volume 36(2), pp. 183-204.
- Kenk, K. & Kirs, J. K. 2013. Mehaanika alused: Dünaamika Analüütiline mehaanika (in Estonian). Tallinn: TTÜ Press.
- Kleis, I. 1988. Rakendusmehaanika (in Estonian). Tallinn: Valgus.
- Lepikson, H. 1998. V-kujulise neljataktilise sisepõlemismootori kinemaatilise skeemi projekteerimine (in Estonian). Tallinn: TTÜ.
- Lepik, Ü. & Roots, L. 1971. Teoreetiline mehaanika (In Estonian). Tallinn: Valgus.
- Leppik, P. 2001. Tunni analüüsimine on huvitav. Tallinn.
- Leppik, P. 2008. Õpetajatöö psühholoogilisi probleeme. Tartu: Tartu Ülikooli Kirjastus.
- Levin, M. & Ulm, S. 1966. Arvutusmeetodite käsiraamat (in Estonian). Tallinn: Valgus.
- Manapa, A. A., Sardanb, N. A. & Riase, R. P. M. 2012. Interactive Learning Application in Microbiology: The Design, Development and Usability. Procedia - Social and Behavioral Sciences, Volume 90, pp. 31 - 40.
- Mekanizmalar, Available at: <http://www.mekanizmalar.com> (5.1.2015).

- Melek, Y., Claudia, N. & Horst, B. 2008. The effects of instructional support and learner interests when learning using computer simulations. *Computers & Education*, Volume 51, pp. 1784-1794.
- Molian, S. 1982. *Mechanism Design: An Introductory Text*. Cambridge University Press.
- Norton, L. R. 1992. *Design of machinery*. McGraw-Hill.
- Norton, R. L. 2009. *Cam design and manufacturing handbook*. New York: Industrial Press Inc..
- Novohatska, T., Grasmanis, B. & Vjaters, I. 2014. Theoretical mechanics for students of engineering profile. *Proceedings Engineering for rural development*, pp. 485-490.
- Ochkov, V. F. 2011a. Steam engine. Available at: <http://communities.ptc.com/videos/2119> (8.10.2014).
- Ochkov, V. F. 2011b. Windshield wipers. Available at: <http://communities.ptc.com/videos/2060> (8.10.2014).
- Ochkov, V. F. 2011c. Chebyshev's Foot Stepping Machine. Available at: <http://communities.ptc.com/videos/2057> (8.10.2014).
- Ochkov, V. F. 2011d. Walk Machine. Available at: <http://communities.ptc.com/videos/2047> (8.10.2014).
- Ochkov, V. F. 2013. ЖИВЫЕ КИНЕМАТИЧЕСКИЕ СХЕМЫ В MATHCAD. *Открытое образование*, Volume 2, pp. 27-33.
- Olt, J. & Heinloo, M. 2011a. The Study of a New Manipulator for a Stone Protector of Stony Soil Tillage Implement. *Journal of Agricultural Science and Technology*, Volume 1(5B), pp. 751-755.
- Olt, J. & Heinloo, M. 2011b. Visualization of motion of fertiliser granules on the planar of spinning spreading disc of a disc spreader. *Proceedings XXXIV CIOCTA-CIGR, Vienna*, pp. 292 - 296
- Picciarelli, V. & Stella, R. 2010. Coupled pendulums: a physical system for laboratory investigations at upper secondary school. *Physics Education*, Volume 45(4), pp. 402-408.
- Piskunov, N. 1981. *Diferentsiaal- ja integraalarvutus 1*. Tallinn: Valgus.

- Preszler, R. W., Dawe, A., Shuster, C. B. & Shuster, M. 2007. Assessment of the Effects of Student Response Systems on Student Learning and Attitudes over a Broad Range of Biology Courses. *CBE Life Sci Educ*, Volume 6, pp. 29-41.
- Recchi, M., Gagliardi, M., Grimellini, N. & Levrini, O. 2006. Different uses of ICT for modelling in Physics Education. *Proceedings GIREP Conference 2006: Modeling in Physics and Physics Education*, pp. 409-417.
- Reintam, A. 1995. Mineraalvætiste ketaslaoturi laotusketta tööprotsessi uurimine matemaatilise modelleerimise teel (in Estonian). *Agraarteadus*, Volume 6(4), pp. 435–448.
- Riess, W. & Mischo, C. 2010. Promoting systems thinking through biology lessons. *International Journal of Science Education*, Volume 32(6), pp. 705-725.
- Ruina, A. & Pratap, R. 2014. *Introduction to Statics and Dynamics*. Oxford University Press.
- Rutten, N., van Joolingen, W. R. & van der Veen, J. T. 2012. The learning effects of computer simulations in science education. *Computers & Education*, Volume 58(1), pp. 136-153.
- Shigley, J., Mischke, C. & Brown, T. 2004. *Standard handbook of machine design*. McGraw-Hill.
- Smith, S. What Are Interactive Learning Materials? Available at: http://www.ehow.com/info_7947754_interactive-learning-materials.html (30.10.2014).
- Soutas-Little, R. W., Inman, D. J. & Balint, D. S. 2008. *Engineering Mechanics: Dynamics - Computational Edition*. Thomson.
- Soutas-Little, R. W., Inman, D. J. & Balint, D. S. 2008. *Engineering Mechanics: Statics-Computational Edition*. Thomson.
- Stern, L., Barnea, N. & Shauli, S. 2008. The effect of a computerized simulation on middle school students' understanding of the kinetic molecular theory. *Journal of Science Education and Technology*, Volume 17(4), pp. 305-315.
- Tamme, E. 1973. *Arvutusmeetodid 2* (in Estonian). Tallinn: Valgus.
- Targ, S. 1968. *Teoreetiline mehaanika* (in Estonian). Tallinn: Valgus.

- Thornton, S. T. & Marion, J. B. 2007. Classical Dynamics of Particles and Systems, Fifth edition. Cengage Learning.
- Zhang, M., Zhang, L. & Zhang, F. 2010. The analysis of link mechanism movement based on MathCAD. Proceedings - 2010 International Forum on Information Technology and Applications, Volume 1, pp. 281-287.

KOKKUVÕTE

Antud doktoritöös esitletakse 11 publikatsiooni ja ühte patenti, millede abil näidatakse, kuidas on võimalik virtuaalmudeleid ja nende liikumise simulatsioone luua inseneri- ja masinamehaanika ning analüütilise mehaanika valdkondadest, mida saab kasutada õpetamisel ja probleemide uurimisel. Luues uuritavast objektist matemaatilise mudeli abil virtuaalmudeli ja simuleerides selle liikumist on võimalik antud probleemist paremini aru saada. Eriti puudutab see inimesi, kes on kunstnikutüüpi kõrgema närvitegevusega ja vajavad arusaamiseks mitmesuguste objektide visualiseerivaid kujutisi (Leppik, 2001; Leppik, 2008). Antud töös leitud probleemide lahendid on visualiseeritud virtuaalmudelitena kui ka uuritud objektide liikumise simuleerimisega.

Õppemeetodite arendamise valdkonnast käsitleti järgnevaid teemasid:

1. Mehaanika loov õpetamine

Selle teema kohta on doktoritöös esitletud kahte artiklit. Artiklis III selgitatakse, kuidas võiks loovalt õpetada inseneri- ja masinamehaanikat. Selles artiklis on toodud näiteid mehaanika probleemide lahenditest, mis on leitud Mathcadi töölehel ja milledele on koostatud objektide liikumist simuleerivad videoklipid. Artiklis II on näidatud, kuidas kasutada interaktiivseid näiteid õppeainele „Analüütiline mehaanika“ interaktiivse loengukonspekti koostamisel. Antud meetodit saaks ka kasutada insenerimehaanika ja masinamehaanika interaktiivse konspekti koostamiseks.

Analüütilise mehaanika interaktiivse konspekti täpsema näitena uuriti töös I kaksikpendli suuri võnkumisi Mathcadi töölehel. Hamiltoni diferentsiaalvõrrandite süsteemi lahendamisel Runge-Kutta IV järku meetodiga leiti kaksikpendlite asendeid määravate nurkade väärtuste sõltuvused ajast. Koostati kaksikpendli virtuaalmudeli liikumise simulatsiooni videoklipp, mis näitab ilmekalt selle pendli kaootilist liikumist.

2. V-kujuline mootori ja nukkmehhanismi arvutipõhine uurimine

Artiklis IV näidati, kuidas arvutipõhiselt teha V-kujulise mootori kinemaatika ja dünaamika arvutusi, koos virtuaalmudeli koostamise ja selle liikumise simuleerimisega. Käsitleti mudeli kinemaatikat ja dünaamikat, kusjuures kolbidele mõjuva jõu määramisel lähtuti neljataktilise mootori indikaatordiagrammist. Koostati videoklipp simulatsiooniga mootori virtuaalmudeli liikumisest.

Töös IX näidati arvutipõhiselt optimaalse radiaalse nuki sünteesi tegemist. Selleks koostati Mathcadi töölehel programm, mis seob omavahel tõukuri eemaldumise ja naasmise võrrandid. Koostati siirde, kiiruse, kiirenduse ja survenurga sõltuvust nuki pöördenergiast näitavad joonised. Nuki optimaalse profiili saamiseks leiti optimaalsed väärtused algringjoone raadiusele ja tõukuri ekstsentrilisusele. Väljastati optimaalse profiiliga nuki koordinaadid, mida saab kasutada nuki väljalõikamisel. Nuki pöörlemist ja tõukuri virtuaalmudeli liikumist simuleeriti vastavas videoklipis

3. Punktmassi liikumisega seotud ülesanded

Seda teemat käsitlevad doktoritöös kolm artiklit. Artiklis VI käsitleti punktmassi liikumist kõveral trajektoiril. Videoklipis simuleeriti punktmassi liikumine mõnedel kõveratel trajektooridel, millel punktmassi normaalkiirendust, tangentsiaalkiirendust, täiskiirendust ja kiirust kujutati geomeetriliste vektoritega. Videoklipis on näha punktmassile etteantud trajektoor, punktmassi asukohast kõverustsentrisse suunatud vektor, punktmassi asukohale vastava trajektoori punkti kõverusringjoon ja evoluuut, mida kujundab kõverusringjoone keskpunkt

4. Sümpaatiliste pendlite uurimine sümbolarvutuse ja Laplace teisendusega.

Töös VII näidati kuidas tuletada diferentsiaalvõrrandeid sümpaatilistele pendlitele väikeste võnkumiste korral ja lahendada need nii programmi Mathcad sümbolarvutuse kui Laplace teisenduse abil. Koostati videoklipp sümpaatiliste pendlite virtuaalse mudeli liikumise simulatsiooniga.

Uurimismeetodite arendamise valdkonnast käsitleti järgnevaid teemasid:

1. Mõnede varbmehhanismide virtuaalmudelite uurimine ja visualiseerimine.

Artiklis V võrreldi sise põlemismootorites levinud ühe kepsuga väntmehhanismi ja kahe kepsuga väntmehhanismi, mis pole laialdast kasutust leidnud. Leiti kolvi siirded, kiirused ja kiirendused mõlemas mehhanismis. Leitud väärtusi võrreldi samadel joonistel. Eraldi võrreldi liugurite survenurka ja reaktsioonjõude, mida avaldaks kolb silindri pinnale. Koostati kaks võrdlevat mehhanismide liikumise simulatsiooni. Esimeses simulatsioonis võrreldi liugurite siirdeid ja teises simulatsioonis - kiirusi, kiirendusi ja survenurki. Leiti, et kahe kepsuga väntmehhanismi korral on nii survenurga kui ka reaktsioonjõu väärtus keskmiselt väiksem kui ühe kepsuga varbmehhanismis. Artiklis X käsitletakse 12 lülilist koostatud mehhanismi, mille liikumine on jala kõndimise liigutuse sarnane. Eeldatakse, et vaadeldava mehhanismi liikumine toimub liikumist takistavas keskkonnas. Muutuvad takistusjõud ja inertsijõud põhjustavad sisendlüli kiiruse kõikumist. Et vähendada selle kiiruse kõikumist näidatakse, kuidas leida sellisele mehhanismile hoorattast. Koostati simulatsioon mehhanismi liikumisest.

2. Punktmassi liikumisega seotud probleemide uurimine ja liikumiste simuleerimine.

Artiklis VIII modelleeriti väetiseosakest punktmassina. Uuriti väetiseosakese trajektoore jaotuskettal, sellel viibimise aega ja laoturilt lahkumise kiirust erinevate väetiselaoturi laba nurkade, hõõrdekoefitsiendi ja väetiseosakese algpositsiooni korral. Koostati videoklipid simulatsioonidega väetiseosakese liikumisest. Töös XI uuriti punktmassina modelleeritud astelpaju marja liikumist, marjade okstest eraldamise konveieri lindil ja pärast sellelt lahkumist. Koostati matemaatiline mudel, mis kirjeldab marja liikumist konveierilindil ja õhus pärast selle eemaldumist lindilt. Leiti marja siire, kiirus, ja kogu liikumise aeg sõltuvalt konveierilindi liikumise kiirusest, kaldenurgast ja hõõrdeegurist marja ning lindi vahel. Koostati konveieri lindi virtuaalne mudel, millel on kujutatud mari. Koostati videoklipp, mis illustreerib marja liikumist konveieril erinevate kaldenurkade korral ja pärast konveierilt lahkumist.

Meetodid ja tulemused, mida antud töös näidati saab kasutada mehaanika ainete õpetamisel visualiseerimaks õpitava mehaanika ülesande objekti virtuaalse mudeli ja simuleerides tema liikumist arvuti ekraanil.

Arvuti programmi Mathcad saab kasutada hea abivahendina, et luua interaktiivseid õppematerjale, mis annavad võimaluse eksperimenteerida õppematerjalidega. Simulatsioonide loomise võimalus teeb õpilaste jaoks õppimise huvitavamaks.

Arvuti programmi Mathcad saab kasutada hea töövahendina, et teha inseneriarvutisi ja simulatsiooni. Simulatsioonid visualiseerivad saadud tulemusi aidates kontrollida lahenduse õigsust.

ACKNOWLEDGEMENTS

The thesis has been completed thanks to the Estonian University of Life Sciences, Institute of Technology.

I would like to thank my supervisor

Professor Mati Heinloo

for leading me and for being always ready to help me.

Thanks to professor Jüri Olt for many advises during my studies.

Special thanks to lecturer Eino Aarend for guiding me on the path of the mechanics.

I would like to thank all my colleagues and friends, especially Marten Madissoo, Tõnu Leemet, Valetina Prigoževa, Jaanus Allas, Peeter Nõmm, Villu Mikita, Aarne Küüt and Risto Ilves.

Thanks to my mother Maimu, father Jaak, sister Terje and brother Teet for always supporting my studies.

Last but not least, many thanks for the support, time and effort from my wife and child Janika and Eliis-Marii.

Aan, A., Aarend, E., Heinloo, M.
On chaotic motion of a double pendulum
Agronomy Research, 10(1), 5 – 12, 2011

On chaotic motion of a double pendulum

A. Aan, E. Aarend and M. Heinloo

Institute of Technology, Estonian University of Life Sciences, Kreutzwaldi 56, EE 51014 Tartu, Estonia, e-mail: aare.aan@emu.ee

Abstract. This paper presents the results of studying the chaotic motion of a virtual double pendulum. Large oscillations of this pendulum were modelled by the system of nonlinear differential equations in the Hamilton form. This system was solved on the worksheet of Computer Package Mathcad numerically, using the Runge-Kutta algorithm of fourth order. The results are illustrated by some frames of video clips visualizing the chaotic motion of a double physical pendulum. The results of this paper can be used in the teaching process of analytical mechanics for students of engineering.

Key words: Analytical mechanics, equations of Hamilton, double pendulum, chaotic motion, Computer Package Mathcad.

INTRODUCTION

Classical analytical mechanics contains a lot of differential equations in the Lagrange and the Hamilton forms. These equations, mostly nonlinear, are practically dead before their numerical solution and imagination of the results. It is convenient to use different computer programs for this purpose, for example, the Computer Package Mathcad. From the point of view of teaching it is useful to simulate, if possible, the motion of a virtual object, modelled by the nonlinear equations of Lagrange or Hamilton. Such an object is, for instance, a double pendulum. It appears that the motion of virtual and physical models of a double pendulum is chaotic. It is possible to find a lot of results on the study of chaotic virtual models of double pendulums on different web sites, for example [1]–[12]. The physical models of a double pendulum are presented, for example, on the web sites [13]–[18].

The purpose of this paper is to use the features of the Computer Package Mathcad and solve numerically, using the Runge-Kutta algorithm of fourth order, the nonlinear system of differential equations in the Hamilton form, modelling the large oscillation of a virtual physical double pendulum, and to visualize its chaotic motion for different initial conditions.

MATERIALS AND METHODS

A mathematical model to study the motion of a double pendulum

Let us consider a physical double pendulum in Fig. 1

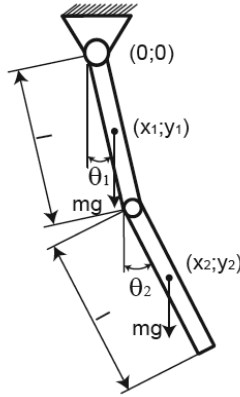


Figure 1. A physical double pendulum.

The double pendulum in Fig. 1 consists of two links of equal length and gravity mg , where g is the acceleration of gravity, joined together by a pivot. The upper pivot of the double pendulum is grounded. In the current position the upper link of the double pendulum has inclination angle θ_1 and the lower link has inclination angle θ_2 . The co-ordinates of the centre of mass of the upper link are (x_1, y_1) and of the lower link (x_2, y_2) .

The mathematical model in the Hamilton form, describing large oscillations of the double pendulum is [18, 19]

$$\theta_1' = \frac{6}{ml^2} \frac{2p_{\theta_1} - 3p_{\theta_2} \cos(\theta_1 - \theta_2)}{16 - 9\cos^2(\theta_1 - \theta_2)}, \quad \theta_2' = \frac{6}{ml^2} \frac{8p_{\theta_2} - 3p_{\theta_1} \cos(\theta_1 - \theta_2)}{16 - 9\cos^2(\theta_1 - \theta_2)}, \quad (1)$$

$$p'_{\theta_1} = -\frac{1}{2} ml^2 \left(\theta_1' \theta_2' \sin(\theta_1 - \theta_2) + 3 \frac{g}{l} \sin(\theta_1) \right),$$

$$p'_{\theta_2} = -\frac{1}{2} ml^2 \left(-\theta_1' \theta_2' \sin(\theta_1 - \theta_2) + \frac{g}{l} \sin(\theta_2) \right),$$

where θ_1 and θ_2 are generalized co-ordinates [19], or inclination angles, of the double pendulum (Fig. 1) and $p_{\theta_1} = \frac{1}{6} ml^2 (8\theta_1' + 3\theta_2' \cos(\theta_1 - \theta_2))$, $p_{\theta_2} = \frac{1}{6} ml^2 (2\theta_2' + 3\theta_1' \cos(\theta_1 - \theta_2))$, are the generalized impulses [20] of the double pendulum. Note, that for small oscillations of a double pendulum, considered in [21], the mathematical model following form equations (1), when $\cos(\theta_1 - \theta_2) \approx 1$, $\sin(\theta_1 - \theta_2) \approx 0$, $\sin(\theta_1) \approx 0$, $\sin(\theta_2) \approx 0$

Let us assume that the special solution of the equations (1) satisfies the following initial conditions:

$$\theta_1(0) = \theta_{10}, \theta_2(0) = \theta_{20}, p_{\theta_1}(0) = p_{\theta_{10}}, p_{\theta_2}(0) = p_{\theta_{20}}, \quad (2)$$

where $\theta_{10}, \theta_{20}, p_{\theta_{10}}, p_{\theta_{20}}$ are constants. Let us consider the first initial position of the double pendulum, shown in Fig. 2 and assume that the motion of the double pendulum begins without initial angular velocities.

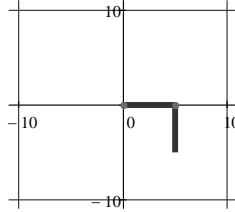


Figure 2. First initial position of the double pendulum.

This assumption means that in the initial conditions (2) the constants must have the following values:

$$\theta_{10} = \frac{\pi}{2}, \theta_{20} = 0, p_{\theta_{10}} = 0, p_{\theta_{20}} = 0, \quad (3)$$

Let us consider now the initial position of the double pendulum, shown in Fig 3 and assume also that the motion of the double pendulum begins without initial angular velocities

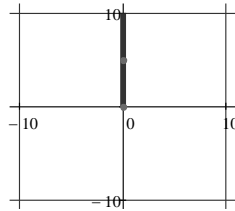


Figure 3. Second initial position of the double pendulum.

This assumption means that in the initial conditions there must be the following values of the constants:

$$\theta_{10} = \pi, \theta_{20} = \pi, p_{\theta_{10}} = 0, p_{\theta_{20}} = 0, \quad (4)$$

Numerical solution of the system of differential equations (1) on the worksheet the Computer Package Mathcad

To use the algorithms programmed in Computer Package Mathcad for solution of system (1) of differential equations on the worksheet of Computer Package Mathcad we have to use the following new variables with array subscripts $y_0 = \theta_1$, $y_1 = y_2 = p\theta_1$, $y_3 = p\theta_2$ and to present the system (1) in normal form

$$y'_0 = f_1(m, l, y), \quad y'_1 = f_2(m, l, y), \quad y'_2 = f_3(m, l, g, y), \quad y'_3 = f_4(m, l, g, y), \quad (5)$$

$$\text{where: } f_1(m, l, y) = \frac{6}{ml^2} \frac{2y_2 - 3y_3 \cos(y_0 - y_1)}{16 - 9 \cos^2(y_0 - y_1)}, \quad f_2(m, l, y) = \frac{6}{ml^2} \frac{8y_3 - 3y_2 \cos(y_0 - y_1)}{16 - 9 \cos^2(y_0 - y_1)},$$

$$f_3(m, l, g, y) = -\frac{ml^2}{2} \left(\frac{36}{m^2 l^4} \frac{[2y_2 - 3y_3 \cos(y_0 - y_1)][8y_3 - 3y_2 \cos(y_0 - y_1)]}{16 - 9 \cos^2(y_0 - y_1)^4} \sin(y_0 - y_1) + \frac{3g}{l} \sin(y_0) \right)$$

$$f_4(m, l, g, y) = \frac{ml^2}{2} \left(\frac{36}{m^2 l^4} \frac{[2y_2 - 3y_3 \cos(y_0 - y_1)][8y_3 - 3y_2 \cos(y_0 - y_1)]}{16 - 9 \cos^2(y_0 - y_1)^4} \sin(y_0 - y_1) - \frac{g}{l} \sin(y_1) \right).$$

Here y is the vector $\begin{pmatrix} y_1 \\ y_2 \\ y_3 \\ y_4 \end{pmatrix}$.

Computer Package Mathcad 14 [22] uses different functions, which present certain numerical algorithms for solution systems of differential equations. One them is the function $\text{rkfixed}(a, t_0, t_N, N, D)$, which uses the algorithm of Runge-Ku. Here

$a = \begin{pmatrix} \theta_{10} \\ \theta_{20} \\ p\theta_{10} \\ p\theta_{20} \end{pmatrix}$ is the vector of constants in the initial conditions, t_0 is the first value of

time t and t_N – its last value; N is the number of intervals between t_0 and t_N ; D – is

notation of the vector $D(t, y) = \begin{pmatrix} f_1(m, l, y) \\ f_2(m, l, y) \\ f_3(m, l, g, y) \\ f_4(m, l, g, y) \end{pmatrix}$ of the right hand sides of the system (1)

The function $\text{rkfixed}(a, t_0, t_N, N, D)$ returns the matrix that is convenient to assign another variable Z : $Z = \text{rkfixed}(a, t_0, t_N, N, D)$. The first column with number 1 contains the values of the variable $y_0 = t$ at the nodes. The second column with number 1 – the values of variable $y_1 = \theta_1$; the third column with number 2 – the values of variable $y_2 = \theta_2$; the fourth column with number 3 – the values of variable $y_3 = p\theta_1$; fifth column with number 4 – the values of variable $y_4 = p\theta_2$.

RESULTS

The results of computations of $y_3 = p_{\theta_1}$ and $y_4 = p_{\theta_2}$ for $t_0 = 0$, $t_N = 100$, $N = 1,000$, $l = 5$, $m = 1$, $g = 9,807$ in the case of initial values (4) are given in the following tables, copied from the worksheet of the Computer Package Mathcad. These tables show that because of the approximate value of the $\pi = 3.141592653589793\dots$, the motion of the double pendulum is possible even from the initial values (4).

	0	
0		0
1		$-9.00728588395204 \cdot 10^{-16}$
2		$-1.8014571767904077 \cdot 10^{-15}$
3		$-2.7021857651856114 \cdot 10^{-15}$
4		$-3.6029143535808155 \cdot 10^{-15}$
5		$-4.503642941976019 \cdot 10^{-15}$
6		$-5.404371530371223 \cdot 10^{-15}$
7		$-6.305100118766426 \cdot 10^{-15}$
8		$-7.205828707161631 \cdot 10^{-15}$
9		$-8.106557295556835 \cdot 10^{-15}$
10		$-9.007285883952038 \cdot 10^{-15}$
11		$-9.908014472347242 \cdot 10^{-15}$
12		$-1.0808743060742447 \cdot 10^{-14}$
13		$-1.170947164913765 \cdot 10^{-14}$
14		$-1.2610200237532854 \cdot 10^{-14}$
15		...

$p_{\theta_1} =$

	0	
0		0
1		$-9.00728588395204 \cdot 10^{-16}$
2		$-1.8014571767904077 \cdot 10^{-15}$
3		$-2.7021857651856114 \cdot 10^{-15}$
4		$-3.6029143535808155 \cdot 10^{-15}$
5		$-4.503642941976019 \cdot 10^{-15}$
6		$-5.404371530371223 \cdot 10^{-15}$
7		$-6.305100118766426 \cdot 10^{-15}$
8		$-7.205828707161631 \cdot 10^{-15}$
9		$-8.106557295556835 \cdot 10^{-15}$
10		$-9.007285883952038 \cdot 10^{-15}$
11		$-9.908014472347242 \cdot 10^{-15}$
12		$-1.0808743060742447 \cdot 10^{-14}$
13		$-1.170947164913765 \cdot 10^{-14}$
14		$-1.2610200237532854 \cdot 10^{-14}$
15		...

$p_{\theta_2} =$

Figs. 4 and 5 show the dependence of the inclination angles θ_1 and θ_2 of links of the double pendulum (Fig. 1) on time in the case of the initial conditions (3) (Fig. 2).

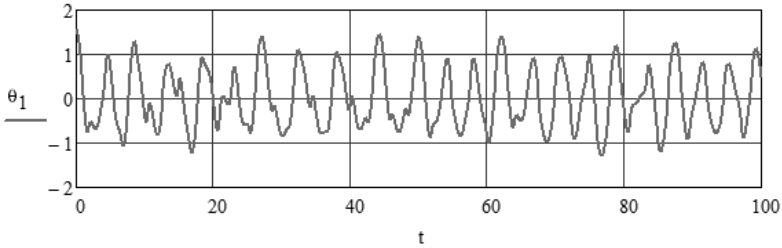


Figure 4. The dependence of inclination angle θ_1 on time in the case of initial values (3).

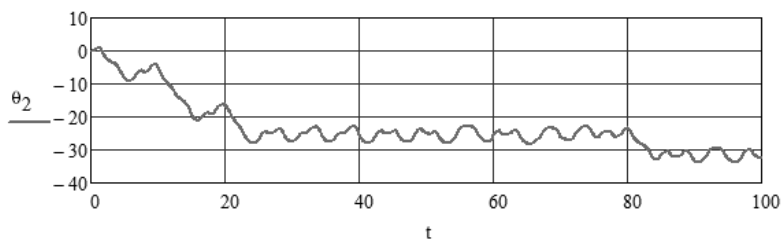


Figure 5. The dependence of inclination angle θ_2 on time in the case of initial values (3).

Figs. 6 and 7 show the dependence of the inclination angles θ_1 and θ_2 of links of the double pendulum (Fig. 1) on time in the case of the initial conditions (4) (Fig. 3).

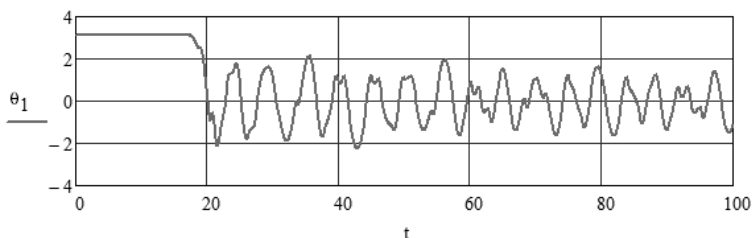


Figure 6. The dependence of inclination angle θ_1 on time in the case of initial values (4).

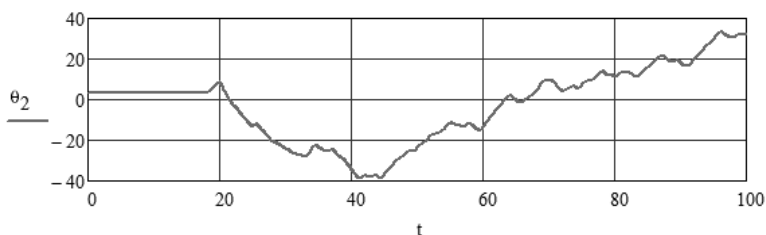


Figure 7. The dependence of inclination angle θ_2 on time in the case of initial values (4).

The diagrams in Figs. 4-7 show that there is chaotic motion of the double pendulum. The video clip <http://www.youtube.com/watch?v=BFIJTAzYdvo> shows a series of frames from this video clip.

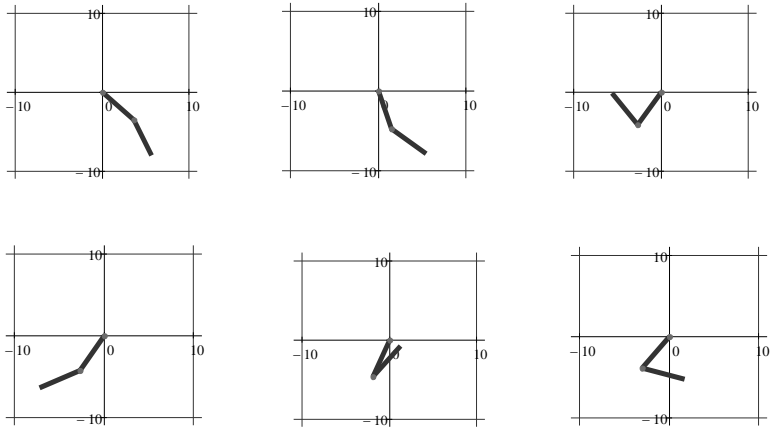


Figure 8. Frames from composed video clip from initial position in Fig. 2.

The video clip <http://www.youtube.com/watch?v=N9eWZR31-VQ> shows the chaotic motion of the double pendulum from initial position in Fig. 3. Fig. 9 shows a series of frames from this video clip

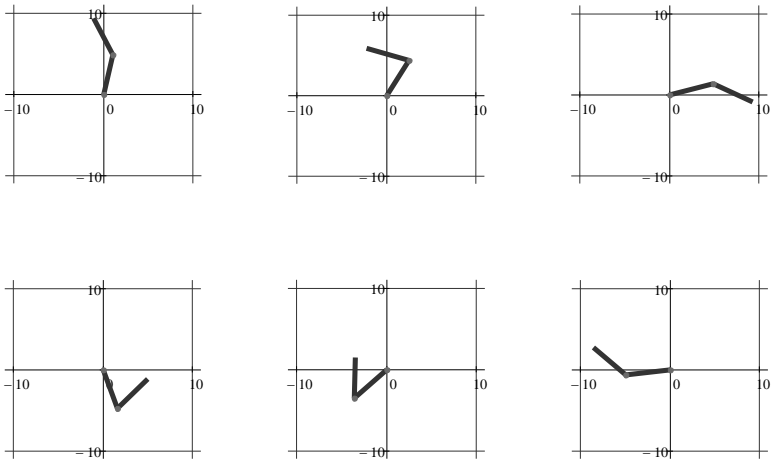


Figure 9. Frames from composed video clip from initial position in Fig. 3.

CONCLUSIONS

This paper shows the features of the Computer Package Mathcad in solution of nonlinear system of differential equations. The nonlinear equations of large oscillations of a double pendulum are solved and the chaotic motion is found out. Note that it is easy to make a physical model of a chaotic double pendulum. Some examples are given in [13]–[18]. Fig. 10 shows a frame from video clip with the chaotic motion of a simple physical pendulum [13].



Figure 10. A frame from video clip, showing chaotic oscillation of the physical model of a double pendulum.

REFERENCES

- [1] <http://scienceworld.wolfram.com/physics/DoublePendulum.html>
- [2] <http://demonstrations.wolfram.com/DoublePendulum/>
- [3] <http://www.maths.tcd.ie/~plynch/SwingingSpring/doublependulum.html>
- [4] <http://www.physics.northwestern.edu/vpl/mechanics/pendulum.html>
- [5] http://tabitha.phas.ubc.ca/wiki/index.php/Double_pendulum
- [6] http://www.physics.usyd.edu.au/~wheat/dpend_html/
- [7] <http://www.physics.usyd.edu.au/~wheat/sdpend/>
- [8] <http://www.youtube.com/watch?v=Uzlcwt5SKc&NR=1>
- [9] http://www.myphysicslab.com/dbl_pendulum.html
- [10] <http://www.chris-j.co.uk/rott.php>
- [11] <http://freddie.witherden.org/tools/doublependulum/>
- [12] <http://www.imaginary2008.de/cinderella/english/G2.html>
- [13] <http://www.youtube.com/watch?v=8VmTivTut6A>
- [14] <http://www.youtube.com/watch?v=z3W5aw-VKKA>
- [15] <http://www.youtube.com/watch?v=O2ySvbL3-yA>
- [16] <http://www.youtube.com/watch?v=cXRXWv5KMgs>
- [17] <http://www.youtube.com/watch?v=Lz8B2ck9o84>
- [18] <http://www.youtube.com/watch?v=BrMQ7G1DtPw>
- [19] http://en.wikipedia.org/wiki/Double_pendulum
- [20] Ü. Lepik, L. Roots. Teoreetiline mehaanika (In Estonian), 1971, Tallinn, 483 p.
- [21] J. Kirs. Mehaanikaliste süsteemide võnkumised (In Estonian), 1998, Tallinn, 124 p.
- [22] http://www.msmiami.com/custom/downloads/Mathcad14_Users_Guide_English.pdf

Aan, A., Heinloo, M., Aarend, E.
Interactive Computer Aided Learning and
Teaching of Analytical Mechanics
International Journal of Engineering Pedagogy,
1(3), 4 – 8, 2011

Interactive Computer Aided Learning and Teaching of Analytical Mechanics

<http://dx.doi.org/ijep.v1i3.1788>

A. Aan, M. Heinloo and E. Aarend
Estonian University of Life Sciences, Tartu, Estonia

Abstract—The aim of this paper is to introduce a new possibility for learning Analytical Mechanics via internet. This subject belongs to the field of engineering, the theoretical parts of lecture materials are available online in PDF format and have special links to switch on the interactive examples on the worksheets of the Computer Package Mathcad.

Index Terms—computer aided engineering, interactivity, attractiveness, internet, analytical mechanics, Computer Package Mathcad.

I. INTRODUCTION

The digital age has transformed education, both formally in the classroom and permanently in any other environment. Although there are many types of interactive materials that have been used in learning for decades, in most cases interactive learning materials are thought of as those that are done on a computer. Many of these materials are made available over the internet, although some are distributed in the form of software [1].

Interactive learning is most commonly defined into three distinct types. These learning types are grouped based on the types of interaction in which they engage students. The first, learner-content, is a type of teaching where the student interacts solely with the facts, readings and information. In the second style, learner-instructor, the primary interaction is with the instructor. The third style is called learner-learner, and this is where the student primarily interacts with his peers to learn new material [2, 3].

U.S. Department of Education report 2009 showed that the most effective interactive learning occurs when all three types of interaction are used [2].

Interactive learning is the counterpart of lecture-type learning. It is the active learning process as opposite to the passive system of a lecture-type. In interactive learning, the students use tangible objects to acquire information. Teachers do not directly pass the information to them. Students acquire the information themselves by allowing them to discover it. Of course, guidance by teachers is necessary. They still provide initial information to the students [4].

In interactive environment students are engaged with the materials rather than simply memorizing the information, the learning is deeper and more lasting. With more engagement student spent more time on the learning task [2]. In interactive learning materials student is in control of the progress of the lesson to some degree. This means in individual learning the learner can make his own pace and studying style of him. In many schools and universities the teachers have lack of time and are unable to give dedicated attention to individual students for very long.

Interactive materials can help provide learning experience without the need for continuous teacher intervention [1].

Engineering teaching material has to be attractive and interactive to make students research technical problems. Attractive learning material means that it is visualized by using many schemes, figures, and animations. Students will understand learning materials better if they can actively engage in the examples of problem-solving via computer screen and change relevant parameters, equations, and simulate the motions. These are hands-on learning materials on the computer. The students can approach to attain information through hands-on interactive experience by using the computer.

There are articles available about interactive learning opportunities in other subjects. For example, Maxima Software – a tool for developing online applications intended for interactive solutions of the examples in Control Theory by K. Zakova [5]. The advantages of the Maxima software include its online availability via internet for all interested users any time, and it can be used locally on the desktop computer or in the notebook. For all technical universities devoted to electrical engineering can use Maxima for computations like useful instrument in an educational process mainly in online and distance forms of education [5]. Also in mathematics we can find interactive learning materials. Heinloo [6] and Talman [7] have made e-courses of mathematics that are interactive and visualized with figures and animations. Heinloo [6] used interactive Mathcad worksheets for lecture notes, examples and exercises. Also there are the links to the video clips, which provide a student with an opportunity to watch and review the example problem solutions at home.

From internet we can find lot of interactive learning materials for different subjects [8, 9, 10].

This paper introduces interactive learning materials on Analytical Mechanics, composed in the Institute of Technology of Estonian University of Life Sciences in Estonian language [11]. These interactive materials are mostly learner-instructor type, but on the computer and over the internet they are also considered learner-content learning material.

II. MATERIALS AND METHODS

Main text of interactive learning materials have been composed by the program Microsoft Word [12] and converted to PDF (Portable Document Format) [13] format. In PDF format all the linked citations work normally as defined. The figures have been composed by using program Adobe Illustrator [14] with occasional addition of pictures. Interactive examples have been composed on the worksheets of the Computer Package Mathcad. Main text

in PDF and Mathcad files are connected with links and are available in Estonian e-Learning Development Centre repository [15].

III. ON VISUALIZATION OF LEARNING MATERIAL

Colorful and, where possible, lifelike figures are used to make the material more attractive for students (Fig. 1). Some of examples in the learning materials are visualized by video clips, for example [16].

IV. INTERACTIVE LEARNING MATERIAL

If the learning materials are on the computer, student can use program features like search, zoom, copy, etc. that accentuate their interactivity.

In terms of collaboration with other computer program features, it is possible to make learning material more interactive by using inside the text links to citations or equation numbers. This gives an opportunity to move inside the text and switch between linked parts on different pages.

Fig. 2 shows a part of the contents of learning material [18] where clicking on the word "Näide 2.6" leads to the page with the solution of the example 2.6

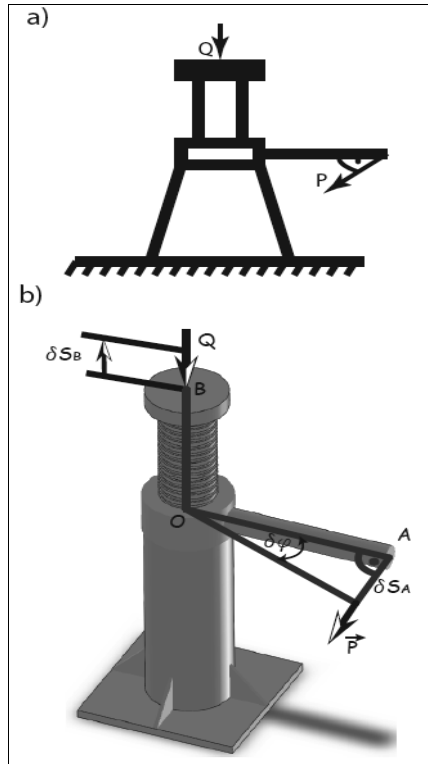


Figure 1. Comparison of traditional (a) [17] and lifelike (b) [18] screw jack calculation figure

In Fig. 3 we can see an example (Näide 2.6), where mass A is connected with cylinder B over wheel O by rope. Cylinder B is moving down and pulling mass A downwards. At the same time cylinder B is spinning off the rope. The question is - what is the acceleration of point C.

In the problem solution (Fig. 4) we can see that one of the equations that has been used is Lagrange equations (Lagrange'i võrrandid) and in the main text it is equation 2.40. Clicking on equation number leads to the explanation (Fig. 5) of the Lagrange equations (Lagrange võrrandid) in the main text.

SISUKORD (contents)	
SISSEJUHATUS	6
1. MEHAANIKA PRINTSIIBID	8
.....	
2.6. Lagrange'i funktsioon	48
Näide 2.5.	48
Näide 2.6. (example)	50

Figure 2. Links in the contents

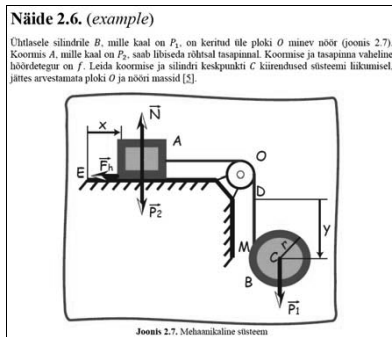


Figure 3. The mechanical system in the example

Lahendus (solution)

Süsteemil on kaks vabadusastet. Valime üldistatud koordinaatideks koormise A kauguse x tasapinna mingist punktist E ja silindri tsentri kauguse y nõõri mingist punktist D ($q_1 = x, q_2 = y$). Antud süsteemi Lagrange'i võrranditeks (equation 2.40) on

$$\frac{d}{dt} \left(\frac{\partial T}{\partial \dot{q}_1} \right) - \frac{\partial T}{\partial q_1} = Q_1,$$

Figure 4. A part of solution of the example problem

If a student wishes to learn more about Lagrange equations, he or she will be directed to corresponding literature by clicking on the citation (Fig. 6).

If the literature is available on the internet, the student can continue from there by using relevant internet addresses. The name of the book can be connected with links to library internet catalog. In Estonia there is library e-catalog Ester that shows the quantity and availability of books in library [19].

Let us consider an interactive example about physical pendulum on Mathcad [20] worksheet to which leads a special link in the main text (Fig. 7).

Lagrange teist tüüpi võrrandeid on k tükki, st sama palju kui on süsteemil vabadusastmeid [3, 5, 6]

$$\frac{d}{dt} \left(\frac{\partial T}{\partial \dot{q}_1} \right) - \frac{\partial T}{\partial q_1} = Q_1$$

$$\frac{d}{dt} \left(\frac{\partial T}{\partial \dot{q}_2} \right) - \frac{\partial T}{\partial q_2} = Q_2 \quad (2.40)$$

$$\frac{d}{dt} \left(\frac{\partial T}{\partial \dot{q}_k} \right) - \frac{\partial T}{\partial q_k} = Q_k$$

Lagrange teist tüüpi võrrandite arv on minimaalne, mis on vajalik süsteemi liikumise määramiseks. Lagrange teist tüüpi . . .

Figure 5. A part in main text with Lagrange equations

KIRJANDUS (literature)

1. TTÜ Eesti Inseneripedaagooika Keskus. Kätesaadav: <http://www.ttu.ee/ttu-eesi-inseneripedaagooika-keskus/> (04.05.2011).
2. Topnik, E. Teoreetiline mehaanika ülesannetest IV. Analüütiline mehaanika. – Tallinn: TPI, 1987. – 160 lk.
3. Lepik, Ü., Roots, L. Teoreetiline mehaanika. – Tallinn: Valgus, 1971. – 484 lk.
4. Topnik, E. Teoreetiline mehaanika IV. Analüütilise mehaanika metoodiline materjal. – Tallinn: TPI, 1985. – 68 lk.
5. Butenin, N., Lunts, J., Merkin, D. Teoreetiline mehaanika. Džnaamika. – Tallinn: Valgus, 1986 – 552 lk.

Figure 6. Literature from main text

Näide 2.5. (example)

Kasutades Lagrange'i võrrandeid koostada füüsikalise pendli võnkumiste võrrandid (joonis 2.6.) Kus P on pendli kaal ja $2l$ pendli pikkus [6].

Joonis 2.6. Füüsikaline pendel

Figure 7. A physical pendulum in the example

Fig. 8 shows the first possible derivation of the equations of motion of physical pendulum in the main text.

Fig. 9 shows the second possible derivation of the equations of motion of physical pendulum, and the link leading to the interactive example on the worksheet of Mathcad.

On Mathcad worksheet a learner can visualize the motion of pendulum by graphs (Fig. 10). A learner can also change the values of inclination angle φ and angular velocity φ' at the initial moment $t = 0$ and observe what happens on figures.

On the worksheet of Mathcad a learner can use controls like slider to define the parameters of pendulum. Fig. 11 shows the slider, defining the length of the pendulum.

Lahendus (solution)

Pendli on üks vabadusaste ja asendi määrab nurk φ . Järelikult $q_1 = \varphi$. Anname nurgale φ positiivse juurdexkavu $\delta\varphi$, et sellel nihkel teeb 160d nimilt raskusjõud P , siis $\delta A_1 = (-P \cdot l \cdot \sin \varphi) \delta\varphi$. Seega $Q_1 = -P \cdot l \cdot \sin q_1$. Pendli kinetiline energia saame valemist (vt. lk. 47)

$$T = \frac{1}{2} \omega^2 \text{ ehk } T = \frac{l \omega^2}{2}$$

Lagrange'i võrrand omab antud juhul kuju

$$\frac{d}{dt} \left(\frac{\partial T}{\partial \dot{q}_1} \right) - \frac{\partial T}{\partial q_1} = Q_1$$

Kuna kinetiline energia T ei sõltu nurgast φ , siis arvutus annab, et

$$\frac{\partial T}{\partial q_1} = 0, \quad \frac{\partial T}{\partial \dot{q}_1} = l_0 \cdot \dot{q}_1, \quad \frac{d}{dt} \left(\frac{\partial T}{\partial \dot{q}_1} \right) = l_0 \cdot \ddot{q}_1$$

Asendades saadud suhtused Lagrange'i võrrandisse saame

$$l_0 \cdot \ddot{q}_1 = -P \cdot l \cdot \sin q_1$$

Figure 8. Derivation of equation of motion for a physical pendulum

Kuna jõud P on potentsiaalne, võib kasutada ka võrrandeid (2.44). Summates z -telje vertikaalselt üles, saame potentsiaalseks energiaks $\Pi = Pz = -P \cdot l \cdot \cos \varphi$. Kasutades Lagrange'i funktsiooni (2.42)

$$L = \frac{l_0 \cdot \dot{q}_1^2}{2} - P \cdot l \cdot \cos q_1$$

Leiame osatuletised

$$\frac{\partial L}{\partial q_1} = -P \cdot l \cdot \sin q_1, \quad \frac{\partial L}{\partial \dot{q}_1} = l_0 \cdot \dot{q}_1, \quad \frac{d}{dt} \left(\frac{\partial L}{\partial \dot{q}_1} \right) = l_0 \cdot \ddot{q}_1$$

Asetades tulemused Lagrange'i võrrandisse, saame sama tulemuse, mis eelnevalt

$$l_0 \cdot \ddot{q}_1 + P \cdot l \cdot \sin q_1 = 0$$

Mathcadi interaktiivne näide. (Mathcad interactive example)

Figure 9. Link to Mathcad interactive example [21]

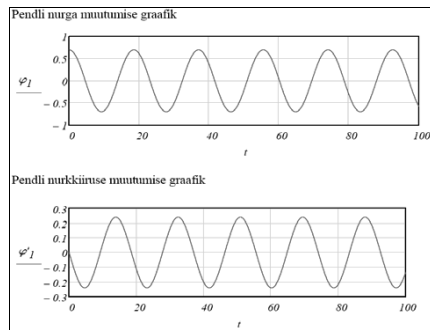


Figure 10. Pendulum angle (upper) and angular velocity (lower) change

PAPER
INTERACTIVE COMPUTER AIDED LEARNING AND TEACHING OF ANALYTICAL MECHANICS

- [19] E-catalog for Tartu libraries. Available at: <http://tartu.ester.ee/search>, Date accessed: 10.06.2011.
- [20] PTC Mathcad, Available at: <http://www.ptc.com/products/mathcad/index-v2.htm>, Date accessed: 10.06.2011.
- [21] A. Aan, M. Heinloo, Näide 4.1, Available at: http://www.e-ope.ee/download/euni_repository/file/1592/N%C3%A4ide%204.1.xmcd?download=true, Date accessed: 10.06.2011.
- [22] A. Aan, Pendulum, Available at: <http://www.youtube.com/watch?v=Ag2MU5tMXj4>, Date accessed: 11.06.2011.
- [23] A. Aan, M. Heinloo, Double Pendulum, Available at: http://www.e-ope.ee/download/euni_repository/file/1592/Double%20pendulum.xmcd?download=true Authors, Date accessed: 22.06.2011.

AUTHORS

A. Aan is with the Institute of Technology, Estonian University of Life Sciences, Kreutzwaldi 64, 51014, Tartu, Estonia (e-mail: aare.aan@emu.ee).

M. Heinloo is with the Institute of Technology, Estonian University of Life Sciences, Kreutzwaldi 64, 51014, Tartu, Estonia (e-mail: mati.heinloo@emu.ee).

E. Aarend is with the Institute of Technology, Estonian University of Life Sciences, Kreutzwaldi 64, 51014, Tartu, Estonia (e-mail: dmmd@emu.ee).

Received 31 August 2011. Published as resubmitted by the authors 26 September 2011.

Aan, A., Heinloo, M.
On creative teaching of engineering mechanics
Annals of DAAAM for 2011 and Proceedings, 1081 – 1082, 2011

ON CREATIVE TEACHING OF ENGINEERING MECHANICS

HEINLOO, M[atij] & AAN, A[are]

Abstract: This paper shows how to use the features of the Computer Package Mathcad for creative teaching of students in engineering mechanics by using its interactive worksheets and visualization the results of computations. As examples of visualization of the problems of engineering mechanics the simulations of motion of virtual four bar linkage, material point on the elliptical trajectory and large oscillations of a virtual double pendulum are considered.

Key words: creativity, interactivity, visualization, engineering mechanics, double pendulum

1. INTRODUCTION

The subjects of engineering mechanics contains a lot of formulas that are dead for engineering students before their visualization by numerical results of computations, graphs, their animations and simulations the motion of virtual objects.

Creative teaching method of engineering mechanics is based first of all on the interactive worksheets of computer packages. On these worksheets a student can change different parameters and initial conditions for studying virtual mechanical objects and make his own simulations of their motions or animations of the figures and examine these. The positive outcome of this method is that students have the possibility for more deep understanding of principles of mechanics. Negative outcome is the dependence of students from computers and special programs.

The purpose of this paper is to show how the Computer Package Mathcad (PTC Corporate, 2011) can be used for creative teaching of engineering mechanics.

2. ON VISUALIZATION THE MOTION OF A FOURBAR

Fig. 1 shows a frame of the video clip (Four bar linkage, 2011) that simulates the motion of a virtual four bar linkage (Norton, 1999) with a con-rod's curve.

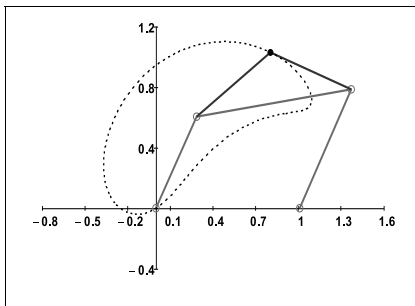


Fig. 1. A four bar linkage with a con-rod's curve

3. ON VISUALIZATION THE MOTION OF A POINT

Fig. 2 shows a frame from another video clip (Kinematics of a Point, 2011) that simulates the motion of a material point on the elliptical trajectory (Targ, 1988). This frame presents the circle of curvature at the point of trajectory, the centre of the curvature, the evolute that draws the centre of curvature and the arrows proportional to the real velocities and accelerations.

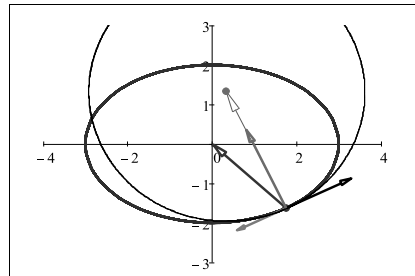


Fig. 2. The elliptical trajectory of the material point, its evolute, circle of curvature, vectors of velocity the accelerations of the moving point and the vector connecting moving point with the centre of curvature

4. ON VISUALIZATION THE MOTION OF A DOUBLE PENDULUM

Motion of a double pendulum can be modeled by the equations of Lagrange of second order or by the equations of Hamilton. It appears that large oscillations of a double pendulum are chaotic. A lot of results on study the double pendulums one can find on the different web sites, for example (Neumann, 2004; Wolfram demonstrations project). The real model of double pendulum is present, in video clip (High performance double pendulum, 2009). A double pendulum is presented in Fig. 3

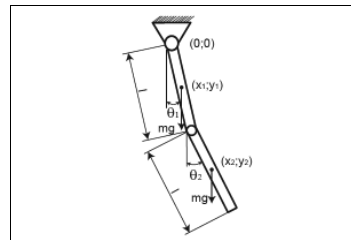


Fig. 3. A double pendulum

lengths l and weights mg , where g is the acceleration. The mathematical model in the Hamilton form, describing large oscillations of the double pendulum is (Wikipedia, 2011)

$$\begin{aligned} \dot{\theta}_1 &= \frac{6}{m l^2} \frac{2 p_{\theta_1} - 3 p_{\theta_2} \cos(\theta_1 - \theta_2)}{16 - 9 \cos^2(\theta_1 - \theta_2)}, \\ \dot{\theta}_2 &= \frac{6}{m l^2} \frac{8 p_{\theta_2} - 3 p_{\theta_1} \cos(\theta_1 - \theta_2)}{16 - 9 \cos^2(\theta_1 - \theta_2)}, \\ \dot{p}_{\theta_1} &= -\frac{1}{2} m l^2 \left(\dot{\theta}_1 \dot{\theta}_2 \sin(\theta_1 - \theta_2) + 3 \frac{g}{l} \sin(\theta_1) \right), \\ \dot{p}_{\theta_2} &= -\frac{1}{2} m l^2 \left(-\dot{\theta}_1 \dot{\theta}_2 \sin(\theta_1 - \theta_2) + \frac{g}{l} \sin(\theta_2) \right), \end{aligned} \quad (1)$$

where θ_1 and θ_2 are generalized co-ordinates (Wikipedia, 2011), or inclination angles, of the double pendulum (Fig. 3) and

$$\begin{aligned} p_{\theta_1} &= \frac{1}{6} m l^2 (8 \dot{\theta}_1 + 3 \dot{\theta}_2 \cos(\theta_1 - \theta_2)), \\ p_{\theta_2} &= \frac{1}{6} m l^2 (2 \dot{\theta}_2 + 3 \dot{\theta}_1 \cos(\theta_1 - \theta_2)), \end{aligned}$$

are the generalized impulses (Lepik & Roots 1971) of the double pendulum.

Let us assume that the special solution of the equations (1) satisfies the following initial conditions:

$$\theta_1(0) = \theta_{10}, \theta_2(0) = \theta_{20}, p_{\theta_1}(0) = p_{\theta_{10}}, p_{\theta_2}(0) = p_{\theta_{20}}, \quad (2)$$

where $\theta_{10}, \theta_{20}, p_{\theta_{10}}, p_{\theta_{20}}$ are constants. Let us consider the initial position of the double pendulum, shown in Fig. 4 and assume that the motion of double pendulum begins without initial angular velocities.

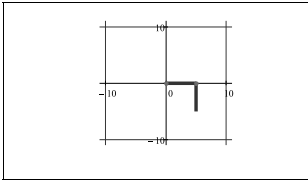


Fig. 4. First initial position of the double pendulum

This assumption means that in the initial conditions (2) the constants must have the following values

$$\theta_{10} = \frac{\pi}{2}, \theta_{20} = 0, p_{\theta_{10}} = 0, p_{\theta_{20}} = 0. \quad (3)$$

The system of equations (1) under conditions (2), (3) (Fig. 4) was solved on the worksheet of the Computer Package Mathcad by using the numerical algorithm of Runge-Kutta.

The computations were made for $l = 5, m = 1, g = 9.807$ in the case of initial values (3) and visualized in Figs. 5 and 6.

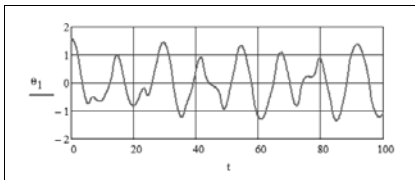


Fig. 5. The dependence of inclination angle θ_1 on time in the case of initial values (3) (Fig. 4)

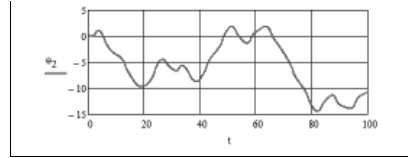


Fig. 6. The dependence of inclination angle θ_2 on time in the case of initial values (3) (Fig. 4)

The diagrams in Figs 5 – 6 and the video clip (Physical double pendulum, 2011) show the chaotic motion of double pendulum. Fig. 7 shows several frames from this video clip

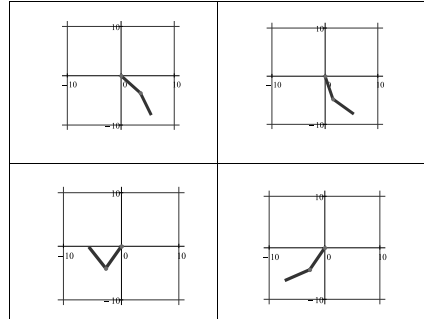


Fig. 7. Frames from composed video clip from initial position in Fig. 4

5. CONCLUSIONS

The enrichment of engineering mechanics by the features of the information technology increases the efficiency of studying different subjects of engineering mechanics and makes teaching process more interesting both for students and teachers.

6. REFERENCES

- Norton, R. L. (1999). *Design of Machinery, An Introduction to the Synthesis and Analysis of Mechanisms and Machines*, Second edition, McGraw-Hill, ISBN , Boston
- Neumann, E. (2004) Double pendulum, http://www.myphysicslab.com/dbl_pendulum.html, Accessed on: 2011-02-13
- PTC Corporate. (2011). Mathcad, <http://www.ptc.com/products/mathcad/>, Accessed on: 2011-01-13
- Targ, S. (1988). *Theoretical Mechanics*, Moscow
- Lepik, Ü; Roots, L. (1971). *Theoretical Mechanics*, Tallinn
- *** (2011) Wikipedia. Double pendulum, http://en.wikipedia.org/wiki/Double_pendulum, Accessed on: 2011-03-03
- *** Wolfram demonstrations project. Double pendulum, <http://demonstrations.wolfram.com/DoublePendulum/>, Accessed on: 2011-02-13
- *** (2011) Kinematics of a Point, <http://www.youtube.com/watch?v=zFbVcd4GOJw>, Accessed on: 2011-01-17
- *** (2011) Four bar linkage, <http://www.youtube.com/watch?v=GgEra0JPoDU>, Accessed on: 2011-01-15
- *** (2011) Physical double pendulum, <http://www.youtube.com/watch?v=BFIJTAzYdvo>, Accessed on: 2011-03-13
- *** (2009) High performance double pendulum, <http://www.youtube.com/watch?v=z3W5aw-VKKA>, Accessed on: 2011-02-13

Aan, A., Heinloo, M., Aarend, E., Mikita, V.
Analysis of four-stroke cycle internal combustion
V-engine in Mathcad environment
Proceedings of 8th International Conference of
DAAAM Baltic Industrial Engineering, 389 – 394, 2012

ANALYSIS OF FOUR-STROKE CYCLE INTERNAL COMBUSTION V-ENGINE IN MATHCAD ENVIRONMENT

Aan, A., Heinloo, M., Aarend, E., Mikita, V.

Abstract: *This paper presents the method and the results of numerical analysis of the virtual model of four-stroke cycle internal combustion V-engine on the worksheet of the Computer Package Mathcad, provided that a crankshaft has constant (load mode) angular velocity and its pistons are loaded by pressures according to the indicator diagram for four-stroke cycle engines. The kinematic and dynamic analysis of V-engine is based on the publication by Lepikson (1998) [1]. Present article also contains a short review of papers that use the Computer Package Mathcad for the analysis of mechanisms and in teaching engineering subjects. The method presented in this paper can be used primarily in teaching process of engineering subject "Mechanics of Machinery" and by engineers of internal combustion engines.*
Key words: Mechanics of Machinery, V-engine, Mathcad, kinematics, dynamics.

1. INTRODUCTION

Advances in computer technology have opened new possibilities to solve engineering problems that require accurate composition of equations and using calculation methods, which are unique for every problem. Virtual reality-based methods allow verifying obtained solutions and simulating the motion of mechanical systems on computer screen that speeds up getting correct solutions, thereby reducing time and costs of product development.

There are several computer package environments (Matlab, Mathematica, Mathcad etc.) that can be used in teaching engineering subjects, to create virtual models for

mechanical systems and to simulate their motion. The Computer Package Mathcad has been used to study the load distribution on the blade of a helicopter rotor [2], to compose the virtual model for planar linkage [3], to create a virtual model for a disk-riding tool and simulation its motion [4], to simulate the motion of fertilizers particles on the spreading disk of a disk spreader [5], to generate the virtual models of four-bars [6], to compose a virtual model for stone protector and simulation its motion [7], to visualize the solutions of problems in engineering mechanics [8] to compose an interactive e-course of engineering analytical mechanics [9], to solve the examples for theoretical mechanics [10].

Common configurations of internal combustion engine are V-, RV-, W- and in-line [11]. This paper presents the method and the results of numerical analysis of the virtual model of four-stroke cycle internal combustion V-engine on the worksheet of Computer Package Mathcad. Special video clip is composed to simulate and verify the motion of the virtual model of V-engine [12].

The method and the results presented in this paper can be used first of all in teaching process of engineering subject "Mechanics of Machinery" and also by engineers in the design of internal combustion engines.

2. THE KINEMATICS SCHEME OF V-ENGINE

The kinematic scheme of V-engine is shown in Fig. 1.

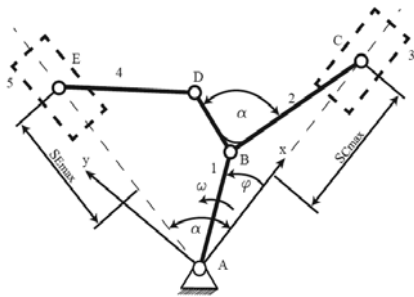


Fig. 1 The kinematic scheme of V-engine

Crankshaft 1 shown in Fig. 1 is supposed to rotate counter clockwise with angular velocity ω . This crankshaft is joined by pivot B to the main connecting rod 2 which moves main piston 3 along track AC in the main cylinder. This connecting rod is also joined by pivot D to the secondary connecting rod 4 that is joined by pivot E to the secondary piston 5 and moves it along the track AE in the secondary cylinder. Constructive angle α between tracks AC, AE and the arms BD, BC of main connecting rod 2 is permanent.

The following V-engine parameters were used in the calculations: lengths of the links $l_{AB}=0.090m$, $l_{BC}=0.322m$, $l_{BD}=0.085m$ $l_{DE}=0.240m$; constructive angle $\alpha=60^\circ$; inside diameters for cylinders $d_s=0.15m$; crankshaft rotation speed $n_m=1000rpm$; masses of links: $m_1=13.7kg$, $m_2=6.25kg$, $m_3=3.6kg$, $m_4=2kg$ and $m_5=3.6kg$. Moments of inertia of links 2 and 4:

$$I_2 = m_2 \cdot 0.174 \cdot l_{BC}^2 kgm^2,$$

$$I_4 = m_4 \cdot 0.083 \cdot l_{DE}^2 kgm^2.$$

Maximum pressure inside the cylinders: $p_{max}=4MPa$.

3. DETERMINATION OF THE POSITIONS OF LINKS

Let us suppose that the origin of the coordinate system Axy is in pivot A (Fig. 1). The x-axis coincides with track AC. The rotation angle of crank AB is φ . Co-ordinates of pivots B and C are

$$x_B = l_{AB} \cdot \cos \varphi \quad (1)$$

$$y_B = l_{AB} \cdot \sin \varphi,$$

$$x_C = x_B + \sqrt{l_{BC}^2 - y_B^2}, \quad (2)$$

$$y_C = 0.$$

Co-ordinates of pivot D can be determined from the following system of equations of restrictions

$$(x_D - x_B) \cdot (x_C - x_B) - (y_D - x_B) \cdot y_B = l_{BC} \cdot l_{BD} \cdot \cos \alpha \quad (3)$$

$$(x_D - x_B)^2 + (y_D - x_B)^2 = l_{BD}^2$$

The first equation in (3) means that during the motion the angle α between arms BD and BC is permanent. The second equation in (3) means that during the motion the distance between pivots B and D is permanent. Co-ordinates of pivot E can be determined from the following system of equations of restrictions

$$y_D = x_E \cdot \tan \alpha$$

$$(x_E - x_D)^2 + (y_E - y_D)^2 = l_{DE}^2 \quad (4)$$

The first equation in (4) means that during the motion pivot E is permanently on track AE. The second equation in (4) means that during the motion the distance between the pivots D and E is permanent. Equations (1), (2) and systems of equations (3), (4) were solved in relation to the values of rotation angle φ of crank AB by using the solve block "Given-Find" of Mathcad. The virtual model in Fig. 2 was composed on Mathcad worksheet by using the results of computations of pivots co-ordinates.

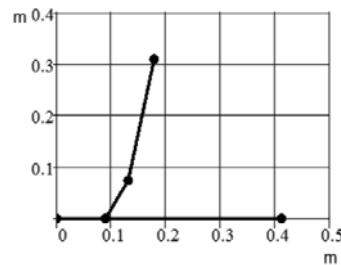


Fig. 2. The virtual model of V-engine

Before composing the video clip with simulation of motion of the composed virtual model in Fig. 2, rotation transformation

was used to turn it to the position (Fig. 3) of the kinematic scheme in Fig. 1.

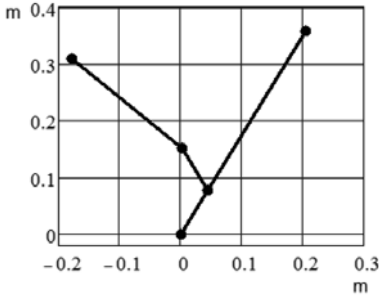


Fig. 3. Virtual model of V-engine, in the position of the scheme in Fig. 1

On the basis of Fig. 3 a video clip [12] simulating the motion of virtual model of V-engine was composed on Mathcad worksheet.

Maximum values of displacements (S) of pivots C (piston 3) and E (piston 5) can be determined by equations

$$S_C = \max_{\varphi} x_C - x_C,$$

$$S_E = \max_{\varphi} \sqrt{x_E^2 + y_E^2} - \sqrt{x_E^2 + y_E^2}.$$

The results of computations are visualized in Fig. 4.

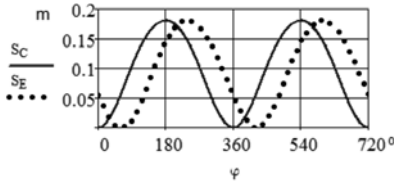


Fig. 4. Maximum values of displacements of the pivots C (main piston 3) and E (secondary piston 5) depending on the values of rotation angle φ of crank AB (Fig. 1)

Experimentally acquired p-V indicator diagram was used to create a diagram where volume (V) values are converted in displacement values in Fig. 5.

Fig. 4 was used to compose four strokes (intake, compression, power, exhaust) in V-engine by the pistons 3 and 5, when the

pressures applied to the pistons change according to the indicator diagram in Fig. 5.

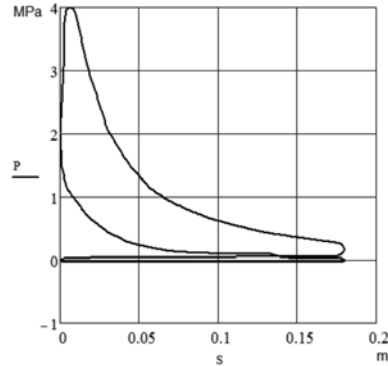


Fig. 5. The indicator diagram for the four-stroke cycle internal combustion engine, where p is the pressure applied to a piston and S is piston displacement

4. DETERMINATION OF THE VELOCITIES OF PIVOTS

The velocity projections of pivot B on the x- and y-axis can be obtained by differentiation of formulas (1)

$$v_{Bx} = -y_B \cdot \omega, \quad v_{By} = x_B \cdot \omega,$$

where

$$x_B = l_{AB} \cdot \cos \varphi, \quad y_B = l_{AB} \cdot \sin \varphi, \quad \omega = \frac{d\varphi}{dt}.$$

The velocity projection of pivot C (main piston 3, Fig. 6) on x-axis can be found out from formula

$$v_{Cx} = v_{Bx} - \frac{y_B \cdot v_{By}}{x_C - x_B}, \quad (5)$$

derived from the formula (2) by time-based differentiation. The results of computations are visualized in Fig. 6.

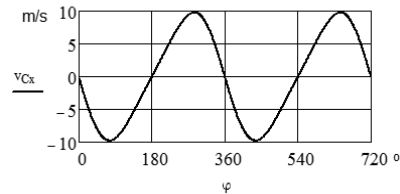


Fig. 6. Pivot C velocity projection v_{Cx} (main piston 3) depending on rotation angle φ

By differentiating the equations (3) and (4) in terms of time one can obtain two linear systems of equations for determining the projections

$$\begin{aligned} v_{Dx} &= \frac{dx_D}{dt}, & v_{Dy} &= \frac{dy_D}{dt}, \\ v_{Ex} &= \frac{dx_E}{dt}, & v_{Ey} &= \frac{dy_E}{dt}, \end{aligned}$$

of the velocity pivots D and E. Composed linear systems of equations were solved on Mathcad worksheet by using inverse matrix method known from linear algebra. The results of computations are visualized in Fig. 7.

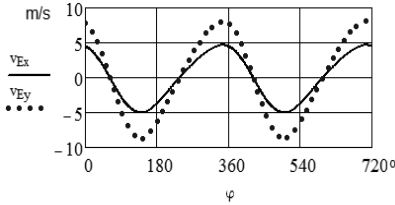


Fig. 7 Pivot E (secondary piston) velocity projections v_{Ex} , v_{Ey} depending on rotation angle φ

5. DETERMINATION OF THE ACCELERATIONS OF PIVOTS

Time-based differentiation of equations (5) gives the following formula to determine the acceleration projection a_{Cx} of pivot C (main piston)

$$a_{Cx} = a_{Bx} - \frac{(v_{By}^2 + y_B \cdot a_{By}) \cdot (x_C - x_B) - y_B \cdot v_{By}' \cdot (v_{Cx} - v_{Bx})}{(x_C - x_B)^2}.$$

The results of computations are visualized in Fig. 8.

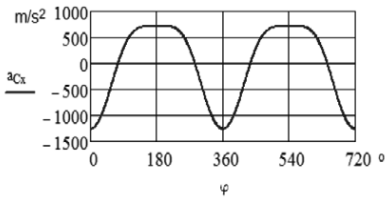


Fig. 8 Pivot C (main piston) acceleration projection a_{Cx} depending on rotation angle φ

When using time-based differentiation of equations (3) and (4) twice one can obtain

two linear equations systems for determining the projections

$$\begin{aligned} a_{Dx} &= \frac{d^2x_D}{dt^2}, & a_{Dy} &= \frac{d^2y_D}{dt^2}, \\ a_{Ex} &= \frac{d^2x_E}{dt^2}, & a_{Ey} &= \frac{d^2y_E}{dt^2}, \end{aligned}$$

where a_{Ex} , a_{Ey} are secondary piston acceleration projections and a_{Dx} , a_{Dy} – the accelerations of the main piston. The results of computations are visualized in Fig. 9.

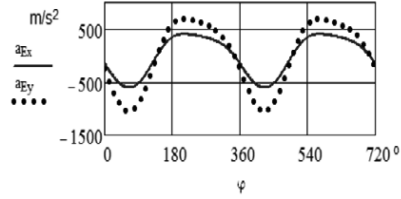


Fig. 9 Pivot E (secondary piston) acceleration projections a_{Ex} and a_{Ey} depending on rotational angle φ

According to [1] links 2 and 4 centres of masses accelerations projections a_{2x} , a_{2y} and a_{4x} , a_{4y} in points x_2 , y_2 and x_4 , y_4 respectively were determined by the following formulas

$$a_{2x} = a_{Bx} + \mu(a_{Cx} - a_{Bx}),$$

$$a_{2y} = (1 - \mu)a_{By},$$

$$a_{4x} = \frac{a_{Dx} + a_{Dx}}{2}, \quad a_{4y} = \frac{a_{Dy} + a_{Dy}}{2},$$

where $\mu=0.27$.

6. DETERMINATION OF THE ANGULAR VELOCITIES AND THE ACCELERATIONS OF LINKS 2 AND 4

Let us consider the following equations:

$$x_E - x_D = l_{DE} \cdot \cos \varphi_4, \quad (6)$$

$$x_B - x_C = l_{BC} \cdot \cos \varphi_2, \quad (7)$$

$$y_E - y_D = l_{DE} \cdot \sin \varphi_4, \quad (8)$$

$$y_B - y_C = l_{BC} \cdot \sin \varphi_2, \quad (9)$$

where φ_4 and φ_2 are the angles between x-axis and connecting links ED (4) and BC (2) accordingly, measured from x-axis counter clockwise. After time-based differentiation of the equations (6) and (9) we have

$$v_{Ex} - v_{Dx} = -l_{DE} \cdot \omega_4 \cdot \sin \varphi_4, \quad (10)$$

$$v_{By} - v_{Cy} = l_{BC} \cdot \omega_2 \cdot \cos \varphi_2, \quad (11)$$

where

$$\begin{aligned} v_{Ex} &= \frac{dx_E}{dt}, & v_{Dx} &= \frac{dx_D}{dt}, \\ v_{By} &= \frac{dy_B}{dt}, & v_{Cy} &= 0, \end{aligned}$$

are the projections of the velocities of pivots E, D, B, C, already computed above.

Substitution of (8) into (10) and (7) into (11) gives

$$v_{Ex} - v_{Dx} = \omega_4(y_D - y_E), \quad (12)$$

$$v_{By} = \omega_2(x_B - x_C). \quad (13)$$

From (12) and (13) we can find the following formulas

$$\omega_2 = \frac{v_{Ex} - v_{Dx}}{y_D - y_E}, \quad \omega_4 = \frac{v_{By}}{x_B - x_C}, \quad (14)$$

that determine the angular velocities of links ED (4) and BC (2) in the case where the positions of pivots and their velocities are known. The results of computations of angular velocities are visualized in Fig 10.

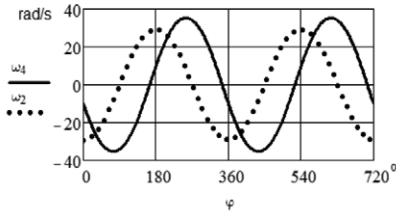


Fig. 10 The dependence of angular velocities ω_2 , ω_4 on rotation angle φ

Time-based differentiation of equations (14) gives the following formulas for determination of angular accelerations of links BC (2) and ED (4).

$$\varepsilon_2 = \frac{a_{By}(x_B - x_C) - v_B(v_{Bx} - v_{Cx})}{(x_B - x_C)^2}, \quad (15)$$

$$\varepsilon_4 = \frac{(a_{Ex} - a_{Dx})(y_D - y_E) - (v_{Ex} - v_{Dx})(v_{Dy} - v_{Ey})}{(y_D - y_E)^2}.$$

The results of computations of angular accelerations are visualized in Fig. 11.

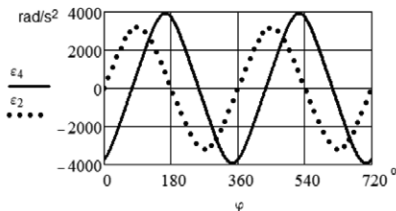


Fig. 11 The dependence of angular velocities ε_2 , ε_4 on rotation angle φ

7. DETERMINATION OF REACTION FORCES

Forces applied to the main piston E (3) and the secondary piston E (5) can be found out by using equations

$$F_C = p_C \frac{\pi d_s^2}{4}, \quad F_E = p_E \frac{\pi d_s^2}{4}.$$

It is supposed that combustion gas pressures are the following

$$\max_{\varphi} p_C \cong \max_{\varphi} p_E \cong 4 \text{ MPa}.$$

It is assumed that the pressures p_C and p_E , applied to the pistons C (3) and E (5) follow the indicator diagram in Fig. 5.

Before calculating the reaction forces it is necessary to determine the dependence of pressures p_C and p_E on rotation angle φ of the crank AB. Found dependencies are visualized in Figs. 12 and 13.

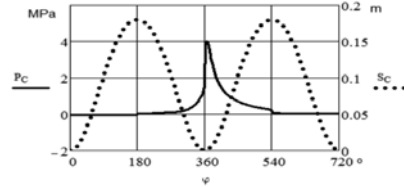


Fig. 12 Displacement S_C of piston C (3) and the pressure p_C in cylinder depending on rotation angle φ

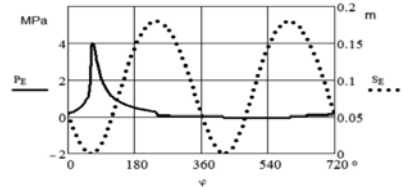


Fig. 13 Displacement S_E of piston C (3) and the pressure p_E in cylinder depending on rotation angle φ

To determine the dynamic reaction forces in pivots and between cylinder walls and pistons, the system of equations on motion for all links was composed according to [13]. Since all accelerations and angular accelerations are determined above, the equations on the motion of links are linear in respect of forces of reaction. The results of computations of reaction forces modules are visualized in Fig. 14.

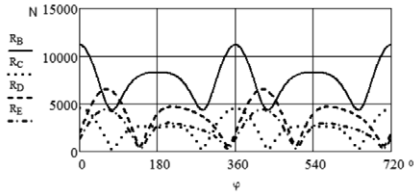


Fig. 14 Reaction forces modules in pivots

8. CONCLUSIONS

1. The Computer Package Mathcad can be considered as a convenient tool for complex analysis of engines.
2. The Computer Package allows the simulation of motion of virtual models of engines.
3. The method presented in this paper can be used in the teaching process of engineering subject "Mechanics of Machinery" and also by engineers of internal combustion engines. This method can also be further developed for more complex and accurate analysis.

9. REFERENCES

1. Lepikson, H. *Design of kinematic scheme for four-stroke internal combustion V-engine (in Estonian)*. Tallinn, 1998, 76 p.
2. Butoescu, V. A vortex model of a helicopter rotor. *INCAS*, 2009, **1**, 23-27.
3. Heinloo, M., Aarend, E., Mägi, M. On The Experience of Mathcad-Aided Analysis of Planar Linkages. *Proc. Tenth World Congress on the Theory of Machines and Mechanisms*. 1999, **1**, 392 – 397.
4. Heinloo, M., Olt J. A Method of Virtual Reality for Creating a Disk-Ridging Tool. *CIGR Ejournal*. 2006, **8**, 21. Available at: <http://www.cigrjournal.org/index.php/Ejournal/article/view/624/618> (05.02.2012).
5. Heinloo, M. Visualization of the working process of a spreading disk of a disk spreader. *Journal of agricultural science*. 2010, **21**, 3-7. Available at: <http://agrt.emu.ee/pdf/20101/heinloo.pdf> (01.02.12).

6. Heinloo, M. Automatic Generation Virtual Models of Fourbars for Visualized e-Courses of Interactive Engineering Mechanics. *Balkan Agricultural Engineering Review*. 2007, **10**.

7. Olt, J; Heinloo, M. Visualization of the Working Process of a Novel Manipulator for a Stone Protector of a Stony Soil Tillage Implement. *Balkan Agricultural Engineering Review*. 2010, **15**.

8. Aan, A., Heinloo, M. On creative teaching of engineering mechanics. *Proc. 22nd International DAAAM World Symposium*. 2011, 1081–1082.

9. Aan, A, Heinloo, M, Aarend, E. Interactive Computer Aided Learning and Teaching of Analytical Mechanics. *Int. J. Eng. Pedagogy (iJEP)*. 2011, **1**, 4-8.

10. Bertjaev, B. D. Mathcad-based *Training in Theoretical Mechanics* (in Russian). Sankt-Peterburg, 2005, 738 p.

11. Pulkrabek, W. W. *Engineering fundamentals of the internal combustion engine*. Prentice Hall, 1997, 411 p.

12. Aan, A., Heinloo, M. Simulation of motion a virtual model of v-engine. Available at: <http://www.youtube.com/watch?v=OyAiXVzfOkI> (01.02.12).

13. Frolov et al. *Theory of mechanism and machines* (in Russian). Moscow, 1987, 496 p.

10. ADDITIONAL DATA ABOUT AUTHORS

MSc (Engn Sc) Aan, Aare (author)
e-mail: aare.aan@emu.ee.

Dr (math) Heinloo, Mati (co-author)
e-mail: mati.heinloo@emu.ee.

MSc (Engn Sc) Aarend, Eino (co-author).

PhD (Engn) Mikita, Villu (co-author)
e-mail: villu.mikita@emu.ee

Institute of Technology,
Estonian University of Life Sciences,
Kreutzwaldi 56, 51014, Tartu, Estonia

Aan, A., Heinloo, M.
Computer based comparison analysis of single and
double-connecting-rod slider-crank linkages
Agronomy Research, 10, 3 – 10, 2012

Computer based comparison analysis of single and double-connecting-rod slider-crank linkages

A. Aan and M. Heinloo

Institute of Technology, Estonian University of Life Sciences, Kreutzwaldi 56, EE51014 Tartu, Estonia; e-mail: aare.aan@emu.ee

Abstract. This paper presents the results of comparative numerical analysis of single and double-connecting-rod slider-crank linkages on the worksheet of Computer Package Mathcad. On the base of composed virtual models of both linkages the motion of the slider (piston) in these linkages is studied thoroughly. This paper has the links to the video clips, comparing the motions of single and double-connecting-rod slider-crank linkages and visualizing the change of vectors of velocities and accelerations in the pivot, where connects two links of double connecting rod. Concluded, that the motion of the slider (piston) and the force of reaction to the track of slider (wall of a cylinder) in these linkages is quite different.

Key words: machine and mechanism theory, linkages, internal combustion engines.

Introduction

Slider-crank linkages can be used in pumps, compressors, internal combustion engines etc. A typical scheme of one cylinder of a four-stroke internal-combustion engine with single connecting rod crank-slider linkage is shown in Fig. 1 (Merriam-Webster, 2006).

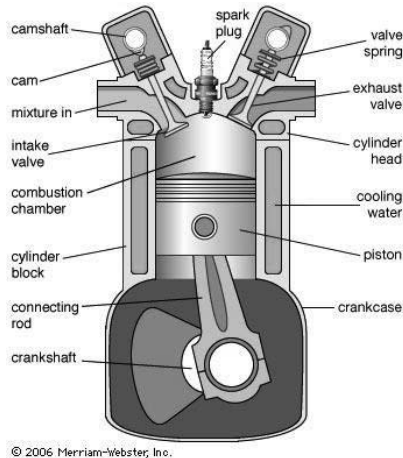


Fig. 1. Cross section showing one cylinder of a four-stroke internal-combustion engine.

A review of different internal combustion engines using single-connecting-rod crank-slider mechanism with multiple cylinders is given in Automotive Handbook (1996).

Mederer (Evert, 2003) proposed to use a double-connecting-rod linkage (Fig. 2) in combustion engines.

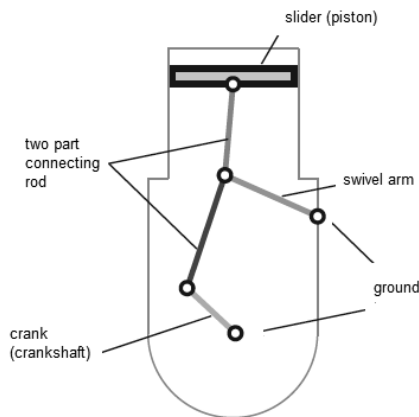


Fig. 2. The scheme of a double-connecting-rod linkage, proposed by Mederer to use in internal combustion engines.

Double-connecting-rod linkage (Fig. 2) consists of ground (cylinder), crank (on crankshaft), two part connecting rod, slider (piston) and a swivel arm. By Mederer this mechanism reduces consumption of fuel and lower emissions, because piston will stay relative long times at area of its uppermost position, and in the compression stroke large parts of counter-pressure is taken by swivel arm, that means less input power is needed for turning a crank in the compression stroke.

The aim of this paper is to present the method and results of comparative numerical analysis of single-connecting-rod and double-connecting-rod slider-crank linkages on the worksheet of Computer Package Mathcad, in the case of constant (idle) crank (crankshaft) angular velocity. On the base of composed virtual models of both linkages the motion of the slider (piston) in these linkages will be studied thoroughly. This paper will have also links to two composed video clips. First video clip compares the motions of single-connecting-rod and double-connecting-rod slider-crank linkages with the same maximum displacement of the slider (piston). Second video clip visualizes the changing geometrical vectors of velocities and accelerations in the pivot, where connects two links of double-connecting-rod slider-crank linkage. This video clip compares also the reaction force in the track of sliders (cylinder wall).

Composition of virtual models of linkages

The links OA, AE, and EC of the four-bar OAEC in the structure of double-connecting-rod linkage can rotate around pivots O, A, E and C, whereby pivots O and C are grounded (Fig. 3). For numerical computations let us assume that the lengths of

the links OA, AE and EC are $l_{OA} = 0.3$ m, $l_{AE} = 0.7$ m, $l_{EC} = 0.735$ m accordingly and the coordinates of the pivot C are $x_C = 0.67$ m, $y_C = 0.7$ m. Let us suppose also that the rotational speed of crank OA is $n = 700$ rpm, that means angular velocity $\omega = 73.304$ rad s⁻¹.

The coordinates of pivot A (Fig. 3) can be found out by equations

$$x_A(\varphi) = l_{OA} \cdot \sin \varphi, \quad y_A(\varphi) = l_{OA} \cdot \cos \varphi.$$

The four-bar OAEC has constraints that the distances between pivots A, E and E, C are permanent. Mathematically these constraints means the following system of nonlinear equations of constraints

$$\begin{aligned} (x_E - x_C)^2 + (y_E - y_C)^2 &= l_{EC}^2, \\ (x_E - x_A(\varphi))^2 + (y_E - y_A(\varphi))^2 &= l_{AE}^2, \end{aligned} \quad (1)$$

where φ is the angle of rotation of the crank OA from y-axis clockwise.

The system of equations (1) was solved on the worksheet of Mathcad numerically relative to x_E and y_E (Fig. 3).

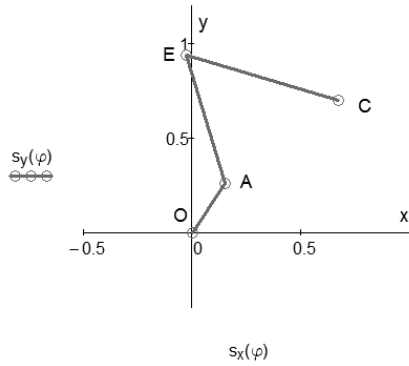


Fig. 3. The virtual model of four-bar OAEC under crank's rotation angle $\varphi = 30^\circ$.

Let us compose the following column vectors

$$s_x(\varphi) = \begin{pmatrix} 0m \\ x_A(\varphi) \\ x_E(\varphi) \\ x_C \end{pmatrix}, \quad s_y(\varphi) = \begin{pmatrix} 0m \\ y_A(\varphi) \\ y_E(\varphi) \\ y_C \end{pmatrix}.$$

Fig. 3 shows the virtual model of linkage OAEC, drawn by these vectors on the worksheet of Mathcad.

Connecting to the pivot E of four-bar in Fig. 3 by a link ED to the pivot pivot D, what is moving along y-axis, we get a virtual model of double-connecting-rod linkage on Figs 2 and 4. Let the length of the link ED be $l_{ED} = 0.7$ m. The y-coordinate of pivot D can be find out from the following equation of restriction

$$y_D(\varphi) = y_E(\varphi) + \sqrt{l_{ED}^2 - x_E(\varphi)^2}. \quad (2)$$

The following vectors

$$s'_x(\varphi) = \begin{pmatrix} x_E(\varphi) \\ 0 \end{pmatrix},$$

$$s'_y(\varphi) = \begin{pmatrix} y_E(\varphi) \\ y_D(\varphi) \end{pmatrix},$$

draw on the worksheet of Mathcad the virtual model of double-connecting-rod crank-slider linkage in Fig. 4a.

To compose the virtual model for typical single-connecting-rod crank-slider linkage in Fig. 4b, we used the following equation of constraint

$$l'_{AD} = \sqrt{(y'_D(\varphi) - y_A(\varphi))^2 + x_A(\varphi)^2}, \quad (3)$$

where l'_{AD} is the permanent length of the link AD in Fig. 4b. In computations were taken $l'_{AD} = l_{AE} + l_{ED} = 1.4$ m. Equation (3) determine the coordinate $y'_D(\varphi)$ of the pivot D by the following formula

$$y'_D(\varphi) = y_A(\varphi) + \sqrt{l_{AD}^2 - x_A(\varphi)^2}.$$

The following vectors

$$ss_x(\varphi) = \begin{pmatrix} 0m \\ x_A(\varphi) \end{pmatrix},$$

$$ss_y(\varphi) = \begin{pmatrix} 0m \\ y_A(\varphi) \end{pmatrix},$$

$$ss'_y(\varphi) = \begin{pmatrix} y'_D(\varphi) \\ y_A(\varphi) \end{pmatrix},$$

draw on the worksheet of Mathcad the virtual model of single-connecting-rod crank-slider linkage in Fig. 4b.

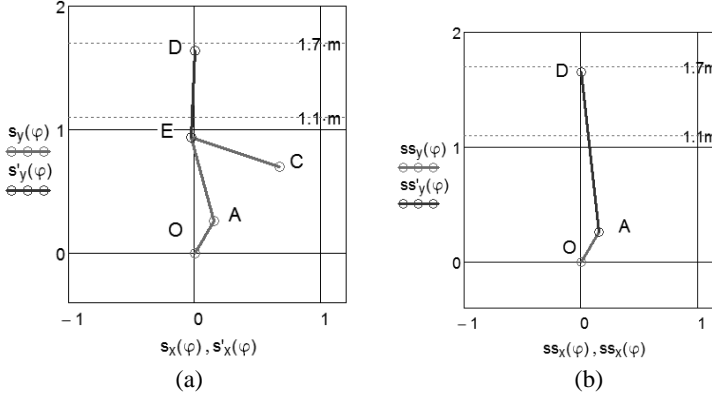


Fig. 4. The virtual models of double-connecting-rod (a) and single-connecting-rod (b) crank-slider linkages under crank's rotation angle $\varphi = 30^\circ$.

Comparison of displacement, velocity and acceleration of a slider (piston)

To compare of displacement, velocity and acceleration, let's give for rotation angle φ the values from 0 with step 0.1 up to $4 \cdot \pi$. This means that the crank OA in Fig. 4 makes two rotations.

According to used assumption, in Fig. 5 at the bottom dead centre (BDC) and the top dead centre (TDC) the pivot D (slider) virtual model displacements for both cases (Fig. 4a and Fig. 4b) are coincidence, but between BDC and TDC displacements are different.

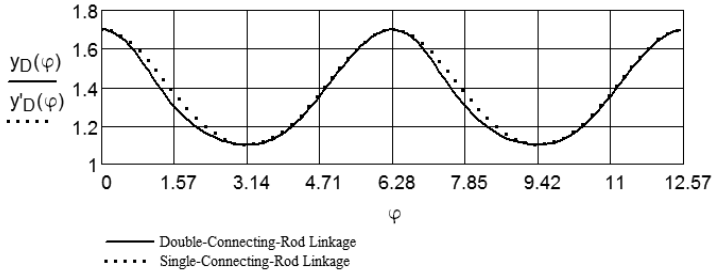


Fig. 5. The Displacement of pivot D (slider) for double-connecting-rod and single-connecting-rod crank-slider linkages dependence from rotational angle φ .

The velocity projections of pivot's D (Fig. 4) are

$$v_{Dy}(\varphi) = \frac{d}{d\varphi} y_D(\varphi) \cdot \omega, \quad v'_{Dy}(\varphi) = \frac{d}{d\varphi} y'_D(\varphi) \cdot \omega.$$

Fig. 6 shows the change of projections of the velocity of the pivot D (Fig. 4) for both virtual models. One can conclude in range of TDC these projections are coincident for both virtual models, but in BTC are not.

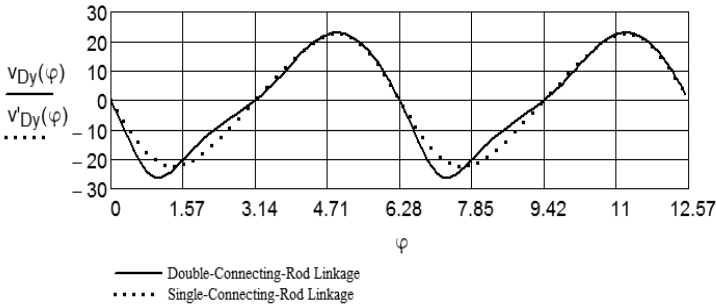


Fig. 6. The velocity of pivot D (slider) for double-connecting-rod and single-connecting-rod crank-slider linkages dependence from rotational angle φ .

The accelerations projections of pivot's D (Fig. 4) are

$$a_{Dy}(\varphi) = \frac{d^2}{d\varphi^2} y_D(\varphi) \cdot \omega^2, \quad a'_{Dy}(\varphi) = \frac{d^2}{d\varphi^2} y'_D(\varphi) \cdot \omega^2.$$

One can conclude from Fig. 7 shows that the projections of accelerations of the pivot D for both virtual models are quite different.

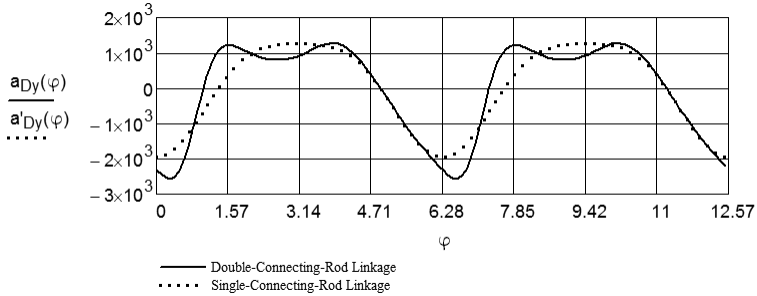


Fig. 7. The accelerations of pivot D (slider) for double-connecting-rod and single-connecting-rod crank-slider linkages dependence from rotational angle φ .

Comparison of angles between the link, connected to the pivot of the slider (piston) and the track of motion

Angles between y-axis (pivot D track) and the links on single connecting rod AD and double connecting rod ED (pressure angle (Kleis, 1988)), can be found out from the equations

$$\beta(\varphi) = a \sin \frac{x_E(\varphi)}{l_{ED}}, \quad \beta'(\varphi) = a \sin \frac{x_A(\varphi)}{l_{AD}}.$$

Fig. 8 shows that the pressure angle β for double-connecting-rod linkage is lower than the correspondent angle β' for single-connecting-rod linkage.

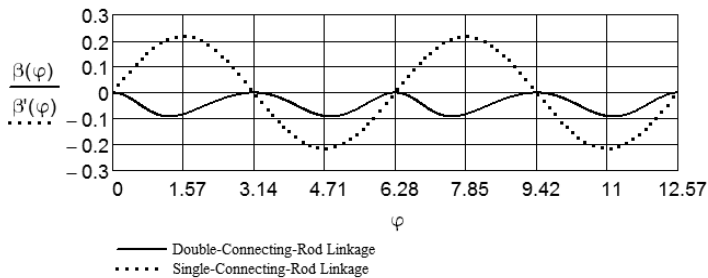


Fig. 8. The pressure angle between the links ED and AD (Fig. 4) relative to the y-axis (track of pivot D) for double-connecting-rod and single-connecting-rod crank-slider linkages dependence from rotational angle φ .

Comparison of the reaction force from the track of slider (the wall of cylinder)

Let's apply force $F_D = 1000$ N to the slider pivot (piston) and take the mass of slider (piston) equal to $m_k = 3$ kg. The equations of motion of the slider (piston) are

$$m_k \cdot a_{Dy}(\varphi) = -F_D + R_E(\varphi) \cdot \cos \beta(\varphi), \quad 0 = R_{Dx}(\varphi) + R_E(\varphi) \cdot \sin \beta(\varphi), \quad (4)$$

where $R_E(\varphi)$ – is the reaction force, applied from link ED in Fig. 4 (a) to the pivot D, $R_{Dx}(\varphi)$ – is the projection of the reaction force, applied to the track of slider (cylinder wall).

From equations (4) one can get the following formula for determination the projection of the reaction force $R_{Dx}(\varphi)$

$$R_{Dx}(\varphi) = (m_k \cdot a_{Dy}(\varphi) + F_D) \cdot \tan \beta(\varphi).$$

Analogous formula is valid for the case Fig. 4b

$$R'_{Dx}(\varphi) = (m_k \cdot a'_{Dy}(\varphi) + F_D) \cdot \tan \beta'(\varphi).$$

From Fig. 9 follows that the average reaction force in the case double-connecting-rod linkage is lower than in the case of single-connecting-rod linkage that means less friction between slider and track (piston and cylinder wall) in double-connecting-rod linkage.

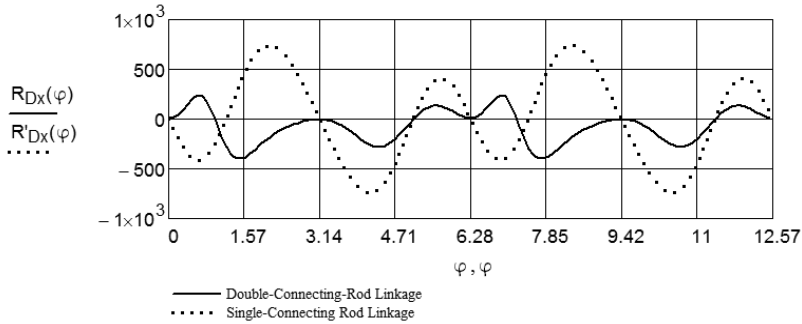


Fig. 9. The projections of the reaction forces between the slider and its track (piston and cylinder) for double-connecting-rod and single-connecting-rod crank-slider linkages dependence from rotational angle φ .

Comparison of visualizing video clips

The Computer Package Mathcad allows also compose of video clips. To visualize the obtained solution and to verify it, two video clips were made. The video clip (Aan & Heinloo, 2012-1), composed on the base of Figs 4 and 5, show visually the change of co-ordinate of pivot D in accordance with motion of corresponding linkage. The video clip (Aan & Heinloo, 2012-2), composed on the base of Figs 4 and 9, shows visually the dependence of reaction force between the link D and the track of it (piston and cylinder wall) in accordance with motion of corresponding linkage. Also on that video clip is visualized change of geometrical vectors of velocity and acceleration of the pivot D and pivot E. These vectors were composed by using the special program on the worksheet of Mathcad, presented by Bertjajev (2005).

Conclusions

- The motion of the slider (piston) in double-connecting-rod linkage and single-connecting-rod linkage is quite different.
- The slider (piston) of double-connecting-rod linkage has lower reaction force on the track of motion (cylinder wall). That means the force, applied to the slider (piston) in double-connecting-rod linkage makes more useful work. Therefore, the motor based on double-connecting-rod linkage could have lower consumption of fuel and lower emissions than the motor with single-connecting-rod linkage.
- The Computer Package Mathcad can be used as convenient tool for composition of video clips for visualization and verify the obtained solution.
- The method and the results of study may be used by teachers of engineering subject 'Machine and Mechanism Theory' and by automobile engineers.

References

- Merriam-Webster. 2006. Internal combustion engine. Available at: <http://www.merriam-webster.com/concise-images/72180.htm> (02.02.2012).
- Robert Bosch GmbH. 1996. *Automotive Handbook 4th edition*. Stuttgart, pp. 892.
- Evert, A. 2003. Buckle- and Double-Connecting-Rod. Available at: <http://www.evert.de/ef774e.htm> (02.02.2012).
- Kleis, I. 1988. *Applied mechanics*. Valgus. Tallinn, pp. 423. (in Estonian).
- Aan, A., Heinloo, M. 2012. Comparison of piston displacements. Available at: <http://youtu.be/LG2h8oijjIU> (02.02.2012).
- Aan, A., Heinloo, M. 2012. Comparison of piston velocities accelerations and reactions. Available at: <http://youtu.be/QvyZAo-Q3Rk> (02.02.2012).
- Bertjajev, B. D. 2005. *Mathcad-based Training in Theoretical Mechanics*. Sankt-Peterburg, pp. 738. (in Russian).

Aan, A., Heinloo, M.
Visualization of the kinematics of a material point
Engineering for Rural Development proceedings, 11, 204 – 209, 2012

VISUALIZATION OF THE KINEMATICS OF A MATERIAL POINT

Aare Aan, Mati Heinloo
Estonian University of Life Sciences
aare.aan@emu.ee, mati.heinloo@emu.ee

Abstract. The reader of this paper will be acquainted with the experiences of visualization of engineering mechanics on the computer screen. The present paper introduces the method of creating a video clip by using the worksheet of the Computer Package Mathcad in order to visualize the motion of a material point on its trajectory, the change of the circle of curvature, the directions of vectors of velocity and vectors of acceleration and the formation of evolute of the trajectory. The results of this paper are illustrated by the video clip and by the figures. Mathcad worksheet as well as already composed video clips can be used by students and teachers of engineering mechanics.

Keywords: visualization, engineering mechanics.

Introduction

Due to the advances in computer technologies there have emerged many new ways to solve engineering problems, the solution of which requires correct equations and calculation methods, which may be unique in each case. Visualization of the studies of mechanical systems on the computer screen accelerates the process of getting correct solutions and thereby reducing the time spent and costs incurred with regard to product development.

Currently there are several computer programs that can create virtual mechanical models, most common of them are Matlab, Mathematica, Maple, Mathcad, etc. In the environment of the Computer Package Matlab we can carry out the studies of virtual models of manipulators with multiple degrees of freedom [1], the study of robot motions [2], the study of the industrial spinning process [3], the visualization of four degrees of freedom parallelogram bipedal robot walking [4]. The Computer Package Mathematica has been used for composing virtual models of four-bar linkage [5], and for the study of the car steering mechanism [5] and vibrations [6].

The authors of the present paper have chosen Computer Package Mathcad [7] for research and teaching purposes, because it is permanently used in the Estonian e-studies community at the universities and vocational schools <http://www.e-ope.ee/>. The developer is periodically updating and upgrading Mathcad in the server of this community.

Mathcad was used to study and visualize the motion of a virtual linkage [8], the motion of the free-active circular link on the top of a potato ridge [9], the working process of the virtual disk-ridging tool of a wide row potato field tillage machine [10], the working process of the virtual model of a blueberry harvester picking reel [11], the distribution of loads on helicopter blades [12], the working process of a novel virtual manipulator for a stone protector of a stony soil tillage implement [13], the motion of fertiliser granules on the plane of the spinning spreading disc of a disc spreader [14], the chaotic motion of virtual double pendulum [15], etc.

There has been composed a review of studies of a virtual manipulator for a scraper of a manure press removal [16].

Visualization of mathematics, mechanics and other engineering subjects allows the engineering students to improve their understanding of these subjects. There has been described an attempt to use Mathcad in teaching of engineering mathematics [17]. Mathcad has been used for composing several e-courses on engineering mathematics and mechanics, available on the website of repository <http://www.e-ope.ee/repository> of Estonia e-University. A proposal has been made to use the Mathcad in creative teaching of engineering mechanics [18]. Also the use of Mathcad in the teaching and learning of analytical mechanics has been described [19].

This paper shows how to create, on the Mathcad worksheet, video clips visualizing the motion of a material point on its trajectory, the change of the circle of curvature, the directions of the vectors of velocity and the vectors of acceleration and the formation of evolute of the trajectory. The Mathcad worksheet as well as the already composed video clips can be used by students and teachers of engineering mechanics.

Basic formulas

If the curve is represented by the parametric equations $x = x(t)$, $y = y(t)$, then the radius of curvature at the point $M(x(t), y(t))$ is [20]

$$R(t) = \frac{v(t)^3}{|a_y(t) \cdot v_x(t) - a_x(t) \cdot v_y(t)|} \quad (1)$$

The centre of curvature co-ordinates x and y are $\alpha(t)$ and $\beta(t)$, respectively

$$\alpha(t) = x(t) - \frac{v(t)^2 \cdot v_y(t)}{a_y(t) \cdot v_x(t) - v_y(t) \cdot a_x(t)}, \quad (2)$$

$$\beta(t) = y(t) + \frac{v(t)^2 \cdot v_x(t)}{a_y(t) \cdot v_x(t) - v_y(t) \cdot a_x(t)}.$$

In (1) and (2)

$$v_x(t) = \frac{d}{dt} x(t), v_y(t) = \frac{d}{dt} y(t) \quad (3)$$

$$a_x(t) = \frac{d^2}{dt^2} x(t), a_y(t) = \frac{d^2}{dt^2} y(t) \quad (4)$$

$$v(t) = \sqrt{v_x(t)^2 + v_y(t)^2} \quad (5)$$

Let us suppose now that a material point M is moving according to the law

$$\begin{aligned} x(t) &= A \cdot \cos(\omega \cdot t) \\ y(t) &= B \cdot \sin(\omega \cdot t) \end{aligned} \quad (6)$$

where a , b and ω are constants and t is the time.

The formulas (6) determine the trajectory of the point M . The formulas (3) and (4) determine the projections of velocity and acceleration of the point M on the x – and y – co-ordinate axes of the co-ordinate system O_{xy} . The formulas (5) represent the modules of the vectors of velocity of the point M .

The direction angles between the x -axis and vectors of velocity $\overline{v(t)}$ and acceleration $\overline{a(t)}$ are

$$\begin{aligned} \alpha_v(t) &= \text{angle}(v_x(t), v_y(t)) \\ \alpha_a(t) &= \text{angle}(a_x(t), a_y(t)) \end{aligned}$$

where $\text{angle}(x, y)$ returns on the worksheet of Mathcad in the direction angle (in radians) of a vector.

The direction angle of the vector, directed from the point M to the centre of curvature, is

$$\alpha_p(t) = \text{angle}(\alpha(t) - x(t), \beta(t) - y(t))$$

where

$$a(t) = \sqrt{a_x(t)^2 + a_y(t)^2}$$

The circle of curvature is determined by the following parametric equations

$$\begin{aligned} x_k(t) &= \alpha(t) + R(t) \cdot \cos(q) \\ y_k(t) &= \beta(t) + R(t) \cdot \sin(q) \end{aligned}$$

where $q = 0, 1, 2, \dots, 2\pi$. The tangential acceleration is defined by the formula [22]

$$a_t(t) = \frac{\alpha_x(t) \cdot v_x(t) + \alpha_y(t) \cdot v_y(t)}{v(t)} \quad (7)$$

and the normal acceleration is defined by the formula

$$a_n(t) = \alpha_x(t) \cdot \frac{(\alpha(t) - x(t))}{R(t)} + \alpha_y(t) \cdot \frac{(\beta(t) - y(t))}{R(t)}. \quad (8)$$

The columns $F(t, \gamma, b, n)^{(1)}$ and $F(t, \gamma, b, n)^{(2)}$ of matrix function

$$F(t, \gamma, b, n) := \begin{cases} x \leftarrow x(t) \\ y \leftarrow y(t) \\ V_0 \leftarrow \begin{pmatrix} x & x & x & x & x \\ y & y & y & y & y \end{pmatrix}^T \\ I \leftarrow \begin{pmatrix} 0 & 0.85 & 0.85 & 1 & 0.85 & 0.85 \\ 0 & 0 & 0.03 & 0 & -0.03 & 0 \end{pmatrix}^T \\ \Omega \leftarrow \begin{pmatrix} \cos(\gamma(t)) & \sin(\gamma(t)) \\ -\sin(\gamma(t)) & \cos(\gamma(t)) \end{pmatrix} \\ V_0 + n \cdot b(t) \cdot I \cdot \Omega \end{cases}$$

of Mathcad [21] can be used to simulate the movement of a geometric vector \vec{b} on Mathcad worksheet. In the function $F(t, \gamma, b, n)$ the following notations are used: $x = x(t)$ and $y = y(t)$ are the coordinates of the origin, $\gamma = \gamma(t)$ is the direction angle, $b(t)$ is the module or projection (if the vector \vec{b} is determined only by one co-ordinate), and b is notation of $b(t)$ of a vector \vec{b} ; m is the coefficient of dimensions and I is the matrix of the shape of a vector \vec{b} on Mathcad worksheet; Ω is the matrix of transformation of rotation, V_0 is the matrix of origin, T denotes the transposed matrix, t is the time.

At the fixed moment of time $t = T$ the columns of the matrix function $F(t, \gamma, b, n)$

$$V_v(T)^{(0)} = F(T, \alpha_v, v, 0.2)^{(0)}, V_v(T)^{(1)} = F(T, \alpha_v, v, 0.2)^{(1)},$$

where v is the notation of module $\sqrt{v_x(t)^2 + v_y(t)^2}$, visualize the vector of velocity, the columns

$$V_a(T)^{(0)} = F(T, \alpha_a, v, 0.1)^{(0)}, V_a(T)^{(1)} = F(T, \alpha_a, v, 0.1)^{(1)},$$

where a is the notation of module $\sqrt{a_x(t)^2 + a_y(t)^2}$ visualize the vector of acceleration, the columns

$$V_{an}(T)^{(0)} = F(T, \alpha_p, a_n, 0.1)^{(0)}, V_{an}(T)^{(1)} = F(T, \alpha_p, a_n, 0.1)^{(1)},$$

where a_n is determined by the formula (8), visualize the vector of normal acceleration, the columns

$$V_{at}(T)^{(0)} = F(T, \alpha_v, a_t, 0.1)^{(0)}, V_{at}(T)^{(1)} = F(T, \alpha_v, a_t, 0.1)^{(1)},$$

where a_t is determined by the formula (7), visualize the vector of tangential acceleration, the columns

$$V_{ap}(T)^{(0)} = F(T, \alpha_p, R, 1)^{(0)}, V_{ap}(T)^{(1)} = F(T, \alpha_p, R, 1)^{(1)},$$

where R is determined by the formula (1), visualize the vector that begins from the point M and is directed towards the centre of curvature (Fig. 1 and Fig. 2).

Results

Let us suppose, that $T = 1.7$ in (6) $A = 3$, $B = 2$, $\omega = \pi$. Then the defined columns are

$$\begin{aligned}
 V_v(T)^{(0)} &= \begin{bmatrix} 1.763 \\ 3.060 \\ 3.037 \\ 3.288 \\ 3.082 \\ 3.060 \end{bmatrix}, & V_v(T)^{(1)} &= \begin{bmatrix} -1.618 \\ -0.990 \\ -0.944 \\ -0.879 \\ -1.036 \\ -0.990 \end{bmatrix}, & V_a(T)^{(0)} &= \begin{bmatrix} 1.763 \\ 0.284 \\ 0.236 \\ 0.023 \\ 0.332 \\ 0.284 \end{bmatrix}, & V_a(T)^{(1)} &= \begin{bmatrix} -1.618 \\ -0.261 \\ -0.313 \\ -0.021 \\ -0.208 \\ -0.261 \end{bmatrix}, \\
 V_{an}(T)^{(0)} &= \begin{bmatrix} 1.763 \\ 0.950 \\ 0.890 \\ 0.806 \\ 1.009 \\ 0.950 \end{bmatrix}, & V_{an}(T)^{(1)} &= \begin{bmatrix} -1.618 \\ 0.062 \\ 0.033 \\ 0.358 \\ 0.091 \\ -0.062 \end{bmatrix}, & V_{a\tau}(T)^{(0)} &= \begin{bmatrix} 1.763 \\ 1.098 \\ 1.109 \\ 0.980 \\ 1.086 \\ 1.098 \end{bmatrix}, & V_{a\tau}(T)^{(1)} &= \begin{bmatrix} -1.618 \\ -1.940 \\ -1.964 \\ -1.997 \\ -1.917 \\ -1.940 \end{bmatrix}, \\
 V_{ap}(T)^{(0)} &= \begin{bmatrix} 1.763 \\ 0.552 \\ 0.464 \\ 0.338 \\ 0.640 \\ 0.552 \end{bmatrix}, & V_{ap}(T)^{(1)} &= \begin{bmatrix} -1.618 \\ 0.883 \\ 0.840 \\ 1.324 \\ 0.925 \\ -0.883 \end{bmatrix}.
 \end{aligned}$$

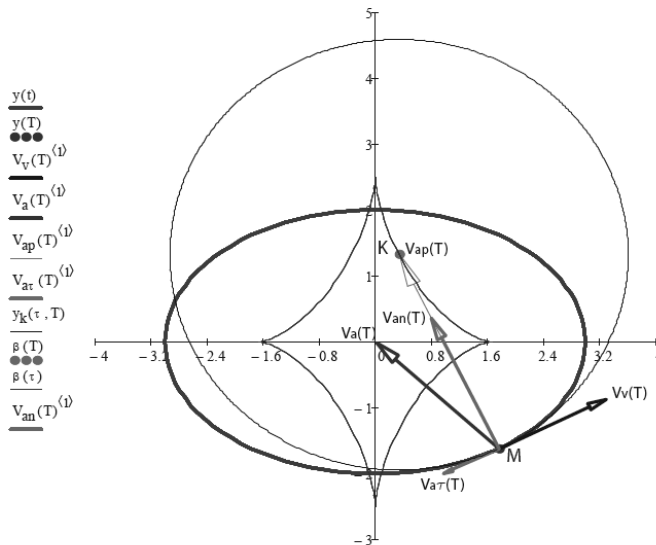
In Fig. 2 these columns draw the vectors shown on the frame of the composed visualized video clip when $T = 1.7$, if in (6) $A = 3$, $B = 2$, $\omega = \pi$. In Fig. 1 the trajectory of the moving point M is a bold curve, the circle of curvature is a thin curve, the curve with corners is the evolute drawn by the centre of curvature K , the bold vector of acceleration is directed to the centre of the co-ordinate system, the bold vector of normal acceleration is directed to the centre of curvature, the bold vector of tangential acceleration is directed opposite the bold vector of velocity (this means that the motion is slowing down at $T = 1.7$), the thin vector connects the point M and the centre of curvature K .

The video clip, with the frame in Fig. 1, clearly shows the change of the point M vector modules of velocity and acceleration in time t . One can also see the motion and change of the radius of the circle of curvature and the creation of the evolute as the trajectory of the centre of curvature.

The composed Mathcad worksheet allows easy modification of Fig. 1. When replacing the law (6) with

$$x(t) = t, y(t) = 0.8 \cdot \sin(3 \cdot t),$$

then the frame 1 in Fig. 1 changes to Fig. 2.



- $x(t), x(T), V_v(T)^{(i)}, V_a(T)^{(i)}, V_{ap}(T)^{(i)}, V_{ar}(T)^{(i)}, x_k(\tau, T), \alpha(T), \alpha(\tau), V_{an}(T)^{(i)}$
 $y(t)$ — Trajectory of the point M
 $y(T)$ ●●● Point M
 $V_v(T)$ — Velocity of the point M
 $V_a(T)$ — Full acceleration of the point M
 $V_{ap}(T)$ — Vector, connecting point M and the centre of curvature
 $V_{ar}(T)$ — Tangential acceleration of the point
 $y_k(\tau, T)$ — Circle of trajectory's curvature at the point M
 $\beta(T)$ ●●● Centre of trajectory's curvature at the point M
 $\beta(\tau)$ — Evolute of the trajectory of the point M
 $V_{an}(T)$ — Normal acceleration at the point M

Fig. 1. Frame from video clip: <http://www.youtube.com/watch?v=zFbVcd4GOJw>

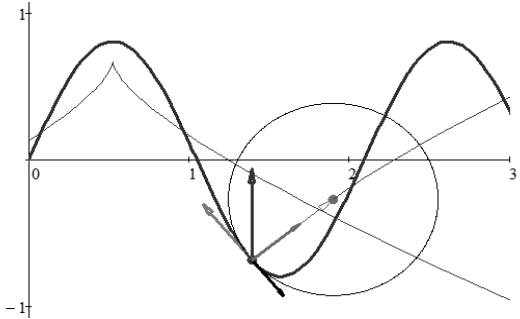


Fig. 2. A frame of possible second video clip:
<http://www.youtube.com/watch?v=2gPSalH9lxU&feature=youtu.be>

Conclusions

1. The composed solution on the Mathcad worksheet and already created video clips allow explaining the kinematics of a material point to the students.
2. The environment of Mathcad allows observing how the formulas actually “work”.

3. It is important that Mathcad detects most of syntax errors.
4. The possibility of experimentation with lecture materials and composing animations makes the study of engineering subjects interesting and attractive for students.
5. Simple procedure of animation on Mathcad worksheet allows visualization of the problems of engineering subjects for students.

References

1. Žlajpah, L. Simulation of n-R planar manipulators. *Simulation Practice and Theory*, vol. 6, 1998, pp 305-321.
2. Žlajpah, L. 2008. Simulation in robotics. *Mathematics and Computers in Simulation*, vol. 79, 1998, pp. 879-897.
3. Tang, Z., Wang, X., Fraser W. B., Wang, L. Simulation and experimental validation of a ring spinning process. *Simulation Modelling Practice and Theory*, vol. 14, 2006, pp. 809-816.
4. Jo H. S., Mir-Nasiri, N. Dynamic modeling and walk simulation for a new four-degree-of-freedom parallelogram bipedal robot with sideways stability control. *Mathematical and Computer Modelling*, 2011
5. Peñuñuri, F., Peón-Escalante, R., Villanueva, C., Pech-Oy, D. Synthesis of mechanisms for single and hybrid tasks using differential evolution. *Mechanism and Machine Theory*, vol. 46, 2011, pp. 1335-1349.
6. Chen, J. T., Chou, K. S., Kao, S. K. One-dimensional wave animation using Mathematica. *Computer Applications in Engineering Education*, vol. 17, 2009, pp. 323–339.
7. Mathcad user's guide. Parametric Technology Corporation, 2007. [online] [31.01.2011]. Available at: http://www.msiami.com/custom/downloads/Mathcad14_Users_Guide_English.pdf.
8. Heinloo, M., Aarend, E., Mägi, M. On the Experience of Mathcad-Aided Analysis of Planar Linkages. *Proc. Tenth World Congress on the Theory of Machines and Mechanisms*, vol. 1, 1999, pp. 392 – 397.
9. Heinloo, M., Olt, J. Motion of the Free-Active Circular Link on the Top of a Potato Ridge Modelled as a Polygonal Cylinder. *Proc. Int. Conf. Perspective Sustainable Technological Process in Agricultural Engineering*, 2001, pp. 99 – 104.
10. Heinloo, M., Olt J. A method of virtual reality for creating a disk-ridging tool. *CIGR Ejournal*, vol. 8, 2006, pp. 21. [online] [31.02.2011]. Available at: <http://cigr-ejournal.tamu.edu/>.
11. Heinloo, M. A virtual reality technology based method for study the working process of a blueberry harvester's picking reel. *CIGR E-journal*, vol. 9, 2007, pp. 12.
12. Butoescu, V. A vortex model of a helicopter rotor. *INCAS*, vol. 1, 2009, pp. 23-27. [online] [31.02.2011]. Available at: http://bulletin.incas.ro/files/valentin_butoescu_v1no1_full.pdf.
13. Olt, J., Heinloo, M. Visualization of the working process of a novel manipulator for a stone protector of a stony soil tillage implement. *Balkan Agricultural Engineering Review*, vol. 15, 2010, pp. 9.
14. Olt, J., Heinloo M. Visualization of Motion of Fertiliser's Granules on the Plane of Spinning Spreading Disc of a Disc Spreader. *Proc. XXXIV CIOSTA CIGR VConference*, 2011, pp. 292 – 296.
15. Aan, A., Aarend, E., Heinloo, M. On chaotic motion of a double pendulum. *Agronomy Research*, vol. 9, 2011, pp. 5 – 12.
16. Leola, T., Heinloo, M. Review of Studies on Press Manure Removal. *Proc. 10.th Int. Sci. Conf. "Engineering for Rural Developments "*, 2011, pp 82 – 87.
17. Heinloo, M., Saks, E. Review of Experiences in the Interactive Teaching of Mathematics and Mechanics. *Proc. EFITA Conference*, 2003, pp. 531–538.
18. Aare, A., Heinloo, M. On Creative Teaching of Engineering Mechanics. *Proc. 22nd DAAAM International World Symposium*, 2011, pp. 1081 – 1082.
19. Aan, A, Heinloo, M, Aarend, E. Interactive Computer Aided Learning and Teaching of Analytical Mechanics. *Int. J. Eng. Pedagogy (iJEP)*, vol. 1, 2011, pp. 4 - 8.
20. Piskunov, N. *Differential and Integral Calculus I*. Moscow, 1969, pp. 492.
21. Bertjaev, B. D. *Mathcad-based Training in Theoretical Mechanics (In Russian)*, Sankt-Peterburg, 2005, pp. 738.
22. Lepik, Ü., Roots, L. *Theoretical mechanics (In Estonian)*. Tallinn, 1971, pp 483.

Aan, A., Heinloo, M.
Composing and solving differential equations for
small oscillations of mathematical spring-coupled pendulums
Agronomy Research, 11(1), 223 – 230, 2013

Computer based comparison analysis of single and double-connecting-rod slider-crank linkages

A. Aan and M. Heinloo

Institute of Technology, Estonian University of Life Sciences, Kreutzwaldi 56, EE51014 Tartu, Estonia; e-mail: aare.aan@emu.ee

Abstract. This paper presents the results of comparative numerical analysis of single and double-connecting-rod slider-crank linkages on the worksheet of Computer Package Mathcad. On the base of composed virtual models of both linkages the motion of the slider (piston) in these linkages is studied thoroughly. This paper has the links to the video clips, comparing the motions of single and double-connecting-rod slider-crank linkages and visualizing the change of vectors of velocities and accelerations in the pivot, where connects two links of double connecting rod. Concluded, that the motion of the slider (piston) and the force of reaction to the track of slider (wall of a cylinder) in these linkages is quite different.

Key words: machine and mechanism theory, linkages, internal combustion engines.

Introduction

Slider-crank linkages can be used in pumps, compressors, internal combustion engines etc. A typical scheme of one cylinder of a four-stroke internal-combustion engine with single connecting rod crank-slider linkage is shown in Fig. 1 (Merriam-Webster, 2006).

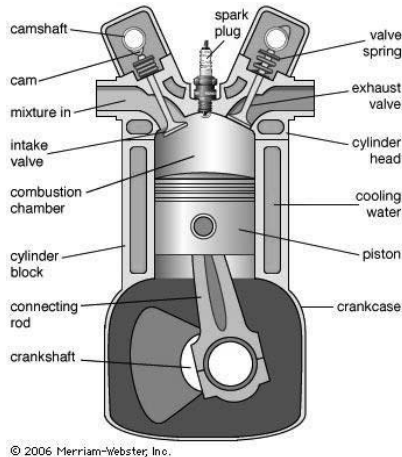


Fig. 1. Cross section showing one cylinder of a four-stroke internal-combustion engine.

A review of different internal combustion engines using single-connecting-rod crank-slider mechanism with multiple cylinders is given in Automotive Handbook (1996).

Mederer (Evert, 2003) proposed to use a double-connecting-rod linkage (Fig. 2) in combustion engines.

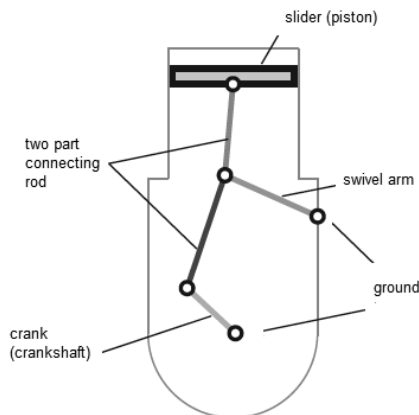


Fig. 2. The scheme of a double-connecting-rod linkage, proposed by Mederer to use in internal combustion engines.

Double-connecting-rod linkage (Fig. 2) consists of ground (cylinder), crank (on crankshaft), two part connecting rod, slider (piston) and a swivel arm. By Mederer this mechanism reduces consumption of fuel and lower emissions, because piston will stay relative long times at area of its uppermost position, and in the compression stroke large parts of counter-pressure is taken by swivel arm, that means less input power is needed for turning a crank in the compression stroke.

The aim of this paper is to present the method and results of comparative numerical analysis of single-connecting-rod and double-connecting-rod slider-crank linkages on the worksheet of Computer Package Mathcad, in the case of constant (idle) crank (crankshaft) angular velocity. On the base of composed virtual models of both linkages the motion of the slider (piston) in these linkages will be studied thoroughly. This paper will have also links to two composed video clips. First video clip compares the motions of single-connecting-rod and double-connecting-rod slider-crank linkages with the same maximum displacement of the slider (piston). Second video clip visualizes the changing geometrical vectors of velocities and accelerations in the pivot, where connects two links of double-connecting-rod slider-crank linkage. This video clip compares also the reaction force in the track of sliders (cylinder wall).

Composition of virtual models of linkages

The links OA, AE, and EC of the four-bar OAEC in the structure of double-connecting-rod linkage can rotate around pivots O, A, E and C, whereby pivots O and C are grounded (Fig. 3). For numerical computations let us assume that the lengths of

the links OA, AE and EC are $l_{OA} = 0.3$ m, $l_{AE} = 0.7$ m, $l_{EC} = 0.735$ m accordingly and the coordinates of the pivot C are $x_C = 0.67$ m, $y_C = 0.7$ m. Let us suppose also that the rotational speed of crank OA is $n = 700$ rpm, that means angular velocity $\omega = 73.304$ rad s^{-1} .

The coordinates of pivot A (Fig. 3) can be found out by equations

$$x_A(\varphi) = l_{OA} \cdot \sin \varphi, \quad y_A(\varphi) = l_{OA} \cdot \cos \varphi.$$

The four-bar OAEC has constraints that the distances between pivots A, E and E, C are permanent. Mathematically these constraints means the following system of nonlinear equations of constraints

$$\begin{aligned} (x_E - x_C)^2 + (y_E - y_C)^2 &= l_{EC}^2, \\ (x_E - x_A(\varphi))^2 + (y_E - y_A(\varphi))^2 &= l_{AE}^2, \end{aligned} \quad (1)$$

where φ is the angle of rotation of the crank OA from y-axis clockwise.

The system of equations (1) was solved on the worksheet of Mathcad numerically relative to x_E and y_E (Fig. 3).

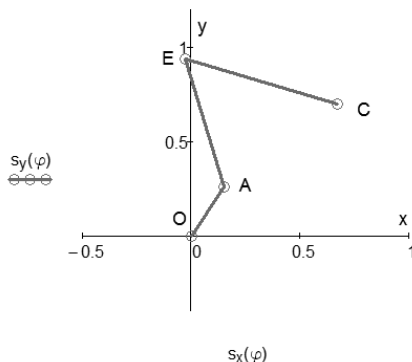


Fig. 3. The virtual model of four-bar OAEC under crank's rotation angle $\varphi = 30^\circ$.

Let us compose the following column vectors

$$s_x(\varphi) = \begin{pmatrix} 0m \\ x_A(\varphi) \\ x_E(\varphi) \\ x_C \end{pmatrix}, \quad s_y(\varphi) = \begin{pmatrix} 0m \\ y_A(\varphi) \\ y_E(\varphi) \\ y_C \end{pmatrix}.$$

Fig. 3 shows the virtual model of linkage OAEC, drawn by these vectors on the worksheet of Mathcad.

Connecting to the pivot E of four-bar in Fig. 3 by a link ED to the pivot pivot D, what is moving along y-axis, we get a virtual model of double-connecting-rod linkage on Figs 2 and 4. Let the length of the link ED be $l_{ED} = 0.7$ m. The y-coordinate of pivot D can be find out from the following equation of restriction

$$y_D(\varphi) = y_E(\varphi) + \sqrt{l_{ED}^2 - x_E(\varphi)^2}. \quad (2)$$

The following vectors

$$s'_x(\varphi) = \begin{pmatrix} x_E(\varphi) \\ 0 \end{pmatrix},$$

$$s'_y(\varphi) = \begin{pmatrix} y_E(\varphi) \\ y_D(\varphi) \end{pmatrix},$$

draw on the worksheet of Mathcad the virtual model of double-connecting-rod crank-slider linkage in Fig. 4a.

To compose the virtual model for typical single-connecting-rod crank-slider linkage in Fig. 4b, we used the following equation of constraint

$$l'_{AD} = \sqrt{(y'_D(\varphi) - y_A(\varphi))^2 + x_A(\varphi)^2}, \quad (3)$$

where l'_{AD} is the permanent length of the link AD in Fig. 4b. In computations were taken $l'_{AD} = l_{AE} + l_{ED} = 1.4$ m. Equation (3) determine the coordinate $y'_D(\varphi)$ of the pivot D by the following formula

$$y'_D(\varphi) = y_A(\varphi) + \sqrt{l_{AD}^2 - x_A(\varphi)^2}.$$

The following vectors

$$ss_x(\varphi) = \begin{pmatrix} 0m \\ x_A(\varphi) \end{pmatrix},$$

$$ss_y(\varphi) = \begin{pmatrix} 0m \\ y_A(\varphi) \end{pmatrix},$$

$$ss'_y(\varphi) = \begin{pmatrix} y'_D(\varphi) \\ y_A(\varphi) \end{pmatrix},$$

draw on the worksheet of Mathcad the virtual model of single-connecting-rod crank-slider linkage in Fig. 4b.

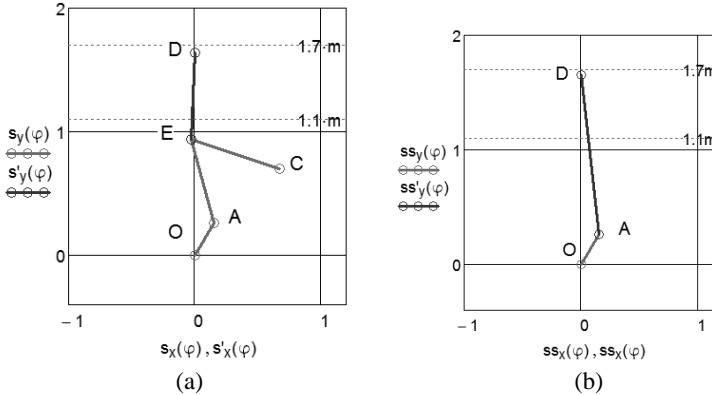


Fig. 4. The virtual models of double-connecting-rod (a) and single-connecting-rod (b) crank-slider linkages under crank's rotation angle $\varphi = 30^\circ$.

Comparison of displacement, velocity and acceleration of a slider (piston)

To compare of displacement, velocity and acceleration, let's give for rotation angle φ the values from 0 with step 0.1 up to $4 \cdot \pi$. This means that the crank OA in Fig. 4 makes two rotations.

According to used assumption, in Fig. 5 at the bottom dead centre (BDC) and the top dead centre (TDC) the pivot D (slider) virtual model displacements for both cases (Fig. 4a and Fig. 4b) are coincidence, but between BDC and TDC displacements are different.

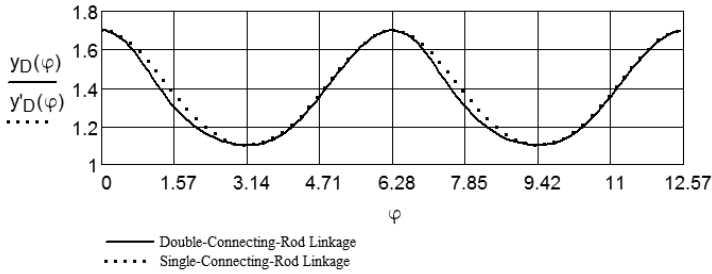


Fig. 5. The Displacement of pivot D (slider) for double-connecting-rod and single-connecting-rod crank-slider linkages dependence from rotational angle φ .

The velocity projections of pivot's D (Fig. 4) are

$$v_{Dy}(\varphi) = \frac{d}{d\varphi} y_D(\varphi) \cdot \omega, \quad v'_{Dy}(\varphi) = \frac{d}{d\varphi} y'_D(\varphi) \cdot \omega.$$

Fig. 6 shows the change of projections of the velocity of the pivot D (Fig. 4) for both virtual models. One can conclude in range of TDC these projections are coincident for both virtual models, but in BTC are not.

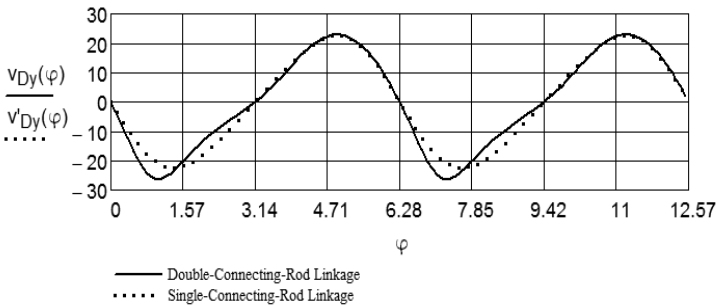


Fig. 6. The velocity of pivot D (slider) for double-connecting-rod and single-connecting-rod crank-slider linkages dependence from rotational angle φ .

The accelerations projections of pivot's D (Fig. 4) are

$$a_{Dy}(\varphi) = \frac{d^2}{d\varphi^2} y_D(\varphi) \cdot \omega^2, \quad a'_{Dy}(\varphi) = \frac{d^2}{d\varphi^2} y'_D(\varphi) \cdot \omega^2.$$

One can conclude from Fig. 7 shows that the projections of accelerations of the pivot D for both virtual models are quite different.

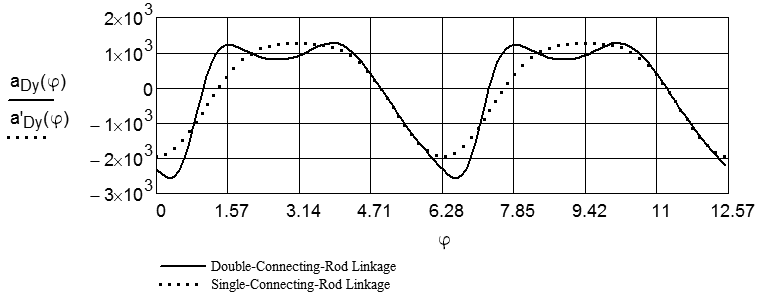


Fig. 7. The accelerations of pivot D (slider) for double-connecting-rod and single-connecting-rod crank-slider linkages dependence from rotational angle φ .

Comparison of angles between the link, connected to the pivot of the slider (piston) and the track of motion

Angles between y-axis (pivot D track) and the links on single connecting rod AD and double connecting rod ED (pressure angle (Kleis, 1988), can be found out from the equations

$$\beta(\varphi) = a \sin \frac{x_E(\varphi)}{l_{ED}}, \quad \beta'(\varphi) = a \sin \frac{x_A(\varphi)}{l_{AD}}.$$

Fig. 8 shows that the pressure angle β for double-connecting-rod linkage is lower than the correspondent angle β' for single-connecting-rod linkage.

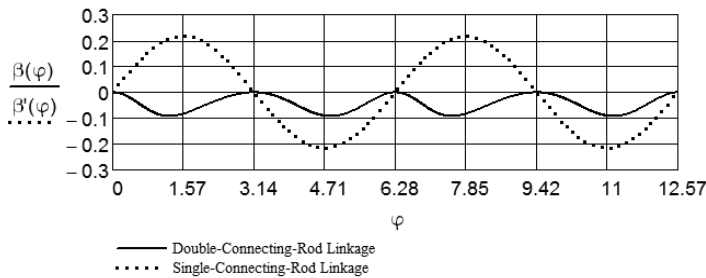


Fig. 8. The pressure angle between the links ED and AD (Fig. 4) relative to the y-axis (track of pivot D) for double-connecting-rod and single-connecting-rod crank-slider linkages dependence from rotational angle φ .

Comparison of the reaction force from the track of slider (the wall of cylinder)

Let's apply force $F_D = 1000$ N to the slider pivot (piston) and take the mass of slider (piston) equal to $m_k = 3$ kg. The equations of motion of the slider (piston) are

$$m_k \cdot a_{Dy}(\varphi) = -F_D + R_E(\varphi) \cdot \cos \beta(\varphi), \quad 0 = R_{Dx}(\varphi) + R_E(\varphi) \cdot \sin \beta(\varphi), \quad (4)$$

where $R_E(\varphi)$ – is the reaction force, applied from link ED in Fig. 4 (a) to the pivot D, $R_{Dx}(\varphi)$ – is the projection of the reaction force, applied to the track of slider (cylinder wall).

From equations (4) one can get the following formula for determination the projection of the reaction force $R_{Dx}(\varphi)$

$$R_{Dx}(\varphi) = (m_k \cdot a_{Dy}(\varphi) + F_D) \cdot \tan \beta(\varphi).$$

Analogous formula is valid for the case Fig. 4b

$$R'_{Dx}(\varphi) = (m_k \cdot a'_{Dy}(\varphi) + F_D) \cdot \tan \beta'(\varphi).$$

From Fig. 9 follows that the average reaction force in the case double-connecting-rod linkage is lower than in the case of single-connecting-rod linkage that means less friction between slider and track (piston and cylinder wall) in double-connecting-rod linkage.

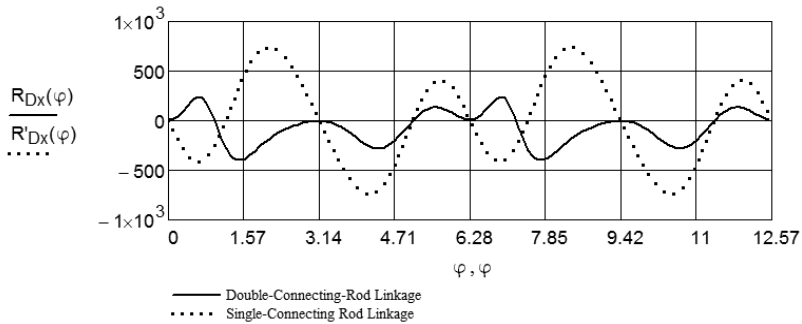


Fig. 9. The projections of the reaction forces between the slider and its track (piston and cylinder) for double-connecting-rod and single-connecting-rod crank-slider linkages dependence from rotational angle φ .

Comparison of visualizing video clips

The Computer Package Mathcad allows also compose of video clips. To visualize the obtained solution and to verify it, two video clips were made. The video clip (Aan & Heinloo, 2012-1), composed on the base of Figs 4 and 5, show visually the change of co-ordinate of pivot D in accordance with motion of corresponding linkage. The video clip (Aan & Heinloo, 2012-2), composed on the base of Figs 4 and 9, shows visually the dependence of reaction force between the link D and the track of it (piston and cylinder wall) in accordance with motion of corresponding linkage. Also on that video clip is visualized change of geometrical vectors of velocity and acceleration of the pivot D and pivot E. These vectors were composed by using the special program on the worksheet of Mathcad, presented by Bertjajev (2005).

Conclusions

- The motion of the slider (piston) in double-connecting-rod linkage and single-connecting-rod linkage is quite different.
- The slider (piston) of double-connecting-rod linkage has lower reaction force on the track of motion (cylinder wall). That means the force, applied to the slider (piston) in double-connecting-rod linkage makes more useful work. Therefore, the motor based on double-connecting-rod linkage could have lower consumption of fuel and lower emissions than the motor with single-connecting-rod linkage.
- The Computer Package Mathcad can be used as convenient tool for composition of video clips for visualization and verify the obtained solution.
- The method and the results of study may be used by teachers of engineering subject 'Machine and Mechanism Theory' and by automobile engineers.

References

- Merriam-Webster. 2006. Internal combustion engine. Available at: <http://www.merriam-webster.com/concise-images/72180.htm> (02.02.2012).
- Robert Bosch GmbH. 1996. *Automotive Handbook 4th edition*. Stuttgart, pp. 892.
- Evert, A. 2003. Buckle- and Double-Connecting-Rod. Available at: <http://www.evert.de/ef774e.htm> (02.02.2012).
- Kleis, I. 1988. *Applied mechanics*. Valgus. Tallinn, pp. 423. (in Estonian).
- Aan, A., Heinloo, M. 2012. Comparison of piston displacements. Available at: <http://youtu.be/LG2h8oijjIU> (02.02.2012).
- Aan, A., Heinloo, M. 2012. Comparison of piston velocities accelerations and reactions. Available at: <http://youtu.be/QvyZAo-Q3Rk> (02.02.2012).
- Bertjajev, B. D. 2005. *Mathcad-based Training in Theoretical Mechanics*. Sankt-Peterburg, pp. 738. (in Russian).

Aan, A., Heinloo, M.
Motion of a granule on fertilizer spreading disc
Proceedings of the 42nd international symposium on agricultural
engineering: Actual Tasks on Agricultural Engineering,
101 – 111, 2014



MOTION OF A GRANULE ON FERTILIZER SPREADING DISC

A. AAN, M. HEINLOO

Institute of Technology, Estonian University of Life Sciences, Tartu, Estonia,
aare.aan@emu.ee

ABSTRACT

This paper reviews the studies on the motion of fertilizer granules on a planar spreading disc in the structure a fertilizer spreader and presents the mathematical model for studying this motion. This model is used to study the dependence of outlet velocity of a fertilizer granule on the coefficient of friction and on adjusting angle. The trajectories of fertilizer granules on the spreading disc are visualized by figures. Video clips are used to simulate the motion of granules on four trajectories. Derived formulae and numerical results of this present paper can be used by the engineers studying discs of fertiliser spreaders. These formulae can also be used for teaching the operation of fertilizer spreader to the students.

Key words: *Agricultural machinery, fertilizer spreader, spreading disk, visualization, Mathcad.*

INTRODUCTION

The first works on modelling the spreading process were carried out nearly half a century ago: Patterson and Reece (1962); Inns and Reece (1962). Modelling of the spreading process has been re-activated during the last years, the models have been enhanced, new methodologies have been introduced, the parameters of the spinning disc of spreader have been optimized and a series of articles has been published. Hofstee (1995) offers many differential equations to describe the motion of a particle. This equations were deduced for various shapes of vanes and discs. Reintam (1995) has presented the differential equation, modelling the motion of a fertilizer particle on the planar spreading disk of a fertilizer spreader with pitched straight vanes at adjusting angle of 60° . Later non-linear differential equation, with numerical solutions for a conical disc with pitched vanes, where presented (Olieslagers, 1997; Dintwa et al., 2004a). In 2005, Villette, Cointault, Piron and Chopinet reported analytical model of fertiliser particle motion. This

mathematical model is derived for a concave disc equipped with pitched straight vanes. Villette et al. 2008 showed that outlet velocity of three-dimensional components in the case of a concave disc could be deduced from the measurement of the horizontal outlet angle. In 2010, Villette et al. introduced the friction coefficient referred to as “equivalent friction coefficient”. This parameter is deduced from a mechanical model of the fertiliser motion on a spinning disc and from the measurement of the outlet angle of the particles.

Van Liedekerke et al. 2006 presented discrete element method (DEM) to simulate particle motion on flat disc with radial vanes. This model took into account interactions between the particles. A new approach consists in investigating entire particle flow by using discrete element method (Van Liedekerke et al., 2009, 2009b; Coetzee and Lombard, 2011). Technical solutions for measuring the speed and direction of fertilizer particles when they leave the disc are used to develop more precise mathematical models according to measurements (García-Ramos, Boné, Serreta and Vidal, 2012). For example, during recent years, the most common technology has been based on the use of different types of optical sensors (Grift, Hofstee, 2002; Swisher, Borgelt and Sudduth, 2002; Villette, Cointault, Chopinet and Paindavoine, 2006). Most studies are focused on particles, but there are also works focusing on the measurement of surface distribution of fertilizer particles (Lawrence, Yule and Coetzee 2007; García-Ramos, Boné, Serreta and Vidal, 2012).

Based on the equations by Reintam (1995), Heinloo (2010) have visualized the motion of fertilizer granules on the planar spreading disc with different contours and with the vanes at adjusting angle of 60° . Olt, Heinloo (2011) have reviewed the studies on spreading discs and studied the motion of fertilizer particles, directed by the vane at adjusting angle of -90° . The first objective of this paper is to apply the results of papers by Reintam (1995), Heinloo (2010) and Olt, Heinloo (2011) to arbitrary adjusting angle, frictional coefficient and the initial distance of a fertilizer granule from the centre of the spreading disc. The second goal of this paper is to compare the trajectories of the motion of fertilizer granules on the planar spinning spreading disc at adjusting angles of 60° and -90° . The third purpose of this paper is to study the influence of friction coefficient of the fertilizer granule (against the vane and the disc) and location of the vane (determined by the initial location of fertiliser granules and by the adjusting angle of the vane) on the outlet time and outlet velocity when granules leave the disc.

MATERIALS AND METHODS

Mathematical model for spreading disc of a disc spreader

Let us consider the scheme of a spreading disc in figure 1 according to Reintam (1995).

In figure 1, R is the radius of the spreading disc; bold intercept denotes the vane for directing the fertilizer granules on the disk, ψ_0 is the adjusting angle of the vane, r – the distance between the centre of the disc and fertilizer granule in the current position A , r_0 – the distance between the centre of the disc and fertilizer granule in the initial position A_0 , ψ – angle between the polar radii of fertilizer granule and the direction of the vane.

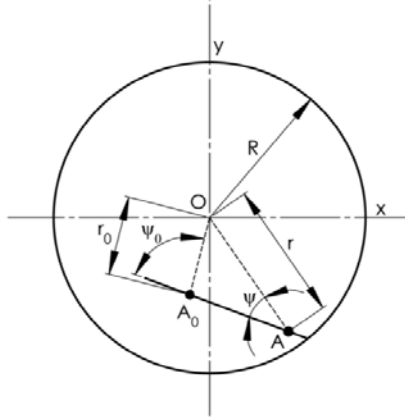


Figure 1 The scheme of a spreading disk. R - spreading disc radius, ψ_0 - adjusting angle of the vane, ψ - angle between the polar radii of a fertilizer granule and the direction of the vane, r - distance between the centre of the disc and fertilizer granule in the current position A , r_0 - distance between the centre of the disc and fertilizer granule in the initial position A_0 .

Fertilizer granule on the spreading disk (fig. 1) is in complex motion. It rotates together with the spreading disk (translation motion) and moves along the vane (relative motion). The projection of equation of relative motion of fertilizer granule on the axis ξ , directed from the initial position A_0 of fertilizer granule along the vane to the border of the spreading disk, can be presented in the form below (Reintam, 1995):

$$m \frac{d^2}{dt^2} \xi(t) = F_1 + F_2 + F_3 + F_4, \quad (1)$$

where $\xi(t) = A_0A$ is the distance between initial and current positions of fertilizer granule; F_1 is the friction force projection on axis ξ between the spreading disk and the vane; F_2 is the translation inertial force projection on axis ξ ; F_3 is the friction force projection on axis ξ , caused by the translation inertial force; F_4 the projection of Coriolis inertial force. The equations for these forces are given below:

$$F_1 = -fmg, \quad F_2 = m\omega^2 r \cos \psi, \quad F_3 = -f m \omega^2 r \sin \psi, \quad F_4 = -2f m \omega \frac{d}{dt} \xi(t).$$

Here m is the mass of the fertilizer granule and ω is constant angular velocity of the spreading disk; f - coefficient of friction between the fertilizer granule and the vane and the spreading disk, g - acceleration of gravity. Placing forces F_1, F_2, F_3, F_4 in the equation (1) and dividing them by m gives the ordinary differential equation with constant coefficients (Reintam, 1995)

$$\frac{d^2}{dt^2}\xi(t) + 2f\omega\frac{d}{dt}\xi(t) - \omega^2(r\cos\psi - fr\sin\psi) + fg = 0. \quad (2)$$

From figure 1 it follows that

$$r\cos\psi = AA_0 + r_0\cos\psi_0 = \xi(t) + r_0\cos\psi_0, \quad r\sin\psi = r_0\sin\psi_0. \quad (3)$$

The adjusting angle ψ_0 of the vane is $\psi_0 > 0$, if it is measured from the vector OA_0 counter clockwise and $\psi_0 < 0$ – if measured clockwise.

Taking into account equations (3), the equation (2) can be written in the following form

$$\frac{d^2}{dt^2}\xi(t) + 2f\omega\frac{d}{dt}\xi(t) - \omega^2\xi(t) = A, \quad (4)$$

where

$$A = \omega^2 r_0 [\cos(\psi_0) - f \sin(\psi_0)] - fg.$$

Differential equation (4) modelling the motion of fertilizer granule on the planar spreading disc with pitched vanes was composed by Reintam (1995).

Let us suppose that fertilizer granule starts motion from its initial position A_0 . In that case, the initial conditions are:

$$\xi(0) = 0, \quad \xi'(0) = 0, \quad (5)$$

where

$$\xi'(0) = \frac{d}{dt}\xi(t)$$

The equation (4) can be solved by standard technique and its solution is

$$\xi(t) = C \left(1 - \frac{\lambda_2 e^{\lambda_1 t} - \lambda_1 e^{\lambda_2 t}}{\lambda_2 - \lambda_1} \right), \quad (6)$$

where $e=2.718...$ and

$$C = \frac{fg}{\omega^2} - r_0 [\cos\psi_0 - f \sin\psi_0], \quad \lambda_1 = \omega \left(-f + \sqrt{1+f^2} \right), \quad \lambda_2 = \omega \left(-f - \sqrt{1+f^2} \right).$$

From figure 1 one can find the relations

$$AA_0 = \xi(t) = \sqrt{r(t)^2 - r_0^2 \sin^2\psi_0} - r_0 \cos\psi_0. \quad (7)$$

From equation (7) and the second equation of (3), we get the following equations

$$r(t) = \sqrt{r_0^2 + 2r_0 \cos \psi_0 \cdot \xi(t) + \xi(t)^2}, \quad (8)$$

$$\psi(t) = \arcsin \left[\frac{r_0 \sin(\psi_0)}{r(t)} \right], \quad (9)$$

where ξ and r are functions of the time t : $\xi = \xi(t)$ and $r = r(t)$. In equation (8), the function $\xi(t)$ is determined by the solution (6) of the differential equation (1). The outlet time t_e can be found out from the equation

$$\xi(t_e) = \sqrt{R^2 - r_0^2 \sin^2 \psi_0} - r_0 \cos \psi_0. \quad (10)$$

Equation (10) was solved numerically similar to t_e by using the solve block on Mathcad worksheet. The angle between vectors OA_0 and OA (fig. 1) can be found out from the equation

$$\alpha(t) = \psi_0 - \psi(t). \quad (11)$$

The rectangular co-ordinates of the current position A of fertilizer granule can be found out by the equations

$$x(t, \varphi_0) = r(t) \cdot \cos[\varphi_0 + \alpha(t) + \omega t], \quad y(t, \varphi_0) = r(t) \cdot \sin[\varphi_0 + \alpha(t) + \omega t], \quad (12)$$

where ω is the angular velocity of the spreading disc and the angle φ_0 determines the initial position of the granule. The projections of the velocity and the module of the fertilizer granule is determined by the following equations

$$v_x(t, \varphi_0) = \frac{d}{dt} x(t, \varphi_0), \quad v_y(t, \varphi_0) = \frac{d}{dt} y(t, \varphi_0),$$

$$v(t, \varphi_0) = \sqrt{v_x(t, \varphi_0)^2 + v_y(t, \varphi_0)^2}. \quad (13)$$

For given parameters of the spreading disc and the fertilizer granule, the velocities (13) were found out by using numerical differentiation on Mathcad worksheet.

RESULTS AND DISCUSSION

Visualization of the motion of fertilizer granules on the planar spinning spreading disc of a disc spreader

By using the mathematical model presented in material and methods of this paper, the computed trajectories of fertilizer granule have been visualized on the spreading disc of fertilizer spreader. The conditions for computations included the following: $R = 0.4$ m; $f = 0.47$; $\omega = 57.6$ s⁻¹; $r_0 = 0.04$ m, $\varphi_0 = -90^\circ$. Figure 2a shows the initial position of the vane and the granule. Figure 2b shows the trajectory of fertilizer granule and the direction of outlet velocity, when $\psi_0 = 60^\circ$.

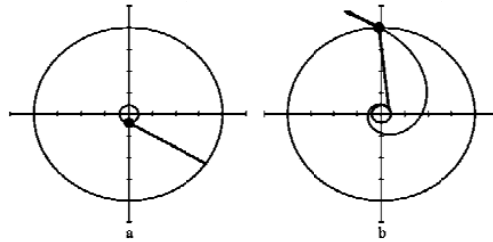


Figure 2 The initial position of the vane and the granule (a), the trajectory of the granule and the outlet velocity (arrow) (b), when $\varphi_0 = -90^\circ$, $\psi_0 = 60^\circ$.

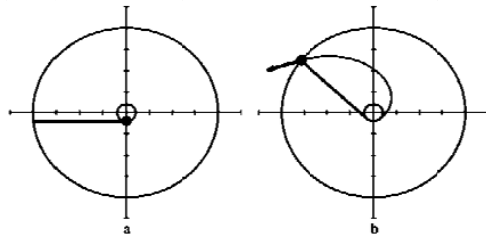


Figure 3 The initial position of the vane and the granule (a), the trajectory of the granule and the outlet velocity (arrow) (b), when $\varphi_0 = -90^\circ$; $\psi_0 = -90^\circ$.

Figure 3a shows the initial position of the vane and the granule. Figure 3b shows the trajectory of fertilizer granule and the direction of outlet velocity, when $\varphi_0 = -90^\circ$; $\psi_0 = -90^\circ$. From Figures 2 and 3 it follows that the trajectory of the granule in the case, where $\psi_0 = -90^\circ$, is shorter than in the case, where $\psi_0 = 60^\circ$.

Figure 4 shows the initial positions, the trajectories and the outlet velocities of granules in the case of four vanes and granules, when $\varphi_0 = 60^\circ, 150^\circ, 240^\circ, 330^\circ$; $\psi_0 = 60^\circ$; relevant angles in Figure 5 are $\varphi_0 = -90^\circ, 0^\circ, 90^\circ, 180^\circ$; $\psi_0 = 60^\circ$.

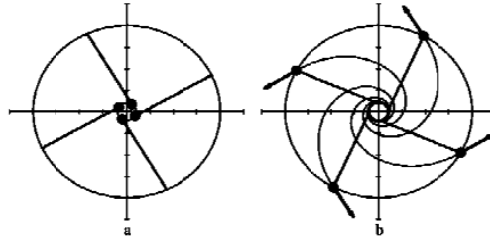


Figure 4 The initial positions (a), the trajectories and the outlet velocities of granules in the case of four vanes (b), when $\varphi_0 = 60^\circ, 150^\circ, 240^\circ, 330^\circ$; $\psi_0 = 60^\circ$.

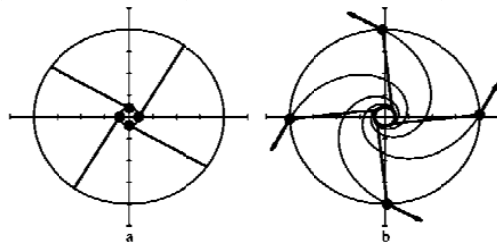


Figure 5 The initial positions (a), the trajectories and the outlet velocities of granules in the case of four vanes (b), when $\varphi_0 = -90^\circ, 0^\circ, 90^\circ, 180^\circ$; $\psi_0 = 60^\circ$.

Heinloo (2010) has shown that polygonal spreading discs may also be used instead of circular spreading discs.

The dependence of the outlet time and outlet velocity of fertilizer granule on the coefficient of friction

Let us assume that $g = 9.807 \text{ m s}^{-2}$; $r_0 = 0.04 \text{ m}$; $R = 0.4 \text{ m}$; $\omega = 60 \text{ s}^{-1}$, $\varphi_0 = -90^\circ$

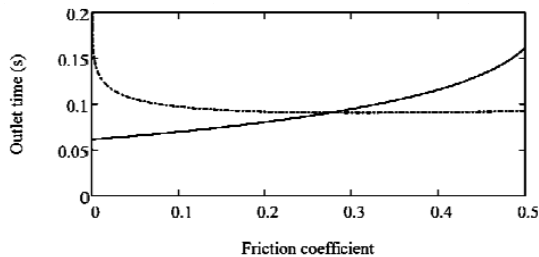


Figure 6 The dependence of the outlet time t_e on friction coefficient f at $\psi_0 = 60^\circ$ (continuous line) and at $\psi_0 = -90^\circ$ (dotted line).

Figures 6 and 7 show the dependence of outlet time (the time, when a fertilizer particle leaves the spreading disc) and the outlet velocity v_e (the velocity of fertilizer granule leaving the spreading disc) on friction coefficient f . The continuous lines in Figures 6 and 7 correspond to $\psi_0 = 60^\circ$ and the dotted line to $\psi_0 = -90^\circ$. It appears from Figure 6 that in case of $\psi_0 = -90^\circ$ along with the increase of friction coefficient f , the outlet time t_e decreases quickly to the constant value, while in the case of $\psi_0 = 60^\circ$ this time increases evenly. Figure 7 indicates that the outlet velocity v_e of the granule in the case, where $\psi_0 = -90^\circ$ is lower than in the case, where $\psi_0 = 60^\circ$.

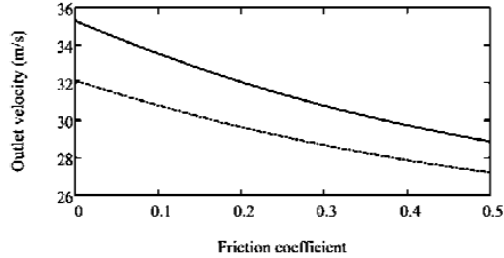


Figure 7 The dependence of outlet velocity v_e on friction coefficient f at $\psi_0 = 60^\circ$ and at $\psi_0 = -90^\circ$ (dotted line).

The dependence of the outlet time and velocity of fertilizer granule on the adjusting angle

Let us assume that $f = 0.3$ (according to Dintwa, et al., 2004b) and $r_0 = 0.04$ m, $R = 0.4$ m, $\omega = 60$ s⁻¹; $\varphi_0 = -90^\circ$. Figures 8 and 9 show the dependence of outlet time t_e and velocity v_e on adjusting angle ψ_0 . Figures 8 and 9 show that outlet time t_e and outlet velocity v_e are determined only when $-90^\circ \leq \psi_0 \leq 72^\circ$. Interestingly, it appears from Figure 8 that the outlet time t_e has minimal value at approximately $\psi_0 = -10^\circ$. Figure 9 shows that the outlet velocity v_e increases evenly along with the increase of the adjusting angle ψ_0 and it may be in the following range: 28.67 m s⁻¹ $\leq v_e \leq 30.85$ m s⁻¹. Figure 8 shows that the outlet time t_e is subject to the following range: 0.061 s $\leq t_e \leq 0.188$ s.

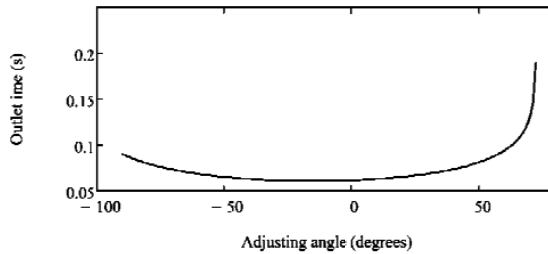


Figure 8 The dependence of outlet time t_e on adjusting angle ψ_0 .

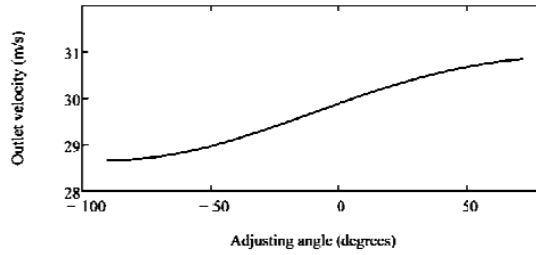


Figure 9 The dependence of outlet velocity v_c on adjusting angle ψ_0 .

The dependence of the outlet time and velocity of fertilizer granule on its initial distance from the centre of the spreading disc

Let us assume that $f = 0.3$, $\omega = 60 \text{ s}^{-1}$, $R = 0.4 \text{ m}$, $\varphi_0 = -90^\circ$. Figures 10 and 11 show the dependence of outlet time t_c and velocity v_c on the distance r_0 of fertilizer particle from the centre of the spreading disc at the initial time, when $\psi_0 = 60^\circ$ (continuous line) and $\psi_0 = -90^\circ$ (dotted line).

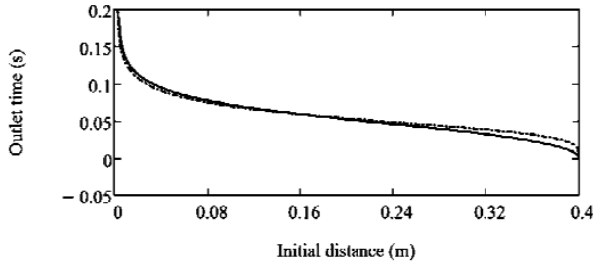


Figure 10 The dependence of outlet time t_c on the initial distance r_0 of fertilizer particle from the centre of the spreading disc at the initial time at $\psi_0 = 60^\circ$ (continuous line) and $\psi_0 = -90^\circ$ (dotted line)

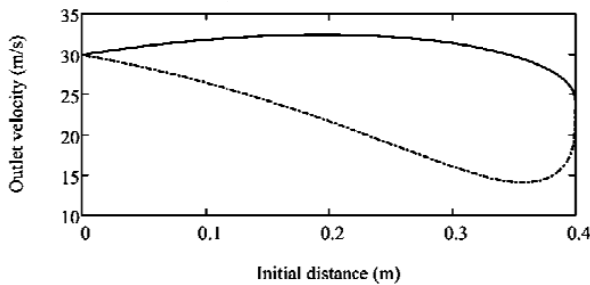


Figure 11 The dependence of outlet velocity v_c on the distance r_0 of fertilizer particle from the centre of the spreading disc at the initial time at $\psi_0 = 60^\circ$ and $\psi_0 = -90^\circ$ (dotted line)

Figure 10 shows that the outlet time t_c dependencies on initial distance r_0 in the case of $\psi_0 = 60^\circ$ and $\psi_0 = -90^\circ$ approximately coincide and decrease along with increasing the values of r_0 . Figure 11 shows that the dependencies of outlet velocity v_c on initial distance r_0 are very different in the cases of $\psi_0 = 60^\circ$, and $\psi_0 = -90^\circ$. In the case of $\psi_0 = 60^\circ$, the outlet velocity v_c has maximum value of 32.5 m s^{-1} approximately at $r_0 = 0.2 \text{ m}$, while in the case of $\psi_0 = -90^\circ$, this velocity has minimum value approximately at $r_0 = 0.36 \text{ s}^{-1}$.

This present paper provides a mathematical model for flat spreading disc equipped with pitched straight vanes. This model describes pure sliding motion of the fertilizer particle between disc and vane. With this mathematical model, it was possible to determine fertilizer particle velocity, which depends on five initial variables: f – friction, r_0 – initial position of the particle on the vane (vane pitch), ψ_0 – adjusting angle of the vane, R – spreading disc radius, and ω – angular velocity of the spreading disc. Comparatively, the study by Villette, Cointault, Piron, Chopiner (2005) uses three variables for flat disc: friction coefficient, disc angular velocity and vane pitch.

The video clips by Aan, Heinloo (2013) on simulation of the motion of the fertilizer granules represent a very good visualisation of the motion of the granules on the spreading disk of a fertilizer spreader. These video clips were composed on Mathcad worksheet by using the methodology presented by Heinloo (2010) and Olt, Heinloo (2011).

CONCLUSIONS

This paper shows the use of the features of the computer program Mathcad in the study of the spreading disc of fertilizer spreader.

According to the results of this paper, in order to ensure maximum outlet velocity of fertilizer granules, it is reasonable to use adjusting angle equal to 72° as possible minimum value of friction coefficient and vane pitch approximately equal to 0.17 m.

The outlet times and velocities can be used to study the motion of fertilizer granules after leaving the spreading disc of the fertilizer spreader, and the virtual sowing of the fertilizer spreader, and to determine the virtual distribution of virtual granules on a virtual field.

The results of this present paper and the corresponding video clips can be used in the process of teaching the students agricultural machinery and by the engineers studying the disc fertiliser spreader.

The scientists, wishing to compose visualizations of motions of the elements involved in agricultural machinery, can consider this paper as an example of visualization of machine elements on Mathcad worksheet and simulation of their motion.

REFERENCES

1. Aan, A., and Heinloo, M. (2013). Video clips on motion a granule on fertilizer spreading disc. Available at: <http://www.youtube.com/watch?v=8d9EYzzxw1s&feature=youtu.be> and http://youtu.be/ZEh0Zv_gixQ. Accessed on 8 August 2013.
2. Coetzee, C.J., and Lombard, S.G. (2011). Discrete element method modelling of a centrifugal fertiliser spreader. *Biosystems Engineering*. 109(4): 308-325

3. Dintwa, E., Van Liedekerke, P., Olieslagers, R., Tijskens, E., and Ramon, H. (2004a). Model for simulation of particle flow on a centrifugal fertiliser spreader. *Biosystems Engineering*, 87(4): 407–415.
4. Dintwa, E., Tijskens, E., Olieslagers, R., De Baerdemaeker, J., and Ramon, H. (2004b). Calibration of a Spinning Disc Spreader Simulation Model for Accurate Site-specific Fertiliser Application, *Biosystems Engineering*, 88(1): 49-62, doi: 10.1016/j.biosystemseng.2004.01.001.
5. García-Ramos, F. J., Boné, A., Serreta, A., and Vidal, M. (2012). Application of a 3-D laser scanner for characterising centrifugal fertiliser spreaders, *Biosystems Engineering*, 113(1): 33-41, doi: 10.1016/j.biosystemseng.2012.06.004
6. Grift, T. E., and Hofstee, J. W. (2002). Testing an online spread pattern determination sensor on a broadcast fertilizer spreader. *Transactions of the ASAE*, 45(3): 561-567.
7. Hofstee, J.W. (1995). Handling and spreading of fertilizers — Part 5. The spinning disc type fertilizer spreader. *Journal of Agricultural Engineering Research*, 62: 143–162.
8. Heinloo, M. (2010). Ketaslaoturi laotusketta virtuaalse tööprotsessi visualiseerimine (in Estonian). *Agraarteadus*, 21(1), 3 – 7, Available at: http://agrt.emu.ee/?Agraarteadus_2010.
9. Inns F. M., and Reece A.R. (1962). The theory of the centrifugal distributor. II: motion on the disc, off-centre feed. *Journal of Agricultural Engineering Research*, 7(4): 345–353.
10. Lawrence, H. G., Yule, I. J., and Coetzee, M. G. (2007). Development of an image-processing method to assess spreader performance. *Transactions of the ASABE*, 50(2): 397-407.
11. Olieslagers, R. (1997). Fertilizer distribution modelling for centrifugal spreader design. PhD Thesis, nr. 341, aan de faculteit landbouwwetenschappen, K.U. Leuven, Belgium
12. Olt, J., and Heinloo, M. (2011). Visualization of motion of fertiliser granules on the planar of spinning spreading disc of a disc spreader. *In: Efficient and safe production processes in sustainable agriculture and forestry: Proc. XXXIV CIOCTA-CIGR V Conference*, 292 - 296.
13. Patterson D.E., and Reece A.R. (1962). The theory of the centrifugal distributor. I: motion on the disc, near-centre feed. *Journal of Agricultural Engineering Research*, 7 (3): 232–240.
14. Reintam, A. (1995). Mineraalväetiste ketaslaoturi laotusketta tööprotsessi uurimine matemaatilise modelleerimise teel (in Estonian). *Agraarteadus*, VI (4): 435–448, available: http://agrt.emu.ee/?Agraarteadus_1995.
15. Swisher, D. W., Borgelt, S. C., and Sudduth, K. A. (2002). Optical sensor for granular fertilizer flow rate measurement. *Transactions of the ASAE*, 45 (4): 881-888.
16. Van Liedekerke, P., Tijskens, E., Dintwa, E., Antonus J., and Ramon, H. (2006). A discrete element model for simulations of a spinning disc fertilizer spreader I: single particle simulation. *Powder technology*, 170(2): 71-85.
17. Van Liedekerke, P., Tijskens, E., Dintwa, E., Rioual, F., Vangeyte, J., and Ramon, H. (2009). DEM simulations of the particle flow on a centrifugal fertilizer spreader. *Powder technology*, 190 (3): 348-360.
18. Van Liedekerke, P., Tijskens, E., and Ramon, H. (2009). Discrete element simulations of the influence of fertiliser physical properties on the spread pattern from spinning disc spreaders. *Biosystems Engineering*, 102 (4): 392-405.

19. Villette, S., Cointault, F., Piron, E., and Chopinet, B. (2005). Centrifugal Spreading: An Analytical Model for the Motion of Fertiliser Particles on a Spinning Disc. *Biosystems Engineering*, 92(2): 157–164.
20. Villette, S., Cointault, F., Chopinet, B., and Paindavoine, M. (2006). Optimizing Hough transform for fertilizer spreading optical control. *Optical Engineering*, 45 (2), Article no. 027006.
21. Villette S., Piron E., Cointault F., and Chopinet B. (2008). Centrifugal spreading of fertiliser: Deducing three-dimensional velocities from horizontal outlet angles using computer vision. *Biosystems Engineering*, 99(4): 496-507.
22. Villette, S., Piron, E., Martin, R., Miclet, D., Boilletot, M., and Gée, C. (2010). Measurement of an equivalent friction coefficient to characterise the behaviour of fertilisers in the context of centrifugal spreading. *Precision Agriculture*, 11(6): 664-683.

Aan, A., Heinloo, M., Allas, J.
Design of a radial cam for the cam-follower mechanism
Proceedings of 8th International Conference of DAAAM Baltic
Industrial Engineering, 11 – 16, 2014

DESIGN OF A RADIAL CAM FOR THE CAM-FOLLOWER MECHANISM

Aan A., Heinloo M., Allas J.

Abstract: This paper presents a method for designing of a radial cam on the worksheet of Mathcad including the calculation of follower's displacements, values of its velocities and accelerations, the optimization of the contour of a cam by choosing the eccentricity of follower and the radius of base circle of cam and the simulation of the working process of the cam mechanism. The optimal coordinates the contour of the cam were calculated. Finally, practical information for exporting cam contour data from Mathcad environment in data format necessary for CNC part program generation is discussed, considering CNC controllers using the most widespread ISO type program format and contouring with linear interpolation.

Key words: cam mechanism, design, optimization, visualization.

1. INTRODUCTION

Cam mechanisms consisting of only two elements, the cam as mechanical driver element and the follower as driven element, are widely used in technical applications due to reduced constructive complexity. Any functional motion of follower due to the movement of cam can be produced [1].

Cam mechanism can be classified in several ways: by follower motion (translating, rotating), by type of cam (radial, cylindrical), by joint closure, by follower (flat, rolling, mushroom), by cam curves [2]. Alaci et al. [3] have showed some aspects concerning the design of cam mechanisms with oscillating flat faced follower by using computer software. They also have generated figures of cam profiles as enve-

lopes of the straight lines paths on the Mathcad worksheet.

In the study of Ahmet Shala and Ramë Likaj [4] an analytical method for synthesis of cam mechanism is presented. They use Mathcad for displacement, velocity and acceleration calculation of the follower.

This paper presents the method and the results of numerical analysis of the radial cam, with translating follower on the worksheet of Mathcad. The visualization of the cam and follower and the simulation of working process of cam-follower mechanism are presented. The coordinates of the visualized cam contour coordinates can be used in the CNC milling machine for the production of the real cam.

2. MATERIALS AND METHODS

2.1 The scheme of cam-follower mechanism

Fig 1 shows the scheme of a cam-follower mechanism

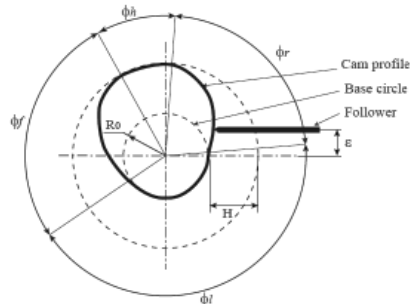


Fig. 1. The scheme cam mechanism, where ϕ_f is the rise angle, ϕ_h – the high dwell angle, ϕ_f – the fall angle, ϕ_l – the low dwell angle, ϵ – the eccentricity, H – the follower stroke

Let us consider the cam-follower mechanism by the following parameters: the rise angle of the follower $\phi_r = 60^\circ$; the high dwell angle of the follower $\phi_h = 60^\circ$; the fall (return) angle of the follower $\phi_f = 60^\circ$; the stroke of the follower $H = 0.005m$; the offset of the follower ε ; the radius of the base circle of the cam R_0 ; the number of positions of cam in computations $N = 360$; angular velocity of the cam $\omega = 10rad/s$.

2.2 Follower's displacement

According to [2] let us describe the displacement of the follower in the rise by the law:

$$s_1(\varphi) = H \left[35 \left(\frac{\varphi}{\phi_r} \right)^4 - 84 \left(\frac{\varphi}{\phi_r} \right)^5 + 70 \left(\frac{\varphi}{\phi_r} \right)^6 - 20 \left(\frac{\varphi}{\phi_r} \right)^7 \right] \quad (1)$$

and in the fall by the law

$$s_2(\varphi) = H - H \left[35 \left(\frac{\varphi - \phi_r - \phi_h}{\phi_f} \right)^4 - 84 \left(\frac{\varphi - \phi_r - \phi_h}{\phi_f} \right)^5 + 70 \left(\frac{\varphi - \phi_r - \phi_h}{\phi_f} \right)^6 - 20 \left(\frac{\varphi - \phi_r - \phi_h}{\phi_f} \right)^7 \right]. \quad (2)$$

In (1), (2) φ is the rotation angle of a cam from the initial position.

The displacement of a follower in one cycle of cam's rotation can be determined by the following program on the worksheet of the Mathcad (Fig. 2)

$$s(\varphi) = \begin{cases} s_1(\varphi) & \text{if } 0 \leq \varphi \leq \phi_r \\ s_1(\phi_e) & \text{if } \phi_r < \varphi \leq \phi_r + \phi_h \\ s_2(\varphi) & \text{if } \phi_r + \phi_h < \varphi \leq \phi_r + \phi_h + \phi_f \\ 0 & \text{otherwise} \end{cases}$$

Fig. 2. Program for determination of the follower displacement

Accordingly to program (Fig. 2) we get follower displacement on fig. 3.

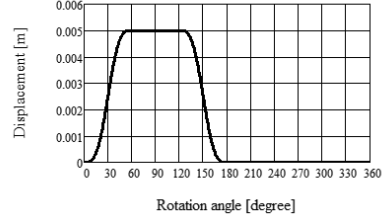


Fig. 3. The dependence of the displacement of the follower on rotation angle φ of the cam

2.3 Follower's velocity

The first derivative from equations (1) and (2) gives the velocity analogue functions:

$$v_1(\varphi) = \frac{d}{d\varphi} s_1(\varphi), \quad (3)$$

$$v_2(\varphi) = \frac{d}{d\varphi} s_2(\varphi). \quad (4)$$

The velocity analogue in one cycle of cam's motion can be determined by the program on the figure 4.

$$v(\varphi) = \begin{cases} v_1(\varphi) & \text{if } 0 \leq \varphi \leq \phi_r \\ 0 & \text{if } \phi_r < \varphi \leq \phi_r + \phi_h \\ v_2(\varphi) & \text{if } \phi_r + \phi_h < \varphi \leq \phi_r + \phi_h + \phi_f \\ 0 & \text{otherwise} \end{cases}$$

Fig. 4. Program for determination of the follower velocity analogue

The program in fig. 4 computes the analogue of the follower's velocity in the dependence on the rotation angle φ of the cam. To determine follower's real velocity (fig. 5) the velocity analogue were multiplied by the angular velocity ω of the cam.

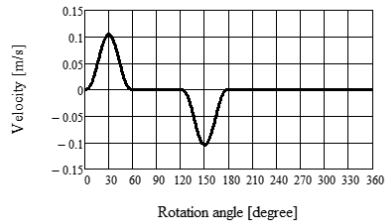


Fig. 5. The dependence of the follower velocity on the rotation angle φ of the cam

2.4 Follower's acceleration

The second derivative from equations (1) and (2) gives the acceleration analogue functions:

$$a_1(\varphi) = \frac{d^2}{d\varphi^2} S_1(\varphi), \quad (5)$$

$$a_2(\varphi) = \frac{d^2}{d\varphi^2} S_2(\varphi). \quad (6)$$

The acceleration analogue for one cycle of cam's motion can be determined by the program on the fig. 6.

$$a(\varphi) = \begin{cases} a_1(\varphi) & \text{if } 0 \leq \varphi \leq \phi_r \\ 0 & \text{if } \phi_r < \varphi \leq \phi_r + \phi_h \\ a_2(\varphi) & \text{if } \phi_r + \phi_h < \varphi \leq \phi_r + \phi_h + \phi_f \\ 0 & \text{otherwise} \end{cases}$$

Fig. 6. Program for determination of the follower acceleration analogue

The program in fig. 6 computes the follower's acceleration analogue in the dependence on the rotation angle φ of the cam. To determine follower's acceleration (fig. 7) the acceleration analogue were multiplied by the square of the cam angular velocity ω^2 .

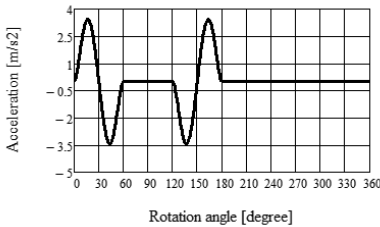


Fig. 7. The dependence of the follower acceleration on the rotation angle φ of the cam

2.5 Optimization of the eccentricity and the radius of the base circle

The pressure angle α (fig. 8) is one of the limiting criteria's for cam design. According to Norton [2] the pressure angle must be between 0 to ± 30 degrees. Pressure angle value can be adjusted by the values of the eccentricity ε and radius R_0 of base circle.

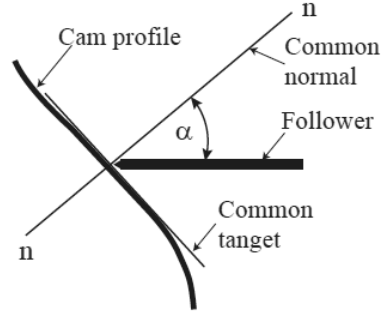


Fig. 8. The pressure angle α between the cam and the follower

According to [2] the pressure angle α of the cam determines the following formula:

$$\alpha(\varphi, R_0, \varepsilon) = \arctan \left(\frac{v(\varphi) - \varepsilon}{s(\varphi) + \sqrt{R_0^2 - \varepsilon^2}} \right). \quad (7)$$

Base circle radius and eccentricity cannot be solved conveniently directly. To find proper R_0 and ε Norton [2] suggest to use special cam design program Dynacam or some equation solvers such as Matlab, TKSolver or Mathcad.

To determine the radius of base circle R_0 and eccentricity ε let us formulate the following problem of optimization:

find such values for R_0 and ε that guarantee satisfaction of the restriction

$$\alpha(\varphi, R_0, \varepsilon) = \alpha_e \quad (8)$$

in the rise and the restriction

$$\alpha(\varphi, R_0, \varepsilon) = \alpha_n \quad (9)$$

in the fall.

With lower accuracy the solution of system of equations (8) and (9) can be obtained also by hand [2], changing the values of R_0 and ε from initial values step by step. Doing so it is useful to know that the change of value ε moves the graph of the function $\alpha(\varphi, R_0, \varepsilon)$ upwards or downwards without changing its shape and the change of value R_0 increases or decreases the external values of the function $\alpha(\varphi, R_0, \varepsilon)$. In such way the solution for system of equations (8) and (9) by low accuracy can be obtained relatively quickly satisfying the need of teaching process.

The solution method of high accuracy for the system of equations (8) and (9) with respect to R_0 and ε by the help of Mathcad will be developed in future.

Let us consider an example with the maximal value of the pressure angle $\alpha(\varphi, R_0, \varepsilon)$ $a_e = 20^\circ$ (in rise) and minimal value of the pressure angle $a_n = -24^\circ$ (in fall). Let's take the initial values $R_0 = 20\text{mm}$ and $\varepsilon = 0\text{mm}$. In this case the curve of the function $\alpha(\varphi, R_0, \varepsilon)$ is presented in fig. 9, showing the pressure angle curve crossing the values of $a_e = 20^\circ$ and $a_n = -24^\circ$. This means that the system of equations (8) and (9) is not satisfied.

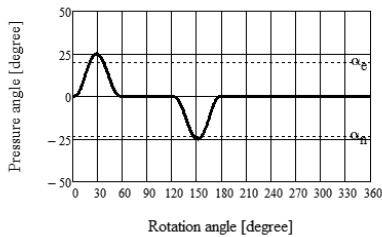


Fig. 9 Cam mechanism pressure angle, $R_0 = 20\text{mm}$ and $\varepsilon = 0$

By changing the values of R_0 and ε step by step one can visually observe the change of the graph of function $\alpha(\varphi, R_0, \varepsilon)$ and quickly obtain the position of this graph, shown in fig. 10. This means that the system of equations (8) and (9) is satisfied with some compromise of accuracy. The case in fig. 10 corresponds approximately to $R_0 = 31\text{mm}$ and $\varepsilon = -1.5\text{mm}$.

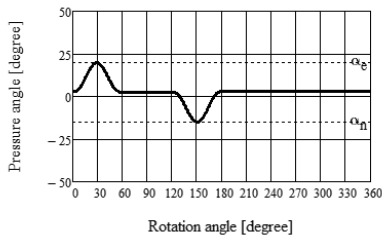


Fig. 10 Cam mechanism pressure angle, $R_0 = 31\text{mm}$ and $\varepsilon = -1.5\text{mm}$

2.6 Visualization of the cam and simulation of the working process of cam-follower mechanism

The polar coordinates $\beta(\varphi), R(\varphi)$ of contact point of the follower and the cam are $R(\varphi) =$

$$\sqrt{s(\varphi)^2 + R_0^2 + 2 \cdot s(\varphi) \sqrt{R_0^2 - \varepsilon^2}}, \quad (10)$$

$$\beta(\varphi) = \varphi - \left(\text{asin}\left(\frac{\varepsilon}{R(\varphi)}\right) - \text{asin}\left(\frac{\varepsilon}{R_0}\right) \right), \quad (11)$$

where $R(\varphi)$ is the polar radius and $\beta(\varphi)$ – the polar angle of the contour point in dependence of angle of cam's rotation φ .

To visualize the contour of the cam let us assume that the cam is not rotating but the follower rotates around the centre of the cam with angle of rotation φ . Then the contact point with polar coordinates $\beta(\varphi), R(\varphi)$ draws the contour of the cam. Fig. 11 visualizes the initial position of the cam in the case $R_0 = 31\text{mm}$ and $\varepsilon = -1.5\text{mm}$.

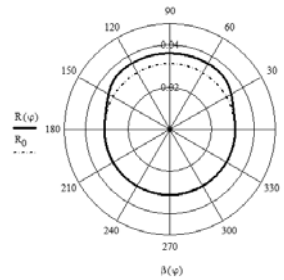


Fig. 11 Cam contour in the polar coordinates $\beta(\varphi), R(\varphi)$

The Cartesian coordinates of the cam contour at the initial position are

$$x(\varphi) = R(\varphi) \cos(\beta(\varphi)), \quad (12)$$

$$y(\varphi) = R(\varphi) \sin(\beta(\varphi)). \quad (13)$$

To simulate the working process of the cam-follower mechanism the cam in fig. 11 [°] is rotated by the angle $\theta = \omega t$, where ω is the angular velocity and t – the time. Equations

$$x_1(\varphi) = x(\varphi) \cdot G(\theta), \quad (14)$$

$$y(\varphi)_1 = y(\varphi) \cdot G(\theta), \quad (15)$$

where

$$G(\theta) = \begin{pmatrix} \cos \theta & \sin \theta \\ -\sin \theta & \cos \theta \end{pmatrix}$$

determine the contour of the cam, turned around the centre of cam by the angle θ counter clockwise.

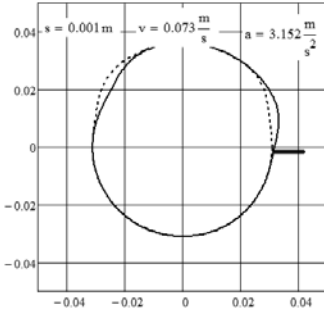


Fig. 12 A frame from video clip [5]

3. PRODUCTION OF CAM

Nowadays any part despite of its complicated shape can be machined on modern industrial CNC machine tools with geometrical accuracy of at least 15 microns, so the machining of the modelled geometrical shape of a cam can be accomplished quite easily with great precision. An ordinary radial cam can be produced in CNC machining centre by contour cutting with a square end mill of suitable type according to cam material and dimensions. Cam geometry points in Cartesian coordinates can be calculated with required accuracy according to equations (12) and (13) (fig. 13) by changing the angular increment of calculations.

$x(\varphi) =$		$y(\varphi) =$	
31	mm	0	mm
30.999		0.271	
30.995		0.541	
30.989		0.811	
30.981		1.082	
30.971		1.352	
30.958		1.622	
30.944		1.893	
...		...	

Fig. 13 Contour coordinates of optimal cam

Different geometrical interpolation techniques for connecting the calculated con-

tour points of cam can be available and used in CNC machine tools depending on the machine tool control options. As discussed by Norton [2], circular and spline fitting interpolation techniques are superior to linear interpolation in terms of vibratory noise in acceleration measurements. Still, on most CNC controllers in everyday use only linear or circular tool movement interpolation is available, so the geometrical accuracy of a machined cam (so called "chordal deviation") compared to mathematical model must be regulated by selecting appropriate angular increment for contour points calculation.

Coordinate values on the fig. 13 can be exported from Mathcad to another different file formats (for example to Microsoft Excel or Notepad) for converting exported data into file format suitable for direct usage in CNC machine tool part program. Majority of CNC part programs are composed in the form of a simple ASCII text file. Widespread CNC controllers using ISO or similar program format accept the input of contour point values for linear interpolation in the form of successive lines of type

```
X...Y... ,
characters X and Y hereby representing the machine tool axes followed by numerical coordinate value, for example (numerical values taken from fig.13)
...
X30.989Y0.811
X30.981Y1.082
X30.971Y1.352 .
```

Coordinate output in showed format can be accomplished from Mathcad calculations. As the cutting tool centre must be offset from cam contour by the radius value of the cutter, CNC controller's cutter radius compensation function must be used in process of machining. The optimal method for bringing the tool into cut for closed contours is to approach the contour tangentially, which helps to avoid contouring mistakes caused by tool deflection, so the tangent line direction for the starting point of

contour cutting must be known. Considering the fact the type of cam contour studied in this work is an arc between rotation angles $\varphi=180\dots360$, we can assume that the tangent line for contour point $\varphi=0=360$ is parallel to Y axis (fig. 14). As the machining of contour is started and finished in point $\varphi=0$, additional tool moves parallel to X and Y axis can be manually added to program for smooth tool transition into and out of the cut.

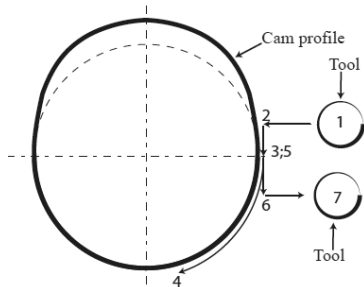


Fig. 14 Tool movement steps: 1 – initial position, 2 – beginning of contour start point tangent line, 3 – starting point of contour cutting, 4 – contour cutting, 5 – end point of contour cutting, 6 – end of contour end point tangent line, 7 – end position

In general the contours are milled using climb cutting, although conventional cutting may give better results in some special cases. The choice between climb and conventional cutting affects the machining direction of a contour, which are accordingly clockwise or counter clockwise for external contours. However, the choice between cutting direction can be easily taken into account while exporting coordinate data from Mathcad. Defining the rotation angle range φ to change clockwise (from 360 to 0 instead) results in contour point coordinates output in clockwise direction and vice versa.

4. CONCLUSION

1. The Computer Package Mathcad can be considered as a convenient tool for design of cams.

2. Mathcad allows the simulation of motion of virtual models of cam mechanisms.

3. Mathcad can be used to compute cam contour coordinates, which can be used for CNC part program.

4. The method presented in this paper can be used in the teaching process of engineering subjects and also by engineers in their work.

5. REFERENCES

1. Shin, J.-H., Kwon, S.-M. & Nam, H. A hybrid approach for cam shape design and profile machining of general plate cam mechanisms, *International Journal of Precision Engineering and Manufacturing*, 2010, **11**(3), 419-472.
2. Norton, R. L. *Cam design and manufacturing handbook*. 2009, Industrial Press Inc., new York.
3. Alaci, S., Ciornei, F. C., Amarandei, D., Filote, C., Patras-Ciceu, S., Prodas, D. *Some aspects regarding computer aided design of cam mechanism with flat face oscillating follower*. *Fiability & Durability*, 2011, **1**(7).
4. Shala, A., Likaj, R. *Analytical method for synthesis of cam mechanism*. *International Journal of Current Engineering and Technology*, 2013, **3**(2).
5. Aan, A. *Simulation the working process of cam-follower mechanism*. 2013. <https://www.youtube.com/watch?v=c43Jlq7-rvc>

6. ADDITIONAL DATA

MSc (Eng Sc) Aan, Aare (author)

e-mail: aare.aan@emu.ee.

Dr (math) Heinloo, Mati (co-author)

e-mail: mati.heinloo@emu.ee.

MSc (Engn Sc) Allas, Jaanus (co-author)

e-mail: jaanus.allas@emu.ee.

Institute of Technology,
Estonian University of Life Sciences,
Kreutzwaldi 56, 51014, Tartu, Estonia

Aan, A., Heinloo, M.
Analysis and synthesis of
the walking linkage of Theo Jansen with a flywheel
Agronomy Research, 12(2), 657 – 652, 2014

Analysis and synthesis of the walking linkage of Theo Jansen with a flywheel

A. Aan* and M. Heinloo

Institute of Technology, Estonian University of Life Sciences, Kreutzwaldi 56, EE51014 Tartu, Estonia; *Correspondence: aare.aan@emu.ee

Abstract. This paper presents the results of cinematic and dynamic calculations of Theo Jansen's walking linkage on the worksheet of Mathcad. To validate the cinematic calculations, a video clip with simulation of the motion of Theo Jansen's mechanism is composed. The synthesis of a flywheel for Theo Jansen's linkage input link to decrease the fluctuation in its rotation is considered in detail.

Key words: theory of mechanisms and machines, Theo Jansen linkage, flywheel, Mathcad.

INTRODUCTION

Humans are mainly using wheeled vehicles for on the ground transportation. But if we look around in the nature, there is no biological creature moving on wheels. To move on the ground, living creatures use legs or crawl. Compared to wheel locomotion, walking has many advantages: lower energy consumption, no need for roads, better to cross over obstacles, the contact with ground is in a determined point, the ground is damaged less (Moldovan et al., 2011). Hence, the scientists are trying to design vehicles which are using legs or other locomotion ways that are inspired from nature.

A Dutch physicist and artist Theo Jansen started to use a twelve-bar mechanism for legs in his kinetic sculptures (Jansen, 2007). This mechanism is now called the 'Theo Jansen linkage' and it can be used for walking vehicles.

There are several studies for the Theo Jansen linkage. Komoda and Wagatsum (2011) proposed an extension mechanism for climbing over bumps. They demonstrated that lifting up of the linkage centre (pivot O_1 , Fig. 1) will raise the leg's orbit upward and the combination of a cycle and up-down motion provides a new elliptic orbit for climbing over bumps with about 10 times the height of the original. In their later work, they propose to move the pivot O_1 (look Fig. 1) periodically, this will also ensure movement over bumps (Komoda & Wagatsum, 2012). Moldovan et al. (2011) showed a walking robot as a part of a mechatronic system and the design of the leg structure based upon the CAD design and forward kinematics. Giesbrecht et al. (2012) optimize the design of the Jansen linkage. The optimization is set up to minimize the energy input and maximize the stride length; they based the optimization on the dynamic of the force analysis.

In this paper, the Jansen linkage movement in a resisting environment is analysed. The fluctuating forces in the resisting environment and the reduced moment of inertia

on the driving link are causing speed fluctuation. To reduce speed fluctuation, a method for calculating a flywheel to the linkages on a Mathcad worksheet is demonstrated. A virtual model of the Jansen mechanism is composed on a worksheet of Mathcad for validation of kinematic calculations. A video clip is composed from the virtual model.

MATERIAL AND METHODS

Description of the walking mechanism of Theo Jansen

The twelve bars of the linkage with measurements are $OA = 250$ mm, $OO_1 = 690$ mm, $AB = 910$ mm, $BO_1 = 650$ mm, $CO_1 = 970$ mm, $BC = 790$ mm, $AE = 1,030$ mm, $EO_1 = 660$ mm, $ED = 790$ mm, $DF = 1,150$ mm, $EF = 670$ mm and $CD = 920$ mm. There are the same measurements for rear links (Fig. 1). The measurements originate from the thesis of Ingram (2006).

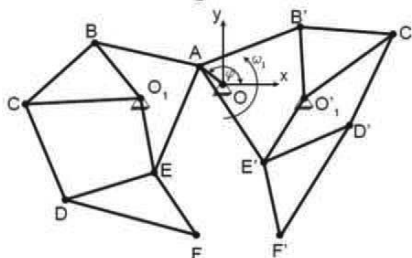


Figure 1. Theo Jansen mechanism.

The link OO_1 is fixed and the constructive angle between the x-axis and the link is $\gamma = 11.16$ degrees. In the calculations, the link OA has constant counter-clockwise angular velocity $\omega_1 = 30$ rad s^{-1} . The movement of the link OA will finally cause movement of the point F and F' , these points are like the leg's feet. The loops of the points F and F' are triangular with these links alignments.

In the calculations, the link masses are found by $m = 0.5 \cdot l$, where l is the length of the link. To determine the moment of inertia of the links, the following formula is used: $I = m \cdot l^2 / 10$. For the triangles BCO_1 , DEF and $B'C'O_1$, the $D'E'F'$ moment of inertia is found by the Huygens-Steiner theorem (Lepik & Roots, 1971).

Determination of coordinates, velocities and accelerations analogues

The kinematic calculations were made on a worksheet of Mathcad; this method has been introduced in previous papers (Aan et al., 2012a; Aan & Heinloo, 2012).

On the basis of kinematic calculations, the simulation of linkage movement with pivot F and F' velocity and acceleration vectors, a video clip was composed on a Mathcad worksheet (Aan, 2014). A frame from the video clip is on Fig. 2.

Analysis of the loops of the pivots F and F'

If we look at Fig. 2, the loops of the pivots F and F' look triangular. On Fig. 3, the lower part of the pivot F loop is zoomed. From there one can see that the lower side of the triangle is not a straight line. By analysis of Fig. 3, the starting point, where the

body weight of the pivot F is taken is set to $x_1 = -1.1498$ m, $y_1 = -1.3708$ m and the end point $x_2 = -0.2055$ m, $y_2 = -1.3708$ m. For the pivot F', the corresponding values are $x'_1 = 0.2055$ m, $y'_1 = -1.3708$ m and $x'_2 = 1.1498$ m, $y'_2 = -1.3708$ m. According to the value of the rotating angle φ , the pivot F is connected with the ground when $\varphi = \varphi_1 = 252$ degrees and leaves the ground when $\varphi = \varphi_2 = 132$ degrees. Pivot F' is connected with the ground when $\varphi = \varphi'_1 = 48$ degrees and leaves the ground when $\varphi = \varphi'_2 = 288$ degrees.

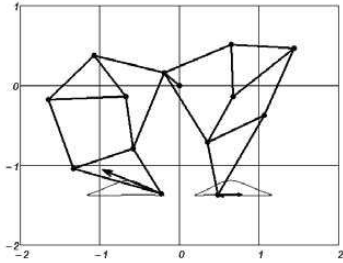


Figure 2. A frame from video clip (Aan, 2014).

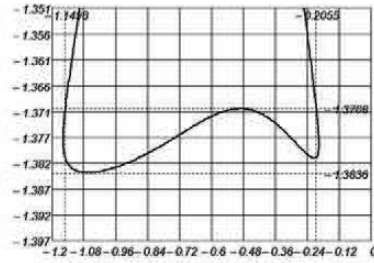


Figure 3. Zoomed lower part of the pivot F loop.

From Fig. 3, one can see that the leg (points F and F') is moving from right to left, it will leave the ground at the point (x_2, y_2) and touch it again at the point (x_1, y_1) . In this study, the foot is moving in the environment (snow, water, mud, etc.) between these points, where resisting forces are applied to it. The resisting force projection on the x axis is $F_{tx} = 250$ N and on the y axis $F_{ty} = 150$ N, same for the rear leg. According to this analysis, the dependency of the resisting force on the rotation angle φ and from points (x_1, y_1) and (x_2, y_2) is defined by the following program on a worksheet of Mathcad (Fig. 4).

$$F_t(\varphi) = \begin{cases} F_t \leftarrow F_t & \text{if } \varphi_2 \leq \varphi \leq \varphi_1 \\ 0 & \text{otherwise} \end{cases} \quad F'_t(\alpha) = \begin{cases} F_t \leftarrow F_t & \text{if } \varphi \leq \varphi'_1 \vee \varphi \geq \varphi'_2 \\ 0 & \text{otherwise} \end{cases}$$

Figure 4. Programs for determination of resisting forces (left point F, right point F'), where F_t – magnitude resisting force.

Reduced resisting torque and moment of inertia

The resisting forces and moment of inertia will be reduced on the link OA. For the resisting forces, the following equation is used:

$$M_r \cdot \omega_1 = \sum_k (F_k \cdot v_k \cdot \cos \alpha_k) + \sum_u (M_u \cdot \omega_u), \quad (1)$$

where: M_r – magnitude of resisting torque on link one (OA in this case); F_k – magnitude of resisting force; v_k – magnitude of velocity; α_k – angle between force and velocity; M_u – pivot's resisting torque and ω_u – pivot angular velocity. In this case, the equation (3) is in the form of

$$M_r(\varphi) = F_t(\varphi) \cdot v_F(\varphi) \cdot \cos 180^\circ + F'_t(\varphi) \cdot v'_{F'}(\varphi) \cdot \cos 180^\circ. \quad (2)$$

The kinetic energy of the linkage was determined by the well-known König theorem (Lepik & Roots, 1971). In order to use the König theorem, the following mechanism links parameters must be determined: moments of inertia, angular velocities, masses and centre of mass velocities; these values are found by the methods which are described above.

The reduced moment of inertia (Artobolevski, 1961) on the link OA can be presented in the form:

$$I_r(\varphi) = I_{OA} + m_{AB} \cdot v_{AB}(\varphi)^2 + I_{AB} \cdot \omega_{AB}(\varphi)^2 + I_{BCO1} \cdot \omega_{BCO1}(\varphi)^2 + m_{CD} \cdot v_{CD}(\varphi)^2 + I_{CD} \cdot \omega_{CD}(\varphi)^2 + I_{EO1} \cdot \omega_{EO1}(\varphi)^2 + m_{AE} \cdot v_{AE}(\varphi)^2 + I_{AE} \cdot \omega_{AE}(\varphi)^2 + m_{EDF} \cdot v_{EDF}(\varphi)^2 + I_{DEF} \cdot \omega_{DEF}(\varphi)^2 + m_{AB} \cdot v'_{AB}(\varphi)^2 + I_{AB} \cdot \omega'_{AB}(\varphi)^2 + I_{BCO1} \cdot \omega'_{BCO1}(\varphi)^2 + m_{CD} \cdot v'_{CD}(\varphi)^2 + I_{CD} \cdot \omega'_{CD}(\varphi)^2 + I_{EO1} \cdot \omega'_{EO1}(\varphi)^2 + m_{AE} \cdot v'_{AE}(\varphi)^2 + I_{AE} \cdot \omega'_{AE}(\varphi)^2 + m_{EDF} \cdot v'_{EDF}(\varphi)^2 + I_{DEF} \cdot \omega'_{DEF}(\varphi)^2, \quad (3)$$

where: I – moment of inertia; m – link mass; ω – link angular velocity; and v – link centre of mass velocity.

Reduction of the fluctuation of the input link's coefficient of speed with a flywheel

Input link OA angular velocity can be determined, in this case with reduced resisting torque (2) and moment of inertia (3), with the following equation (Artobolevski, 1961)

$$\omega(\varphi) = \sqrt{\frac{I_r(0) \cdot \omega_0^2}{I_r(\varphi)} + \frac{2}{I_r(\varphi)} \cdot \Delta T(\varphi)}, \quad (4)$$

where: $I_r(0)$ – value of reduced moment of inertia at $\varphi = 0$; ω_0 – unknown value of $\omega(\varphi)$ at $\varphi = 0$; and $\Delta T(\varphi)$ – change of the linkage kinetic energy. The exact formula for the determination of ω_0 cannot be derived. To find ω_0 , one can use an approximate formula (Lepikson, 1998)

$$\omega_0 = \frac{n \cdot \omega_1}{\sum_{i=0}^n \sqrt{\frac{I_r(0)}{I_{ri}} + \frac{4 \cdot \Delta T_i}{I_{ri} \cdot \omega_1^2}}}, \quad (5)$$

where in this case $n = 360$, because the calculations are made with a step 1 degree, started at $\varphi = 0$ until $\varphi = 360$ degrees.

In equation (4), change of the linkage kinetic energy is determined with the following equation

$$\Delta T(\varphi) = M_m \cdot \varphi + \int_0^\varphi M_r(\varphi) d\varphi, \quad (6)$$

where M_m – constant driving torque of the link OA.

The results of equation (4) are shown on Fig. 5. Because of the reduced moment of inertia in equation (3) and the fluctuating resisting forces, angular velocity is also not constant.

The coefficient of speed fluctuation is defined as

$$\delta = \frac{\max(\omega(\varphi)) - \min(\omega(\varphi))}{\frac{\max(\omega(\varphi)) + \min(\omega(\varphi))}{2}} \quad (7)$$

Accordingly to equations (4) and (7), with these linkage parameters, the speed fluctuation is $\delta = 0.47$. When the fluctuation is ≥ 0.2 , large variation must be allowed in the mechanism (Shigley et al., 2004). To decrease fluctuation, a flywheel must be added to the mechanism and equation (4) takes the form

$$\omega(\varphi) = \sqrt{\frac{(I_r(0)+I_f) \cdot \omega_0^2}{I_r(\varphi)+I_f} + \frac{2}{I_r(\varphi)+I_f} \cdot \Delta T(\varphi)}, \quad (8)$$

where I_f is the moment of inertia of the flywheel.

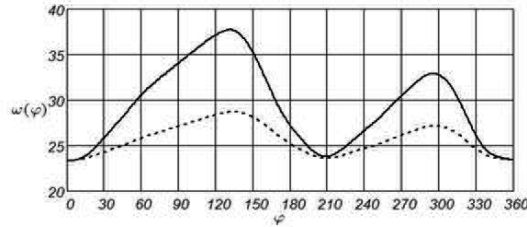


Figure 5. Link OA angular velocity according to formulas (6) and (10) $I_f = 1 \text{ kg} \cdot \text{m}^2$ (dotted line).

In consideration of equations (7) and (8), a program can be used on a worksheet of Mathcad to find fluctuation as a function of the flywheel's moment of inertia (Fig. 6).

$$U(I_f) = \begin{cases} \text{for } n \in 0..360 \\ \omega(\varphi)_n \leftarrow \sqrt{\frac{(I_r(0) + I_f) \cdot \omega_0^2}{I_{r_n} + I_f} + \frac{2}{I_{r_n} + I_f} \cdot \Delta T_n} \\ \delta \leftarrow \frac{\max(\omega(\varphi)) - \min(\omega(\varphi))}{\frac{\max(\omega(\varphi)) + \min(\omega(\varphi))}{2}} \end{cases}$$

Figure 6. Program to find fluctuation as a function of the flywheel's moment of inertia.

The results according to the program on Fig. 6 are shown on Fig. 7. For example, if fluctuation must be $\delta \leq 0.1$, then according to Fig. 7, the flywheel's moment of inertia must be $I_f \geq 3 \text{ kg} \cdot \text{m}^2$.

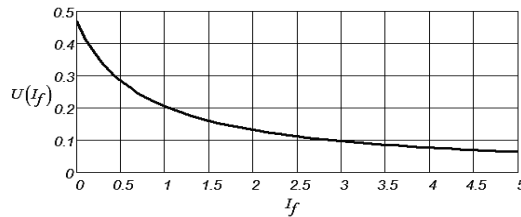


Figure 7. Fluctuation according to the flywheel's moment of inertia.

CONCLUSIONS

1. In this paper, the results of the calculations of Theo Jansen's mechanism are presented on a worksheet of the Computer Package Mathcad. According to the kinematic calculations, a video clip was composed on a Mathcad worksheet, where linkage motion is simulated together with the pivots' F and F' velocity and acceleration vectors.
2. The loops of the pivots F and F' are analysed and their movement under resisting forces determined.
3. The results of synthesis of a flywheel for the Theo Jansen's linkage are presented.

The method presented in this paper can be used in the teaching process of the engineering subject 'Mechanics of Machinery' and also by engineers in their everyday work.

REFERENCES

- Aan, A. & Heinloo, M. 2012. Computer based comparison analysis of single and double-connecting-rod slider-crank linkages. *Agronomy Research* **10**, 3–10.
- Aan, A., Heinloo, M., Aarend, E. & Mikita, V., 2012. Analysis of four-stroke cycle internal combustion V-engine in Mathcad environment. *8th International DAAAM Baltic Conference 'Industrial Engineering'*, Tallinn, TTU Press, 389–394.
- Aan, A. 2014. Jansen linkage. Available at: http://www.youtube.com/watch?v=B_dR2_O3ujc (30.01.2014)
- Artobolevski, I.I. 1961. *Theory of mechanism and machines* (in Estonian). Tallinn, 743 p.
- Moldovan, F., Dolga, V., Ciontos, O. & Pop, C. 2011. Cad design and analytical model of a twelve bar walking mechanism. *Scientific Bulletin, Series D*, **73**(2).
- Jansen, T. 2007. *Theo Jansen: The Great Pretender*. Rotterdam, 010 Publisher, 240 p.
- Komoda, K. & Wagatsuma, H. 2011. A study of availability and extensibility of Theo Jansen mechanism toward climbing over pumps. *The 21st Annual Conference of the Japanese Neural Network Society*. OIST, Okinawa.
- Komoda, K. & Wagatsuma, H. 2012. A proposal of the extended mechanism for Theo Jansen linkage to modify the walking elliptic orbit and a study of cyclic base function. *Proceeding 7th Annual dynamic walking conference*. IHMC, Florida, 143–145.
- Giesbrecht, D., Wu, C.Q. & Sepehri, N. 2012. Design and optimization of a eight-bar legged walking mechanism imitating a kinetic sculpture, 'Wind Beast'. *Transactions of the Canadian Society for Mechanical Engineering* **36**(4), 343–355.
- Ingram, A.J. 2006. Phd thesis: *A new type of mechanical walking machine*. University of Johannesburg, 158 p
- Lepik, Ü. & Roots, L. 1971. *Theoretical mechanics* (In Estonian). Tallinn, pp 483.
- Lepikson, H. 1998. *Design of kinematic scheme for four-stroke internal combustion V-engine* (in Estonian). Tallinn, 76 p.
- Shigley, J., Mischke, C. & Brown, T. 2004. *Standard handbook of machine design*. McGraw-Hill, 1200 p.

Aan, A., Heinloo, M.
Dynamics of a frozen sea buckhorn berry in a separator
Procedia Engineering, 100, 689 – 698, 2015



25th DAAAM International Symposium on Intelligent Manufacturing and Automation, DAAAM 2014

Dynamics of a Frozen Sea Buckhorn Berry Motion in a Separator

Aare Aan*, Mati Heinloo

Estonian University of Life Sciences, Institute of Technology, Fr.R.Kreutzwaldi 56, Tartu 51014, Estonia

Abstract

After removing frozen sea buckthorn berries from the branches of sea buckthorn tree in a separator (patent EE05717B1), the berries fall onto separator's moving conveyer belt under a certain angle of inclination, thus guiding the berries in the collector of separator. This paper presents the mathematical model of the berry motion along the conveyer and after falling from it. The nonlinear differential equations describing the berry motion on the conveyer and after falling from it take into account air resistance depending on the square value of berry's absolute velocity. All these equations were solved numerically by using Runge-Kutta method of 4th order on Mathcad worksheet. This paper focuses on berry motion depending on belt velocity, friction coefficient between belt and berry, and inclination angle of the belt. Composed video clip visualizes berry motion and demonstrates how the berry moves from the initial position in the same direction as conveyer belt velocity, down to lower edge of the belt and falls from conveyer. Results of this paper can be used by engineers designing conveyors and by educators teaching agricultural machinery.

© 2015 The Authors. Published by Elsevier Ltd. This is an open access article under the CC BY-NC-ND license (<http://creativecommons.org/licenses/by-nc-nd/4.0/>).

Peer-review under responsibility of DAAAM International Vienna

Keywords: berry separator; mathematical modelling; berry motion; visualization; Mathcad; belt conveyer

1. Introduction

Moving different materials on belt conveyors is a very common solution used in various industries because of their high efficiency in comparison to other transport methods [1]. Therefore, belt conveyors are widely researched and developed.

Ibishi et al. showed the method for calculating the tension force of the belt. The purpose of the method is to recognize the tension force upper limit, exceeding of which may damage belt transportation equipment [2]. Zanoelo

* Corresponding author. Tel.: +3727313302.
E-mail address: aare.aan@emu.ee

and et al. studied mate leaves dryer and proposed to control the velocity of the belt by the mathematical drying model to ensure the accepted range of moisture in mate leaves [3]. There are energy models that can be used for efficiency optimization of the belt conveyor's operation [4]. In recent studies by Göttlich et al., mathematical model was used to simulate a conveyor belt where the cargo is separated by means of a rigid singularizer. They also validated their model with real data tests [5].

This paper aims at providing a model and simulation of continuous belt conveyor on sea buckhorn berry separator (Fig. 1). The function of this belt conveyor is to separate the frozen berries, leaves and small branches which cannot be removed with sieve. The belt carries leaves and branches away while berries roll over the belt due to its inclination (Fig. 1). This paper presents the possibility to model mathematically berry motion on the conveyor belt. Calculations are based on the numerical method Runge-Kutta that was also used by above-mentioned authors in the field of conveyor modelling. The motion of the berry is visualized by graphs and by a video clip. Results of this paper can be used for designing berry conveyors and for analysing their motion. It also introduces some methods to be used with math program Mathcad, which is used also in other studies for engineering calculations [6] [7].

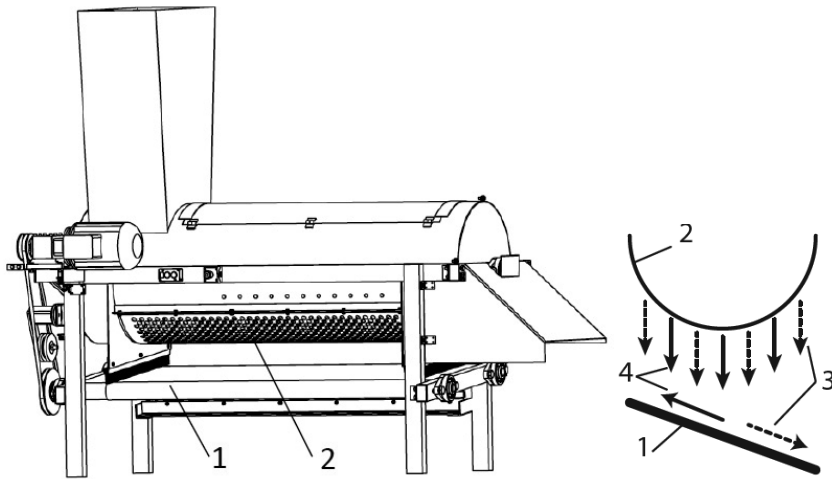


Fig. 1. Left: device for separation of deep-frozen sea buckhorn berries from twigs [8]. Right: principal scheme of the sea buckhorn berries separator sieve and conveyor belt. Where: 1 - inclined conveyor belt, 2 - sieve, 3 – sea buckhorn berries, 4 - leaves and small branches.

Nomenclature

v_k	velocity of the conveyor belt, m/s
l	width of the belt, m
s	axis, with origin at the point B along the conveyor belt, m
s_0	initial value on s-axis, m
s'	berry's velocity, m/s
β	inclination angle of the conveyor belt, degrees
m	berry particle mass, kg
g	acceleration of gravity, m/s^2
f	friction coefficient between berry particle and conveyor belt

ρ	air density, kg/m^3
c_d	air resistance constant
A	surface of the frontal area, m^2
s''	berry particle acceleration, m/s^2
t	time, s
t_0	the time when berry motion begins, s
t_N	the time when berry motion ends, s
N	the number of subintervals within the interval (t_0, t_N)

2. Materials and Methods

The kinematic scheme of the cleaning belt conveyor of buckhorn berry separator is shown on Fig 2.

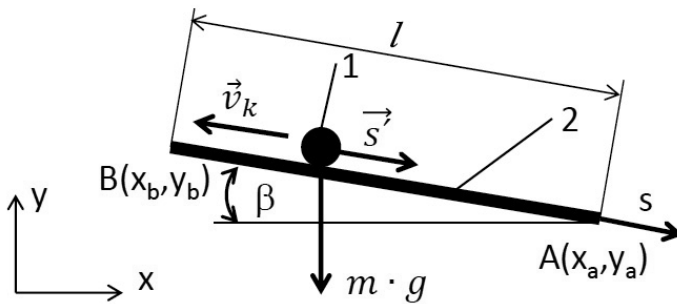


Fig. 2. The computational scheme of belt conveyor: 1 – berry particle, 2 – conveyor belt between points AB, l – width of the belt (distance between points AB), v_k – velocity of the conveyor belt, s – axis, with origin at the point B along the conveyor belt, s' – berry's velocity, β – inclination angle of the conveyor belt, m – berry particle mass, g – acceleration of gravity.

2.1. Berry motion on the belt

Berry particle motion can be modelled by using the following differential equation

$$m \cdot s'' = m \cdot g \cdot \sin \beta - f \cdot m \cdot g \cdot \cos \beta - \frac{1}{2} \cdot \rho \cdot (s' - v_k)^2 \cdot c_d \cdot A, \quad (1)$$

where f – friction coefficient between berry particle and conveyor belt,
 ρ – air density,
 c_d – air resistance constant,
 A – surface of the frontal area,
 s'' – berry particle acceleration.

Last part on the right in equation (1) models air resistance [9].

The initial conditions for equation (1) are

$$s(t_0) = s_0, s'(t_0) = s'_0 - v_k \quad (2)$$

where $t_0 = 0$ and $s'_0 = 0$.

The initial value s_0 must be chosen presuming that the solution meets the condition $s > 0$ (Fig. 2). To solve the equation (1) on Mathcad worksheet, it had to be presented as the following system of two equations of the first order

$$\begin{aligned} y'_0 &= y_1, \\ y_0 &= g \sin(\beta) - f g \cos(\beta) - \frac{\rho (y_1 - v_k)^2 c_d A}{2 M} \end{aligned} \tag{3}$$

where $y_0 = s$, $y_1 = s'$.

Nonlinear system of equations (3) was solved numerically by using the algorithm of Runge-Kutta IV order, under conditions (2) by the following Mathcad function

$$Z(t_N, f, \beta, v_k) = \begin{bmatrix} D(t, y) \leftarrow \begin{bmatrix} y_1 \\ g \sin(\beta) - f g \cos(\beta) - \frac{\rho (y_1 - v_k)^2 c_d A}{2 M} \end{bmatrix} \\ Z \leftarrow \text{rkfixed} \left[\left(\begin{matrix} s_0 \\ s'_0 - v_k \end{matrix} \right), t_0, t_N, N, D \right] \end{bmatrix}$$

where the function

$$\text{rkfixed} \left[\left(\begin{matrix} s_0 \\ s'_0 - v_k \end{matrix} \right), t_0, t_N, N, D \right]$$

is the differentiation equation solver. D - the notation of the function

$$D(t, y) = \begin{bmatrix} y_1 \\ g \sin(\beta) - f g \cos(\beta) - \frac{\rho (y_1 - v_k)^2 c_d A}{2 M} \end{bmatrix}$$

of the right side of the system (3). Here y is the vector $y = \begin{pmatrix} y_0 \\ y_1 \end{pmatrix}$. t_0 – the time when berry motion begins, t_N – the time when berry motion ends, N – the number of subintervals within the interval (t_0, t_N) , $\begin{pmatrix} s_0 \\ s'_0 - v_k \end{pmatrix}$ – the matrix of initial values. Function $Z(t_N, f, \beta, v_k)$ returns the matrix with columns $Z(t_N, f, \beta, v_k)^{<1>}$, $Z(t_N, f, \beta, v_k)^{<2>}$, $Z(t_N, f, \beta, v_k)^{<3>}$, where $<1>$, $<2>$, $<3>$ denote the 1st, 2nd, 3rd column of this matrix. At that $t = Z(t_N, f, \beta, v_k)^{<1>}$ is the vector of the values of time, $s_t = Z(t_N, f, \beta, v_k)^{<2>}$ is the vector of the berry coordinates and $s'_t = Z(t_N, f, \beta, v_k)^{<3>}$ is the velocity vector of the berry. While t_N is also the value of time t , when the berry reaches point A (Fig. 2), its value can be calculated from equation

$$t_N = \text{root}[(Z(t_N, f, \beta, v_k)^{<2>})_N - l, t_N, 0.1, 10], \tag{4}$$

where the function $\text{root}(f(x), x, a, b)$ returns the solution of an equation $f(x) = 0$ in the closed interval $[a, b]$. In (4), $(Z(t_N, f, \beta, v_k)^{<2>})_N$ gives the N th value of the coordinate s_t at point A (Fig. 2) and l is the width of the belt. The value is supposed to be in the closed interval $[0.1, 10]$.

The Cartesian coordinates of the berry on belt during motion are

$$x_t(t_N, f, \beta, v_k) = x_a - (l - Z(t_N, f, \beta, v_k)^{<2>}) \cdot \cos \beta, \tag{5}$$

$$y_t(t_N, f, \beta, v_k) = y_a - (l - Z(t_N, f, \beta, v_k)^{<2>}) \cdot \sin \beta. \tag{6}$$

Point B (Fig. 2) coordinates are

$$x_b = x_a - l \cdot \cos \beta, \tag{7}$$

$$y_b = y_a + l \cdot \cos \beta. \tag{8}$$

2.2. Berry falling in the air

After berry has left the belt’s lower point A at the moment of the time t_N , it starts free fall in the air. This motion is described by the following equations

$$m \cdot y'' = -m \cdot g + \frac{1}{2} \cdot \rho \cdot y'^2 \cdot c_d \cdot A, \tag{9}$$

$$m \cdot x'' = -\frac{1}{2} \cdot \rho \cdot x'^2 \cdot c_d \cdot A, \tag{10}$$

where x'' and y'' are accelerations, x' and y' are velocities in the direction of x - and y -axis. Initial conditions for the equations (9) and (10) are

$$\begin{aligned} x(t_N, f, \beta, v_k) &= x_t(t_N, f, \beta, v_k), x'(t_N, f, \beta, v_k) = x'_t(t_N, f, \beta, v_k), y(t_N, f, \beta, v_k) = y_t(t_N, f, \beta, v_k), \\ y'(t_N, f, \beta, v_k) &= y'_t(t_N, f, \beta, v_k). \end{aligned} \tag{11}$$

To determinate the coordinates x and y during free fall, equations (9) and (10) were solved under initial conditions (11) numerically similar to the solution of equation (1).

3. Results and discussion

3.1. Berry displacement and velocity on belt

Let’s presume that berry and belt conveyor have the following values: berry mass $m = 0.02kg$, belt velocity $v_k = 1m/s$, friction coefficient between berry particle and conveyor belt $f = 0.01$, air density $\rho = 1.2 kg/m^3$, air resistance constant $c_d = 0.47$ (considering that sea buckthorn berry is almost a sphere), surface frontal area $A = \pi \cdot r^2 = 0.00031m^2$, width of the belt (distance between points AB) $l = 0.6m$, point A coordinates $x_a = 0.8m$ and $x_a = 0.5m$. Under initial conditions (2) $s_0 = 0.3m$, it means that the berry touches the belt in the center, because $AB = l = 0.6m$.

The analysis of the separator’s construction (Fig. 1) shows that there are mainly three possible values used for adjusting the separation process of the conveyor belt: inclination angle, velocities and friction coefficient (Fig. 3 – Fig. 5).

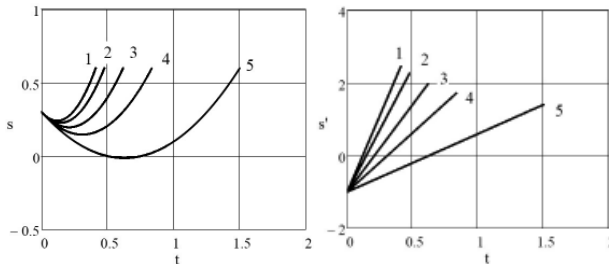


Fig. 3. Left: berry displacement along conveyor belt. Right: berry velocity along conveyor belt. Corresponding different inclination angles of the conveyor belt: 1) $\beta = 60^\circ$, 2) $\beta = 45^\circ$, 3) $\beta = 30^\circ$, 4) $\beta = 20^\circ$, 5) $\beta = 10^\circ$; $v_k = 5m/s$ and $f = 0.01$.

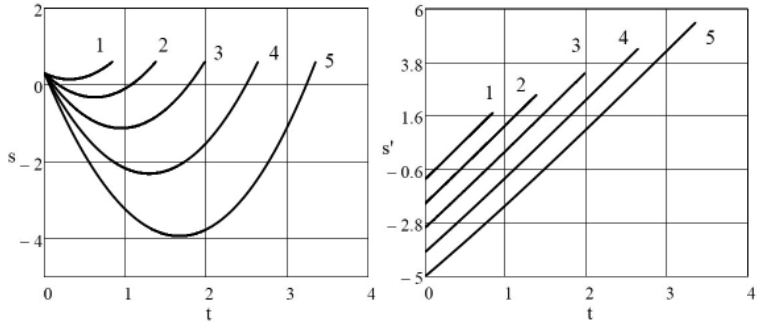


Fig. 4. Left: berry displacement along conveyor belt. Right: berry velocity along conveyor belt. Corresponding different velocities of the conveyor belt: 1) $v_k = 1m/s$, 2) $v_k = 2m/s$, 3) $v_k = 3m/s$, 4) $v_k = 4m/s$, 5) $v_k = 5m/s$; $\beta = 20^\circ$ and $f = 0.01$.

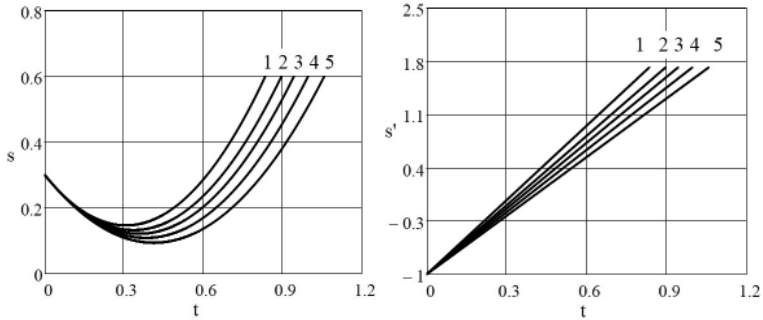


Fig. 5. Left: berry displacement along conveyor belt. Right: berry velocity along conveyor belt. Corresponding different friction coefficient between berry particle and conveyor belt: 1) $f = 0.01$, 2) $f = 0.05$, 3) $f = 0.1$, 4) $f = 0.15$, 5) $f = 0.2$; $v_k = 5m/s$ and $\beta = 20^\circ$.

Figures 3-5 show that after contacting the belt, the berry first starts to move in the direction of belt with velocity v_k and then, due to inclination angle and gravity, moves down along the belt until it reaches point A (Fig. 2). Displacement decrease and negative velocity indicate berry movement along the belt with velocity v_k . Negative displacement means that berry moves over the point B (Fig. 2). In reality, it means that berry will fall over point B along with leaves and small branches (Fig. 1).

The calculation of berry displacement and velocities indicates that there are possible values, in which case the berry moves along with velocity v_k and will not move in the correct direction at all. This can be adjusted with all three parameters (v_k, f, β) and also initial values s_0 and s'_0 .

3.2. Berry trajectory on the belt and in the air

For visualization of the belt according to equations (5) and (6) (Fig. 2, line AB), the coordinates are defined as matrixes on the Mathcad worksheet

$$c_x = \begin{pmatrix} x_b \\ x_a \end{pmatrix}, c_y = \begin{pmatrix} y_b \\ y_a \end{pmatrix}.$$

Berry trajectory can be visualized with the following matrixes according to equations (3) and (4), where $\min(x_t)$ and $\max(y_t)$ are built-in Mathcad functions for finding minimum and maximum values

$$b_x = \begin{pmatrix} \min(x_t) \\ x_t \end{pmatrix}, b_y = \begin{pmatrix} \max(y_t) \\ y_t \end{pmatrix}.$$

On Fig. 6 we can see that if the berry touches the belt in point $s_0 = 0.3m$, it will first move in the direction of belt with velocity v_k , like we saw on Fig. 3 - 5. On Fig. 6, when $\beta = 10^\circ$, the berry will move close to point B, i.e. berry can fall over the belt if point B is on the edge of the belt.

On Fig. 6, when $\beta = 30^\circ$ and $\beta = 60^\circ$, the berry will not reach point B and will stay on the belt until point A.

For example, if $s_0 = 0.3m$ and $s'_0 = 0.5m/s$, then, provided that $\beta = 60^\circ$, the berry will move towards point A instantly after touching the belt (Fig. 7). When $\beta = 10^\circ$ and $\beta = 30^\circ$, it will still show movement along the belt with velocity v_k in the beginning (Fig. 7).

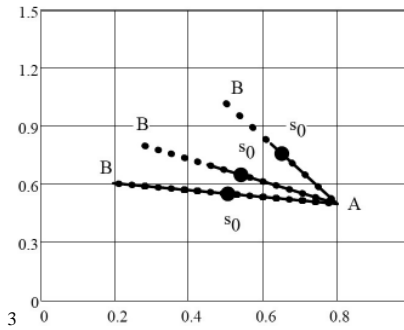


Fig. 6. The berry (continuous line) and the belt (dotted line) trajectories, s_0 location (large dot): 1) $\beta = 10^\circ$, 2) $\beta = 30^\circ$, 3) $\beta = 60^\circ$; $f = 0.01$, $v_k = 1m/s$, $s_0 = 0.3m$, $s'_0 = 0$.

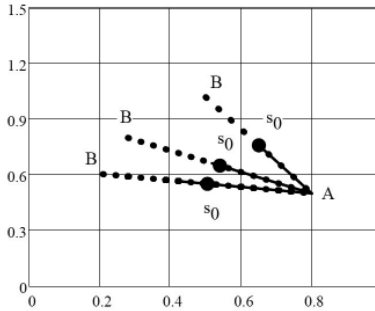


Fig. 7. The berry (continuous line) and the belt (dotted line) trajectories, s_0 location (large dot): 1) $\beta = 10^\circ$, 2) $\beta = 30^\circ$, 3) $\beta = 60^\circ$; $f = 0.01$, $v_k = 1m/s$, $s_0 = 0.3m$, $s'_0 = 0.5m/s$.

When summing up the solutions of equations (5), (6), (7), (8), (9) and (10), we get the entire trajectory of the berry on the belt and through the air (Fig 8). Based on the air trajectories, it is possible to determine the location of the collector or measuring box under the sea buckthorn berries separator.

The motion of the berry particle according to calculations, with different conveyor inclination angle, is visualized in video clip [10].

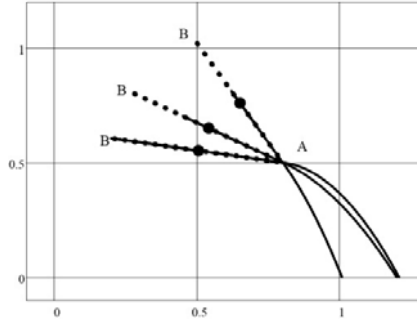


Fig. 8. Berry's entire trajectory on the belt and through the air, when 1) $\beta = 10^\circ$, 2) $\beta = 30^\circ$, 3) $\beta = 60^\circ$; $v_k = 1\text{m/s}$, $f = 0.01$, $s_0 = 0.3\text{m}$, $s'_0 = 0$.

3.3. Total time of berry motion

The total time of berry motion depending on inclination angle β , velocity of conveyor belt and friction coefficient was also determined.

Fig. 9 shows total time of berry motion according to the inclination angle (Fig. 2) of the conveyor belt. The total time decreases when angle increases.

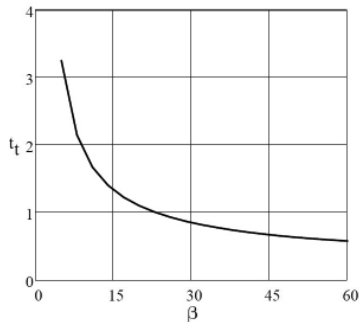


Fig. 9. Total time of berry motion depending on inclination angle β of conveyor belt if $v_k = 1\text{m/s}$, $f = 0.01$, $s_0 = 0.3\text{m}$, $s'_0 = 0$.

Fig. 10 shows total time of berry motion according to different velocity of the conveyor belt (Fig. 2). The total time increases when velocity increases. The relation of total time and conveyor belt velocity increase are almost linear.

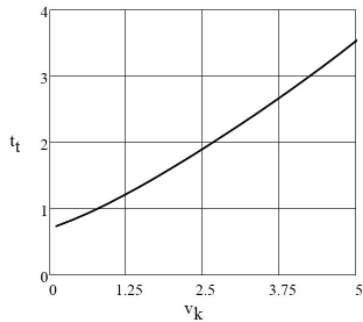


Fig. 10. Total time of berry motion depending on velocity of the conveyor belt if $f = 0.01$, $\beta = 20^\circ$, $s_0 = 0.3m$, $s'_0 = 0$.

Fig. 11 shows total time of berry motion depending on the friction coefficient. The total time increases when friction coefficient increases.

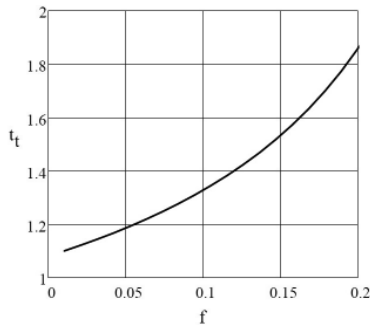


Fig. 11. Total time of berry motion according to different friction coefficients, berry particle and conveyor belt: $v_k = 1m/s$, $\beta = 20^\circ$, $s_0 = 0.3m$, $s'_0 = 0$.

The outcomes indicated in the results and discussion sections are theoretical and must be validated with experimental data. First steps are made to build a prototype of the sea buckthorn berries separator according to patent EE05717B1. Results of experimental data will be discussed in future papers.

Conclusions

This paper shows that: 1) From the initial position at beginning of motion, a berry moves along the belt in the direction of the conveyer belt at certain velocity, stops and then moves along the belt to the lower point of the belt and falls down. 2) There are initial berry values s_0 and s'_0 , in which case the berry does not reach the upper edge of the belt. 3) Total time of berry motion depends substantially on the inclination angle of the belt, coefficient of friction between berry and belt and velocity of the conveyer belt. 4) Composed video clip provides visual representation of full motion of the berry in separator under different angles of inclination of conveyer belt. Mathematical program Mathcad turned out to be a convenient tool for solving problems related to mechanics.

Results of this paper can be used by engineers for designing the conveyors and by educators for creative teaching of mechanics and engineering mechanics [11] of agricultural machinery.

References

- [1] S. Zhang, X. Xia, Optimal control of operation efficiency of belt conveyor systems, in: J. Yan (edi.), *Applied Energy*, 87(6) (2010) 1929-1937
- [2] I. Ibishi, A. Latifi, G. Ibishi, K. Sejdiu, M. Shala-Galica, B. Latifi, Calculation of tension force of belt conveyor, *International Journal of Engineering Science and Technology* 4(12) (2012) 4886 – 4892.
- [3] E.F. Zanoelo, A. Abitante, L.A.C. Meleiro, Dynamic modeling and feedback control for conveyors-belt dryers of mate leaves, in: R.P. Singh (edi.), *Journal of Food Engineering*, 84(3) (2008) 458-468.
- [4] S. Zhang, X. Xia, Modeling and energy efficiency optimization of belt conveyors, in: J. Yan (edi.), *Applied Energy* 88(9) (2011) 3061-3071
- [5] S. Göttlich, S. Hoher, P. Schindler, V. Schleper, A. Verl, Modeling, simulation and validation of material flow on conveyor belts, in: J. Sienc (edi.), *Applied Mathematical Modelling* 38(13) (2014) 3295-3313.
- [6] I. Pantea, I. Stanasel, F. Blaga, The simulation of the profiling technology of tothing knives, in: B. Katalinic (edi.), *Annals of DAAAM for 2008 and 19th International DAAAM Symposium, Trnava, 2008*, pp. 1015-1016.
- [7] M. Tierean, L. Baites, L. Eftimie, Design of the bridges structures using MathCAD, in: B. Katalinic (edi.), *Annals of DAAAM for 2008 and 19th International DAAAM Symposium, Trnava, 2008*, pp. 1389-1390.
- [8] P. Nömm, A. Aan, Device for separation of deep-frozen sea-buckthorn berries from twigs. Estonian patent: EE05717B1 (15.02.2014)
- [9] H. R. Harrison, T. Nettleton, *Advanced Engineering Dynamics*, John Wiley & Sons Inc., 1997.
- [10] A. Aan, (2014), Particle of the berry on inclined moving conveyor belt. Available at: <http://youtu.be/g0Axx5gmwIk> (2.09.2014)
- [11] M. Heinloo, A. Aan, On creative teaching of engineering mechanics, in: B. Katalinic (edi.), *Annals of DAAAM for 2011 and proceedings: 22nd international DAAAM symposium, Vienna, 2011*, pp. 1081 – 1082.

CURRICULUM VITAE

Personal data

Name: Aare Aan
Date of birth: 21. December 1983
Address: Estonian University of Life Sciences, Kreutzwaldi
56, Tartu
Phone: +372 58088219
E-mail: aare.aan@emu.ee

Education

2011 - ... Phd studies, Estonian University of Life Sciences,
Institute of Technology
2009 – 2011 Master's degree studies, Estonian University of Life
Sciences, Production Engineering
2006 – 2009 Bachelor's degree studies, Estonian University of
Life Sciences, Production Engineering
2005 – 2006 Lapland Vocational College, Forwarder operator
2004 - 2005 Luua Forestry School, Forwarder operator
2002 - 2003 Tallinn Polytechnic School, Introduction to infor-
mation technology
1999 – 2002 Koeru High School

Research activity

Degree information:

2011 MSc Production Engineering, Estonian University
of Life Sciences, Institute of Technology

Intellectual property:

2012 Device for the separation of deep-frozen sea-
buckthorn. EE 05717 B1. Nõmm, P., Aan, A. Own-
er: Estonian University of Life Sciences
2013 Hemp harvester. EE 05740 B1. Olt, J., Aan, A.
Owner: Estonian University of Life Sciences

Honours and degrees:

2012 Invention contest of Institute of Technology „Engi-
neering Student Invents 2012“ III place. „Device for
separation of sea-buckthorn berries“

Complementary education:

- 2013 – 2014 Engineering pedagogy courses, Tallinn University of Technology
- 2013 Intensive course: Current trends in process type production and discrete type manufacturing, Estonian University of Life Sciences
- 2012 Intensive course: Scientific trends in automation and manufacturing, Tallinn University of Technology
- 2012 Seminar: Innovated production, Tallinn University of Technology

Career

- 2011 - ... Estonian University of Life Sciences, Assistant (Mechanics of machinery)
- 2010 – 2011 Estonian University of Life Sciences, Specialist
- 2007 – 2010 AS Info-Auto Tartu, Car spare parts salesman

ELULOOKIRJELDUS

Isikuandmed

Nimi: Aare Aan
Sünniaeg: 21. Detsember 1983
Aadress: Eesti Maaülikool, Kreutzwaldi 56, Tartu
Telefon: +372 58088219
E-post: aare.aan@emu.ee

Haridustee

2011 - ... Eesti Maaülikool, Tehnikainstituut, Doktorant
2009 - 2011 Eesti Maaülikool, Tootmistehnika, Magistriõpe
2006 – 2009 Eesti Maaülikool, Tootmistehnika, Bakalaureuseõpe
2005 – 2006 Lapin Ammattiopisto (Soome), Forwarderi operaator
2004 – 2005 Luua Metsanduskool, Forwarderi operaator
2002 – 2003 Tallinna Polütehnikum, Infotehnoloogiaalused
1999 - 2002 Koeru Keskkool

Teadustegevus

Teaduskraadi info:

2011 Magistrikraad tootmistehnika erialal, Eesti Maaülikool

Patentsed leiutised:

2012 Sügavkülmutatud astelpajumarjade okstest eraldamise seade. EE 05717 B1. Nõmm, P., Aan, A.
Omanik: Eesti Maaülikool
2013 Kanepikoristi. EE 05740 B1. Olt, J., Aan, A.
Omanik: Eesti Maaülikool

Teaduspreemiad ja –tunnustused:

2012 Üliõpilaste leiutuskonkursil „Tehnikatudeng leiutab 2012“ III koht tööga „Astelpaju eraldustrummel“

Täiendkoolitused:

2013 – 2014 Inseneripedagoogika kursused, Tallinna Tehnikaülikool
2013 Kursus: Current trends in process type production and discrete type manufacturing, Eesti Maaülikool

- 2012 Kursus: Scientific trends in automation and manufacturing, Tallinna Tehnikaülikool
- 2012 Täiendkoolitus: Uuenduslik tootmine (Masinaehituse TAK, Paindootmissüsteemide tehnoloogiad ja automatiseerimine, Materjalid), Tallinna Tehnikaülikool

Teenistuskäik

- 2011 - ... Eesti Maaülikool, assistent (masinamehaanika)
- 2010 – 2011 Eesti Maaülikool, Tehnikainstituut, spetsialist
- 2007 - 2010 AS Info-Auto Tartu, varuosamüüja

ETTEKANDED

Suulised ettekanded rahvusvahelistel konverentsidel:

International Scientific Conference Biosystem Engineering 2011, Tartu, Eesti, Eesti Maaülikool, On chaotic motion of a double pendulum, **Aan, A.**; Aarend, E.; Heinloo, M.

22nd International DAAAM Symposium "Intellegent Manufacturing and automation: Power of Knowledge and Creativity", 2011, Austria, Viin, On creative teaching of engineering mechanics, **Aan, A.**; Heinloo, M.

8th International Conference of DAAAM Baltic Industrial Engineering, 2012, Tallinn, Eesti, Analysis of four-stroke cycle internal combustion V-engine in Mathcad environment, **Aan, A.**; Heinloo, M.; Aarend, E.; Mikita, V.

International Scientific Conference Biosystem Engineering 2012, Tartu, Eesti, Eesti Maaülikool, Computer based comparison analysis of single and double-connecting-rod slider-crank linkages, **Aan, A.**; Heinloo, M.

International Scientific Conference Biosystem Engineering 2013, Tartu, Eesti, Eesti Maaülikool, Composing and solving differential equations for small oscillations of mathematical spring-coupled pendulums, **Aan, A.**; Heinloo, M.

42nd international symposium on agricultural engineering: Actual Tasks on Agricultural Engineering, 2014, Opatija, Horvaatia, Motion of a granule on fertilizer spreading disc, **Aan, A.**; Heinloo, M.

9th International Conference of DAAAM Baltic Industrial Engineering, 2014, Tallinn, Eesti, Tallinna Tehnikaülikool, Design of a radial cam for the cam-follower mechanism, **Aan, A.**; Heinloo, M.; Allas, J.

International Scientific Conference Biosystem Engineering 2014, Tartu, Eesti, Eesti Maaülikool, Analysis and synthesis of the walking linkage of Theo Jansen with a flywheel, **Aan, A.**; Heinloo, M.

Stendettekanded rahvusvahelistel konverentsidel:

25th DAAAM International Symposium Intelligent Manufacturing & Automation: Focus on Sustainability, 2014, Viin, Austria, Dynamics of a frozen sea buckhorn berry in a separaator, **Aan, A.**; Heinloo, M.